

Effective Interaction and Charge Fluctuations in a Hot Pion Gas

Diploma Thesis

submitted to the Department of Physics
at the Westfälische–Wilhelms–Universität Münster

Michael Döring ¹
Planckstr. 1
64291 Darmstadt
Germany

April 1, 2002

¹M.Doering@theory.gsi.de, MDoering@lbl.gov

Contents

1	Introduction	1
1.1	The Search for the Quark Gluon Plasma	1
1.2	Charge Fluctuations per Degree of Freedom	2
2	Theoretical Framework	6
2.1	Grand Canonical Ensemble and Observables	6
2.2	The Statistical Operator	7
2.2.1	Grand Partition Function for a Free Bose Gas	8
2.2.2	Charge Fluctuations of a Free Bose Gas	10
2.3	Finite Temperature Field Theory	11
2.3.1	Functional Representation / Generating Functional	12
2.3.2	Self Interacting Charged Bose gas	13
2.3.3	Perturbation Series expansion	15
2.3.4	Diagrammatic Expansion	17
2.3.5	Evaluating Matsubara Sums	18
3	Effective Interaction	23
3.1	QCD Lagrangian	23
3.1.1	Quantum Chromodynamics	24
3.1.2	Chiral Effective Models	25
3.2	The High Mass Limit	28
3.2.1	Effective Interaction Lagrangian of the High Mass Limit	30
3.2.2	Gauging the π^4 Effective Lagrangian: Photon Field	30
3.3	Vacuum Feynman Rules from the $(\rho)\pi\gamma$ -Lagrangian — Processes without π^0	32
3.3.1	Scalar QED Feynman Rules	32
3.3.2	Vertices Including the Effective Interaction	33
3.3.3	Vacuum Feynman Rules including π^0	35
3.4	Feynman Rules at Finite Temperature	35
3.4.1	Summary of Feynman Rules in the order e^2g^2	36
4	Charge Fluctuations and Self Energy	37
4.0.2	Conserved Current of the Gauged $(\rho)\pi\pi$ -Lagrangian	37
4.1	Charge Fluctuations and Charge Density	38
4.2	Charge Density and Self Energy Diagrams	38
4.2.1	Charge Density as Imaginary Time Propagator	38
4.3	Ward-Takahashi Identity (WTI) for sQED	41
4.3.1	The Ward Identity	41
4.3.2	The Ward Identity in Different Orders	42

4.4	Applying the WTI in the Construction of Self Energy Diagrams in sQED	43
4.5	The WTI for $\lambda(\phi^*\phi)^2$ -theory	44
4.5.1	Proof to all Orders	46
4.6	The WTI for 4-point Functions in Effective ρ -Coupling	47
4.7	Ward Identity for 2-point Functions in the Effective Coupling	48
4.8	Construction of Self Energy Diagrams in the Effective Theory	48
4.9	The Transversality of Diagrams in a Simple Example	49
4.9.1	Matter Part of $q_\mu \Pi^{\mu\nu}$, $\nu = 1, 2, 3$	50
5	Self Energy in the High Mass Limit	53
5.0.2	The Bubble and the Tadpole Diagram in e^2	53
5.1	The <i>Duck</i> Diagram	54
5.1.1	Complete Self Energy of the <i>Duck</i> Diagram	55
5.2	Moving the Limit	57
5.2.1	Further Exchanges of Summation and Limits	59
5.3	Classifications of Diagrams and Result	62
5.3.1	The contribution of neutral pions	62
5.4	The Ward Identity in $\lambda(\phi\phi^*)^2$ -theory (Vacuum)	63
5.5	The Ward Identity in the Order $e^2 g^2$	66
5.5.1	Mapping the problem (Matter)	66
6	Numerical Results and Outlook	71
6.1	Entropy in g^2	71
6.2	Numerical Results for the Charge Fluctuations per Entropy	71
6.2.1	The Tadpole Diagram and the Simple Bubble	72
6.3	Charge Fluctuations per Entropy	75
6.4	The ρ -meson at Finite Mass	77
7	Summary and Conclusions	82
A	Details of Calculations	83
A.1	Motivation of the Path Integral	83
A.2	Gauging the Effective Lagrangian	85
A.3	Vacuum Feynman Rules including Neutral Pions.	87
A.4	Calculations in the Frame of the Ward-Takahashi Identity (WTI)	89
A.4.1	Proof of the WTI for sQED (see 4.3)	89
A.4.2	Loop Insertion	93
A.4.3	Proof of the WI for Four-Point Functions in the Effective Theory	94
A.4.4	Vacuum Part in e^2 : Dimensional Regularization	96
A.5	Evaluation of the Self Energy in $e^2 g^2$	99
A.5.1	Further Analysis of the <i>Duck</i> Diagram in Fig. 5.1	99
A.5.2	The <i>Specs</i> Diagram	101
A.5.3	Chain Diagrams — Resummation	103
A.5.4	The <i>Snowman</i> Diagram	104
A.5.5	The <i>Mouse</i> Diagram	106
A.5.6	The <i>Propeller</i> Diagram	107
A.5.7	Numerical Test of the Computation of Contour Integrals	108
A.6	Proof of J_D as Conserved Current — no π^0	109
A.7	Fitting the Bubble and the Tadpole Diagram	110
A.8	A Questionable Calculation	111

<i>CONTENTS</i>	3
B References	113
B.1 <i>Mathematica</i> ® Notebooks	113
B.1.1 Reference of Software	113
C Acknowledgement	116

Abstract

The primary goal in the studies of heavy ion collisions is to produce evidence of the quark gluon plasma (QGP). Reduced charge fluctuations, due to the fractional charge of the quarks in the QGP, may provide a signature of its production. In the hadronic phase, fluctuations may be screened or enhanced by hadronic interaction. Using an effective Lagrangian, based on vector dominance, we calculate the charge fluctuations up to second order in a hot pion gas applying finite temperature field theory.

Chapter 1

Introduction

1.1 The Search for the Quark Gluon Plasma

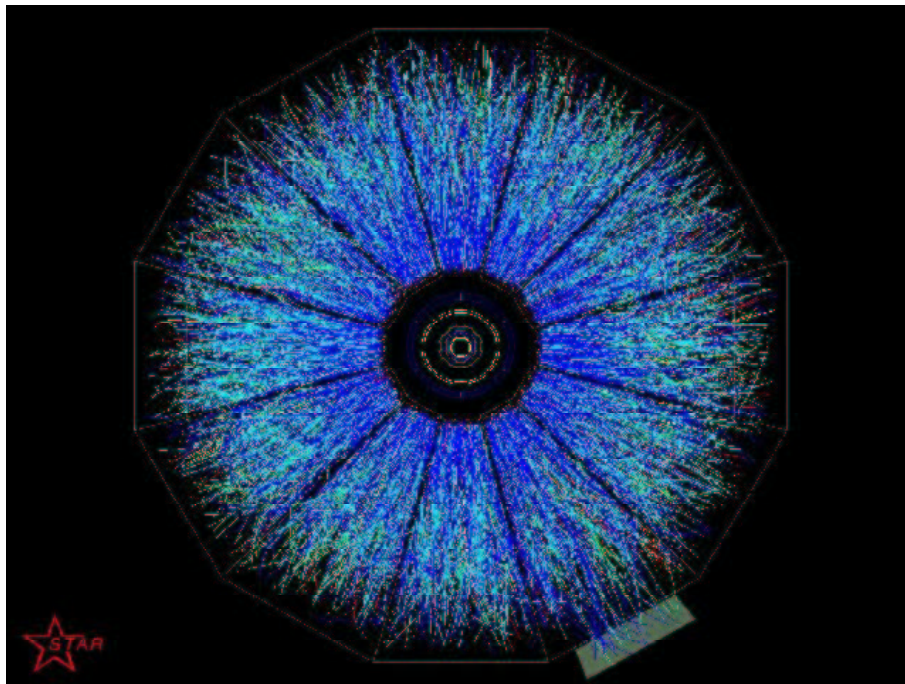


Figure 1.1: Event 53 in the STAR-detector at RHIC (200 GeV / nucleon) [1]. View along the beam axis. The particles leave traces in the gas chamber (TPC) while their transversal trajectory is bent by magnetic fields.

The Quark Gluon Plasma (QGP) is postulated as the fundamental matter phase in which the constituents of the hadronic matter, quarks and gluons, are deconfined. It is assumed to be the predecessor of hadronic matter at the origin of the universe. The QGP is not only of cosmological interest, but could also exist in the core of neutron stars. There, the extreme pressure provides the necessary high energy

densities. Lattice calculations have shown that the caloric curve of matter shows a phase transition, which is a strong evidence that the QGP exists.

The detection of the QGP in heavy ion collisions is not easy. After the collision of two heavy nuclei like $Au + Au$ or $Pb + Pb$ (A–A–collisions) as performed at RHIC or CERN, different scenarios could occur: There is a pure hadron gas that expands until the freeze-out, at which point the reaction products stop interacting. There could also be a mixed phase of QGP and hadrons in the beginning as well as pure QGP. In the latter case the QGP undergoes a phase transition, the hadronization. This results in an expanding fireball which is dominated by pions. The thermal movement of the pions is superposed by a collective expansion flow. The chemical freeze-out first takes place at a certain temperature and density, after which the chemical equilibrium (the consistency) no longer changes, although the particles can still interact with each other. Following chemical freeze-out, the thermal freeze-out takes place and the particles stop interacting as they travel to the detector. In Fig. 1.1 a typical event at RHIC is depicted.

A possible signature of the QGP is the J/Ψ -suppression (Matsui, Satz [2]). The basic mechanism for deconfinement in dense matter is Debye screening of the quark color charge. When the screening radius becomes less than the binding radius of the quark system, i.e. less than the hadron radius at sufficiently high densities, the confining force can no longer hold the quarks together and hence deconfinement sets in. This affects the charmonium binding ($c\bar{c}$). The c - \bar{c} -resonance action leads to J/Ψ production [2]. If the screening length $r_D(T)$ becomes too small at high temperatures, the charge of the c and \bar{c} is screened. In a semiclassical model we can write for the Coulomb $c\bar{c}$ -potential

$$V(r) = -\frac{\alpha_{\text{eff}}}{r} e^{-\frac{r}{r_D(T)}}$$

where T is the temperature and α_{eff} is the Coulomb interaction coupling. There is a minimum value of $r_D^{\text{min}} \sim 0.76$ fm below which no bound $c\bar{c}$ state can exist. Since the J/Ψ production only takes place at temperatures above $T = 200$ MeV, the suppression should be a sensitive signal of the primordial consistency of the matter in a heavy ion collision.

Similar considerations apply for the excited state of the J/Ψ , the Ψ' and χ .

More recent approaches than the initial work [2] propose that the J/Ψ -suppression can be also caused by rescattering with comoving hadronic matter in the hadronic phase (Quark Matter Conference 2001 [3]).

Other possible signatures are strangeness enhancement, real or virtual photons, and the p_T distribution (transverse momentum) of the secondary hadrons [4][5]. The strangeness enhancement, however, can undergo a suppression in the hadronic phase (Strange Quark Matter Conference 2002 [6]).

1.2 Charge Fluctuations per Degree of Freedom

Charge fluctuations have been recently proposed as a possible sign of evidence for the Quark Gluon Plasma ([7],[8]). This section summarizes the paper by Jeon and Koch [7] and [9].

Quarks carry a fractional charge of $1/3$ and $2/3$. They cause charge fluctuations that are smaller than those from a mixed initial phase (QGP + hadron gas) or a pure hadron gas. Hadrons always carry the charge $|q| = 1$. Their charge fluctuations are therefore bigger since the observable D_{CF} is sensitive to the *square* of the charge. The aim is to define an observable in order to measure charge fluctuations.

Charge fluctuations measure the deviation from charge neutrality in a subset of the produced particles in a heavy ion collision from event to event. Although the net charge of the total system is conserved, the subset will show fluctuations.

The subset can be chosen in different ways. In the Bjorken-model, a strong longitudinal flow occurs, suggesting that it may be advantageous to concentrate on a window in rapidity space of the longitudinal expansion: Then, the particles are likely to interact perpendicular to their movement, but their longitudinal interaction should be reduced.

Two constraints are imposed on the window: With $y = \text{arctanh}(v)$ ($c = 1$) being the rapidity of the expanding particles,

$$\Delta y_{\text{total}} \gg \Delta y_{\text{accept}} \gg \Delta y_{\text{charge-transport}}.$$

The rapidity range y_{total} which is allowed by the kinematics of the reaction must be much larger than the width of the measuring window. Then, the subsystem can be assumed as being embedded in an infinite heat bath (The total amount of produced particles) with the possibility of the exchange of particles and energy. This is the grand canonical ensemble. On the other hand, the ensemble must not be too small (second constraint). If it is too small, leakage effects may overshadow the signal. From transport theory the minimal size must not lie below $\Delta y_{\text{charge-transport}} \sim 1$ ¹.

One can understand this as a surface-to-volume effect. If the subsystem becomes too small, the ratio drops and unwanted leakage effects of the particles violate the assumption of local charge conservation.

In [7] different ansatzes are discussed as possible observables. Instead of the ratio $F = Q/N_{ch}$, with the net charge $Q = N_+ - N_-$ and charge multiplicity $N_{ch} = N_+ + N_-$, the ratio

$$R = \frac{N_+}{N_-}$$

is favored. It is essential to divide by the number of charged particles in order to cancel the fluctuations of the volume from event to event due to the fluctuating impact parameter. With the deviation $\delta x = x - \langle x \rangle$ of a quantity x from the mean value, R obtains a factor of 4:

$$\langle \delta R^2 \rangle = \langle R^2 \rangle - \langle R \rangle^2 \simeq 4 \langle \delta F^2 \rangle \left(+ \mathcal{O} \left[\left(\frac{\langle Q \rangle}{\langle N_{ch} \rangle} \right)^2 \right] \right)$$

in the limit $\langle Q \rangle \ll \langle N_{ch} \rangle$.

The fluctuation of an average ratio is dominated by the fluctuation in the smaller quantity if both differ considerably [9]. A ratio of $\langle Q \rangle / \langle N_{ch} \rangle \sim 5\%$ is expected at RHIC. (note: $\langle Q \rangle / \langle N_{ch} \rangle \rightarrow 0$ for a rising ensemble size in a finite heat bath). Then the fluctuation is dominated by the fluctuation in Q so that

$$\langle \delta F^2 \rangle \sim \frac{\langle \delta Q^2 \rangle}{\langle N_{ch} \rangle^2}$$

We multiply this with the expectation value of the number of charged particles in order to obtain the observable

$$D_{CF} := \langle N_{ch} \rangle \langle \delta R^2 \rangle = 4 \langle N_{ch} \rangle \langle \delta F^2 \rangle = 4 \frac{\langle \delta Q^2 \rangle}{\langle N_{ch} \rangle}. \quad (1.1)$$

The expectation value $\langle N_{ch} \rangle$ is closely related to the entropy of the quarks and gluons in a QGP and the hadrons (pions and resonances) in the case of a hadronic phase. Therefore we want to calculate the entropy as well. Charge fluctuations are normalized by the degrees of freedom in order to obtain an intensive quantity.

Firstly, consider a free pion gas. The fluctuation in the net charge is the sum of the fluctuations of positive and negative pions: $\delta Q = \delta N_{\pi^+} - \delta N_{\pi^-}$. Therefore,

$$\langle \delta Q^2 \rangle = \langle \delta N_+^2 \rangle + \langle \delta N_-^2 \rangle = w_\pi \langle N_{ch} \rangle$$

¹This is not a contradiction to the assumption of a grand canonical ensemble. Of course we are interested in the transition of charge into and out from the system. But at very short scales quantum effects are not negligible any more. In Landau, §112 [14], one can find an estimation of what the minimal size of an ensemble must be. By using the Heisenberg uncertainty relation the fluctuation of the entropy is calculated. Since the entropy determines the probability of finding a state in a given interval, its fluctuation must not be too large.

From a more mathematical point of view, the fluctuations must not be too large because the Taylor expansion (2.1) in the derivation of the grand canonical ensemble will fail because the coefficients show too large fluctuations.

with $N_\pi = N_+ + N_-$ and $w_\pi = \langle \delta N_\pi^2 \rangle / \langle N_\pi \rangle$. Here, we have assumed that there is no correlation $\langle \delta N_{\pi^+} \delta N_{\pi^-} \rangle = 0$ between the fluctuations of positive and negative pions.

In order to calculate w_π we find from Landau, §118 [14] that

$$w_\pi = 1 \pm \frac{\langle n_I^2 \rangle}{\langle n_I \rangle} \quad (1.2)$$

with n_I being the integrated Bose distribution (upper sign) or Fermi–Dirac distribution (lower sign)

$$n_I(\beta) = \int \frac{d^3 \mathbf{p}}{(2\pi)^3} \frac{1}{e^{\beta \sqrt{\mathbf{p}^2 + m_\pi^2}} \mp 1} \quad (1.3)$$

This can be numerically solved, leading to $w_\pi = 1.13$ at $T = 170 \text{ MeV}$. In the range $T \in [150, 200]$, w_π is within the range $w_\pi \in [1.11, 1.15]$ (Bertsch [10]). The value of D in a classical gas then is

$$D_{\text{pion}} \simeq 4$$

with a 10% correction due to Bose–Einstein statistics. (see also [33], §9.2). The deviation from 4 is rather small compared to other uncertainties as the influence of resonances on charge fluctuations.

Second we consider a free gas of thermalized massless quarks. Since only the quarks carry charge we can write $\delta Q = Q_u \delta(N_u - N_{\bar{u}}) + Q_d \delta(N_d - N_{\bar{d}})$. Assuming lack of correlations we obtain

$$\langle \delta Q^2 \rangle = Q_u^2 w_u \langle N_{u+\bar{u}} \rangle + Q_d^2 w_d \langle N_{d+\bar{d}} \rangle$$

where $N_{q+\bar{q}}$ denotes the number of quarks and anti-quarks. Choosing the lower sign in (1.2) and (1.3) we obtain a value for w_q slightly smaller than 1. In order to make an estimate of how the final charged particle multiplicity N_{ch} is related to the primordial number of quarks and gluons we assume the conservation of entropy. In the massless, non-interacting limit, we can then relate the entropy density to the particle number density. It is $\sigma_B = 3.6 n_B$ and $\sigma_F = 4.2 n_F$ for bosons and fermions respectively. The bosonic coefficient will be derived later. From this follows the total entropy of a quark–gluon plasma in a volume V :

$$S = V\sigma = 3.6 \langle N_g \rangle + 4.2 (\langle N_{u+\bar{u}} \rangle + \langle N_{d+\bar{d}} \rangle).$$

N_g is the number of gluons in the volume. After a collision of heavy ions, the reaction volume V expands and cools down, and all quarks and gluons are converted into pions. Since the entropy is conserved, the number of pions must be

$$\langle N_\pi \rangle = \frac{S}{3.6} = \langle N_g \rangle + \frac{4.2}{3.6} (\langle N_{u+\bar{u}} \rangle + \langle N_{d+\bar{d}} \rangle).$$

The final charge multiplicity is obtained from this by applying a factor $2/3$ due to isospin symmetry (the neutral pion does not contribute). The resulting value for D_{CF} is then

$$D_{\text{QGP}} = \langle N_{\text{ch}} \rangle \langle \delta R^2 \rangle |_{\text{QGP}} \sim 0.75$$

Clearly, the value for the observable D differs by a factor of more than five from the hadron gas case to the Quark Gluon Plasma case.

Of course, there are deviations due to different influences.

- First of all, the influence of resonances reduces the charge fluctuations in the hadronic phase to a value of 3 [9]. Neutral ρ^0 and ω -mesons decay in the particles of interest, the pions. Two pions originating from such a 2-body decay, of course, show a very strong correlation.
- Lattice calculations have shown that the fluctuations in a QGP are bigger than in the massless quark model, $D = 1.2 - 1.5$ (See Gottlieb [28]).

- The ratio of charge fluctuation to entropy can only increase during the expansion. If the net charge is set in the QGP-phase, it is fixed to all times (apart from leaking effects). Then, only the entropy can increase during hadronization, further lowering the value of D and thus strengthening the signal.
- The initial state is a mixture of QGP and hadron gas. If there is a 50 % mixture, the signal is still visible.
- Enhancement or screening of the charge fluctuations in the (interacting) pion dominated hadronic phase. This is the topic of this thesis.

Furthermore, the effects of rapidity correlations, finite acceptance corrections and rescattering play a role [7].

This thesis aims at getting insight into the enhancement respectively suppression of charge fluctuations in the hadronic phase. The initial charge fluctuations, may they originate from a hadron gas or a QGP, undergo screening effects in the hadronic phase.

In the next chapter we will calculate this effect in a gas of free pions. Then, an interaction with the ρ -meson is introduced and an effective Lagrangian is constructed. Relating the charge fluctuations per entropy to self energy diagrams, this Lagrangian is expanded in the linear order of the strong coupling.

Many of the calculations in this thesis have been performed using *Mathematica*®. At the end of the thesis (B.1) a reference of the relevant programs is given.

Chapter 2

Theoretical Framework

2.1 Grand Canonical Ensemble and Observables

Statistical physics is a tool to describe properties of many-particle systems. Although it is not possible to determine the microscopic behavior of the system, averaged quantities like pressure, energy and entropy can be extracted. The concept is to work with so-called statistical ensembles. We can visualize them as a set of identical system that obey certain constraints. Although the microscopic state of each probe is different, we are only interested in the average over all ensembles. There are three different types of constraints on such a system:

- In the microcanonical ensemble all thermodynamical quantities are expressed in terms of energy, volume and the number of particles (E, V, N) . The system is isolated from its environment.
- In the canonical ensemble, (T, V, N) , where T is the temperature, are the independent quantities. Here, the energy is decreed by the heat exchange of the ensemble with an external heat bath which is assumed to be infinite. For a single particle the microcanonical and the canonical description mean a very different situation. Where the first corresponds to a particle in an empty box with sharp energy in all possible positions and with all possible momenta equally possible (according to the fundamental rule of statistical mechanics), the latter describes a particle with an unsharp distribution of the energy. However, in a macroscopic system the deviation of the total energy from the mean value vanishes, since fluctuations in an N -particle system behave like $1/\sqrt{N}$.
- If we even allow the exchange of particles between the heat bath and the ensemble, the number of particles in the ensemble is not fixed any more. The fundamental variables are the set (T, V, μ) . Here, μ is the so-called chemical potential. It is the free Gibbs energy per particle (see below). It describes the energy difference if one particle is added to the ensemble (see Fliessbach [11]). The grand canonical ensemble is the appropriate assumption in a relativistic quantum theory that is used to describe heavy ion collisions. The number of particles can vary due to the production of new particles. However, there are conserved quantities like the net charge which can be associated with a chemical potential μ_i . The μ_i 's determine the mean net value of the number of particles, mean net charge and so on in the grand canonical ensemble. Of course, the mean number is in fact the number of particles minus the number of antiparticles. Those numbers are not conserved separately (see Kapusta [12]).

In the grand canonical ensemble we can calculate the probability of finding a microscopical state r . For that we imagine the total system which is split in a small system and the rest B which serves as the heat bath and particle reservoir. Between the subsystems, both heat and particles can be exchanged. We call

$\Omega(E, N)$ the number of possible states of the total system. All possible states have equal probability. If the microscopical state r is realized in the small subsystem, the reservoir can realize $\Omega_B(E - E_r, N - N_r)$ states. Since it is so much bigger, this equals approximately the number of states of the total system (if the subsystem is still in r). Then, the possibility to find one of the $\Omega_B(E - E_r, N - N_r)$ states in the total number of $\Omega(E, N)$ is

$$P_r = \frac{\Omega_B(E - E_r, N - N_r)}{\Omega(E, N)}.$$

Since the subsystem is so small, we have $E_r \ll E$ and $N_r \ll N$. The expansion of $\log \Omega_B(E - E_r, N - N_r)$

$$\log \Omega_B(E - E_r, N - N_r) = \log \Omega_B(E, N) - \frac{\partial \log \Omega_B}{\partial E} E_r - \frac{\partial \log \Omega_B}{\partial N} N_r + \dots \quad (2.1)$$

in terms of E_r and N_r can therefore be terminated after the linear contributions. The partial derivatives can be evaluated by using the thermodynamical relations:

$$\beta = \frac{\partial \log \Omega_B(E, N)}{\partial E} \quad \text{and} \quad -\beta\mu = \frac{\partial \log \Omega_B(E, N)}{\partial N}.$$

From this we have

$$P_r(T, V, \mu) = \frac{e^{-\beta(E_r(V, N_r) - \mu N_r)}}{\sum_r e^{-\beta(E_r(V, N_r) - \mu N_r)}}. \quad (2.2)$$

The sum in the denominator normalizes the probability. (Details of the calculation in [11])

Using P_r we can determine thermodynamical observables e.g.

$$E(T, V, \mu) = \overline{E_r} = \sum_r P_r(T, V, \mu) E_r(V, N_r). \quad (2.3)$$

We have identified P_r with the grandcanonical weighting function that allows to calculate expectation values. So far, no physics has taken place — the difficulty lies in the determination of the energy levels E_r . This depends on the statistics and the properties of the system. We have to find the eigenvalues of the Hamiltonian which can be classical (thermodynamics) or quantized.

2.2 The Statistical Operator

We consider a system described by a Hamiltonian H and a set of conserved quantities \hat{N}_i with associated chemical potentials μ_i in the grand canonical ensemble. We are working in second quantization from now on. For an introduction see [15] and Fetter–Walecka [27]. The operators \hat{N}_i of the conserved quantities all have to commute with the Hamiltonian. We define the statistical operator in analogy to the distribution of states P_r in statistical mechanics (2.2) by

$$\hat{\rho}_G = e^{-\beta(H - \sum_i \mu_i \hat{N}_i)}. \quad (2.4)$$

We can think of it as the distribution of states in the ensemble. The physics lies in the determination of the eigenstates of $\hat{K} = \hat{H} - \sum_i \mu_i \hat{N}_i$, often referred to as grand canonical Hamiltonian.

The ensemble average of an operator \hat{O} is defined by

$$\langle \hat{O} \rangle = \frac{\text{Tr}(\hat{\rho}_G \hat{O})}{\text{Tr} \hat{\rho}_G} \quad (2.5)$$

The Tr operation is the sum over a complete set of states, e.g. the eigenstates of the Hamiltonian. Those are weighted by the distribution function $\hat{\rho}_G$. The denominator of (2.5) is then the normalization with

respect to $\hat{\rho}_G$. We see the close relation to the calculation of expectation values in statistical physics as it is shown in one example in (2.3).

We define the grand canonical partition function by

$$Z = \text{Tr} \hat{\rho}. \quad (2.6)$$

It is the most fundamental quantity in statistical physics from which all observables can be derived.

2.2.1 Grand Partition Function for a Free Bose Gas

As an example which we will need later on, we want to calculate the grand partition function for an ideal Bose Gas (starting with the one dimensional case). With the creation and destruction operators of the harmonic oscillator a and a^\dagger , the Hamiltonian of a free Bose gas in one dimension (one degree of freedom) can be rewritten as

$$\hat{H} = \omega \left(\hat{N} + \frac{1}{2} \right). \quad (2.7)$$

Here, ω is the energy determined by the system properties. The motivation of (2.7) can be found in e.g. in Peskin–Schroeder [13]. For simplicity we ignore the zero-point energy which is justified as long as no background fields are present. From the form of the Hamiltonian we see that the eigenstates $|n\rangle$ are simultaneously eigenstates of the Hamiltonian and the number operator. Therefore the number of particles is a conserved quantity, and we can assign a chemical potential μ to the particles. In a pion gas, the π^+ boson obtains a positive chemical potential $\mu > 0$ and the π^- obtains the value $-\mu$.

Then the partition is easily computed in a geometrical series:

$$\begin{aligned} Z &= \text{tr} \left(e^{-\beta(\hat{H} - \mu \hat{N})} \right) = \text{tr} \left(e^{-\beta(\omega - \mu) \hat{N}} \right) \\ &= \sum_{n=0}^{\infty} \langle n | e^{-\beta(\omega - \mu) \hat{N}} | n \rangle = \sum_{n=0}^{\infty} e^{-\beta(\omega - \mu)n} \\ &= \frac{1}{1 - e^{-\beta(\omega - \mu)}} \end{aligned} \quad (2.8)$$

From

$$N = T \frac{\partial \log Z}{\partial \mu}$$

we obtain the energy distribution of the particles

$$n[\omega, T] := N = \frac{1}{e^{\beta(\omega - \mu)} - 1}$$

which is the well known Bose-distribution with the mean energy $E = \omega N$. If $n[\cdot]$ appears with only one argument in the following chapters, always the energy is meant. The second argument is reserved for the temperature although we will also write $n[\omega, \beta]$. Then, the inverse temperature is the argument. Misunderstandings are excluded.

The next step is to generalize this result to a box containing a free boson gas (three degrees of freedom). This can be done in analogy to how the one dimensional oscillator is generalized to a three dimensional one [12]. Obeying the boundary conditions for bosons (modes l_x , l_y and l_z) and splitting the Hamiltonian in the three spatial directions leads to the expression

$$\log Z = \sum_{l_x=1}^{\infty} \sum_{l_y=1}^{\infty} \sum_{l_z=1}^{\infty} \log Z_{l_x, l_y, l_z}.$$

This sum can be replaced by the (positive!) 3-d integral

$$\log Z = -V \int \frac{d^3 \mathbf{p}}{(2\pi)^3} \log \left(1 - e^{-\beta(\omega(\mathbf{p}) - \mu)} \right)$$

with the relativistic dispersion relation $\omega(\mathbf{p})^2 = m^2 + \mathbf{p}^2$.

From this we can compute the entropy of a free boson gas. We assign the subscript 0 to all free gas thermodynamical quantities in order to distinguish between the interacting case we will compute once we know the tools of finite temperature field theory. We have (with $\mu = 0$ which will be motivated later)

$$\log Z_0 = -V \int \frac{d^3 \mathbf{p}}{(2\pi)^3} \log \left(1 - e^{-\frac{\omega}{T}} \right) = V \int \frac{d^3 \mathbf{p}}{(2\pi)^3} \log (-n[-\omega]) \quad (2.9)$$

By using

$$\frac{\partial}{\partial T} n[\omega, T] = \left(-\frac{\omega}{T} \right) \frac{\partial}{\partial \omega} n[\omega, T] \quad (2.10)$$

we obtain

$$\frac{\partial}{\partial T} Z_0 = -\frac{V}{T} \frac{1}{2\pi^2} \int_{m_\pi}^{\infty} d\omega \, \omega \left(\frac{\omega^2}{p} + p \right) \log[-n[-\omega]].$$

after a partial integration.

Therefore,

$$S_0 = \frac{\partial(T \log Z_0)}{\partial T} = -\frac{V}{2\pi^2} \int_{m_\pi}^{\infty} d\omega \left(\frac{\omega^3}{p} + 3\omega p \right) \log[-n[-\omega]]. \quad (2.11)$$

The connection to the result

$$S_0 = \int \frac{d^3 \mathbf{p}}{(2\pi)^3} [(n+1) \log(n+1) - n \log(n)] \quad (2.12)$$

from statistical physics (Lifschitz [32]) is easily established: Using the definition of the Bose distribution n we rearrange (2.12), evaluate the angle integration and switch to ω as integration variable, leading to

$$\begin{aligned} S_0 &= \frac{1}{2\pi^2} \int_{m_\pi}^{\infty} d\omega \, \omega p \left(-\frac{\log(1 - e^{-\beta\omega})}{1 - e^{-\beta\omega}} + \frac{\log(1 - e^{-\beta\omega}) + \beta\omega}{e^{\beta\omega} - 1} \right) \\ &= \frac{1}{2\pi^2} \int_{m_\pi}^{\infty} d\omega \, \omega p \left(-\log[1 - e^{-\beta\omega}] + \frac{\beta\omega}{e^{\beta\omega} - 1} \right). \end{aligned} \quad (2.13)$$

Performing a partial integration in the second term leads exactly to (2.11).

In a massless theory, $\omega \rightarrow p$ and

$$S_{0 \text{ massless}} = -\frac{V}{2\pi^2} 4 \int_0^{\infty} dp \, p^2 \log[1 - e^{-\beta p}] = \frac{4V}{2\pi^2} \left(\frac{1}{45} \pi^4 T^3 \right) \simeq 0.439 V T^3. \quad (2.14)$$

Relation between Self energy and Number of Particles

The number of particles is given by

$$\langle \hat{N} \rangle = V \int \frac{d^3 \mathbf{p}}{(2\pi)^3} \frac{1}{e^{\beta\omega} - 1} = \frac{V}{2\pi^2} \int_0^\infty dp p^2 n[\omega] \quad (2.15)$$

at zero chemical potential. Exact in the low temperature limit, the relation

$$\log n(-n[-\omega]) = \log(1 - e^{\beta\omega}) \simeq -e^{-\beta\omega} \simeq -\frac{1}{e^{\beta\omega} - 1} = -n[\omega] \quad (2.16)$$

holds and hence

$$\langle \hat{N} \rangle \simeq -\frac{V}{2\pi^2} \int_0^\infty dp p^2 \log(1 - e^{-\beta\omega}).$$

Comparing this with (2.14), we find the low-temperature relation $S \simeq 4\langle \hat{N} \rangle$ for massless particles.

Reminder of the chemical potential

In general, the chemical potential is defined in the fundamental thermodynamic identity

$$dE = T dS - P dV + \mu dN.$$

Then, after two Legendre transformations [27] and with the thermodynamical potential

$$\Omega(T, V, \mu) = E - TS - \mu N$$

in the (T, V, μ) -”basis”, we find

$$N = - \left(\frac{\partial \Omega}{\partial \mu} \right)_{TV}$$

We will need this in the derivation of (4.2). In the (T, P, N) -basis we have

$$\mu = \left(\frac{\partial G}{\partial N} \right)_{TP}. \quad (2.17)$$

The chemical potential is the free Gibbs energy per particle. It ”measures” the energy which a grand canonical ensemble gains if one particle is added.

The convention of [12] defines the chemical potential inclusive the rest mass of the particle. This has to be subtracted if results are compared with the non-relativistic theory as in [27].

2.2.2 Charge Fluctuations of a Free Bose Gas

In order to calculate the numerator of our quantity D , we exploit the relation between the fluctuations of a conserved quantity and the pressure P [33]

$$\langle \delta \hat{Q}^2 \rangle = e^2 V T \frac{\partial^2}{\partial \mu^2} P(\mu, T)|_{\mu=0} = e^2 T^2 \frac{\partial^2}{\partial \mu^2} \log Z_0|_{\mu=0}.$$

Acting with the second derivate on (2.9) gives

$$e^2 T^2 \frac{\partial^2}{\partial \mu^2} \log Z_0 = -\frac{e^2 V}{4} \int \frac{d^3 \mathbf{p}}{(2\pi)^3} \frac{1}{\sinh^2 \left(\frac{1}{2} \beta \omega \right)}$$

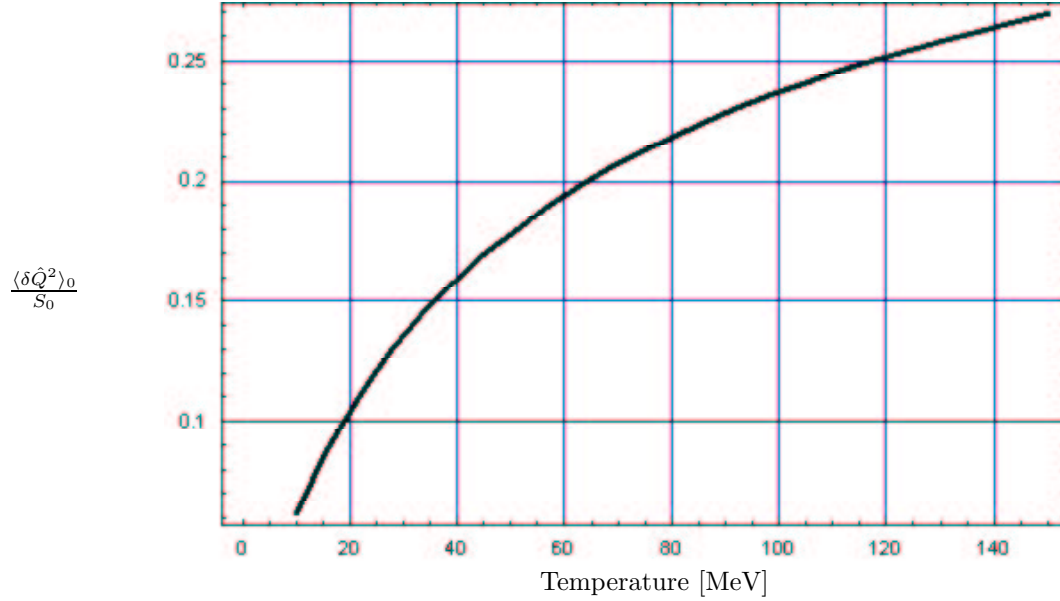


Figure 2.1: Charge Fluctuations of a free Bose gas in a box for one species of particles.

Using (2.11) we obtain therefore

$$\frac{\langle \delta \hat{Q}^2 \rangle_0}{S_0} = -\frac{1}{4} \frac{\int_0^\infty dp p^2 \frac{1}{\sinh^2(\frac{1}{2} \beta \omega)}}{\int_{m_\pi}^\infty d\omega \left(\frac{\omega^3}{p} + 3\omega p \right) \log(1 - e^{-\frac{\omega}{T}})}. \quad (2.18)$$

The charge fluctuations per entropy show an asymptotically constant high temperature behavior. The result is displayed in Fig. 2.1.

The asymptotic value is $\frac{\langle \delta \hat{Q}^2 \rangle_0}{S_0} \simeq 0.38$ for one species of particles. In a Bose gas with π^+ , π^- and π^0 , the charge fluctuations have to be multiplied with a factor of 2 (neutral pions do not contribute to charge fluctuations), whereas the entropy obtains a factor of 3. This leads to a value of $D_{\text{CF}} \simeq 4.05$ as $T \rightarrow \infty$ by using the approximate relation $S \simeq 4\langle \hat{N} \rangle$ from above.

2.3 Finite Temperature Field Theory

One necessary tool in order to calculate in-medium effects on charge fluctuations is finite temperature field theory. It is a field theoretical approach to describe many-body systems and calculate statistical quantities like entropy and fluctuations.

When we introduced the statistical operator, we were able to calculate the grand canonical partition function for a free Boson gas. If the bosons interact with themselves, with an electromagnetic field or with other particles like the ρ -meson, the energy levels are shifted and it is therefore not possible to perform the easy geometrical series as in the case of the free Boson gas (2.8). Finite temperature field theory allows to solve this problem perturbatively. One approach is the canonical formalism, applying Wick's theorem and evaluating Feynman rules. A good introduction to this method is [27], chapter 3–9.

We want to follow another train of thought here, the path integral approach (functional integral representation of the grand canonical partition function). This is totally equivalent to the latter case but much more compact in representation. We follow Kapusta [12], chapters 2–3.

2.3.1 Functional Representation / Generating Functional

In section A.1 the path integral is motivated as the product of integrations over fields $\phi(t_i)$ and conjugate momenta $\pi(t_i)$ at discretized points in time t_i . This linearizes the time evolution operator which carries the Hamiltonian in the exponent. Taking the continuum limit of (A.15) we arrive at the result

$$\begin{aligned} \langle \phi_a | e^{-i\hat{H}t_f} | \phi_a \rangle &= \int [d\pi] \int_{\phi(\mathbf{x}, \mathbf{0})=\phi_a(\mathbf{x})}^{\phi(\mathbf{x}, \mathbf{t}_f)=\phi_a(\mathbf{x})} [d\phi] \\ &\quad \exp \left[i \int_0^{t_f} dt \int d^3\mathbf{x} \left(\pi(\mathbf{x}, \mathbf{t}) \frac{\partial \phi(\mathbf{x}, \mathbf{t})}{\partial \mathbf{t}} - \mathcal{H}(\pi(\mathbf{x}, \mathbf{t}), \phi(\mathbf{x}, \mathbf{t})) \right) \right] \end{aligned} \quad (2.19)$$

The $[\dots]$ -brackets are defined by the limit of the product in (A.9).

We are now ready to express the partition function in terms of (2.19). Recall

$$Z = \text{Tr} e^{-\beta(\hat{H} - \mu_i \hat{N}^i)} = \int d\phi_a \langle \phi_a | e^{-\beta(\hat{H} - \mu_i \hat{N}^i)} | \phi_a \rangle$$

where the sum runs over all states. In order to simplify (2.19) we introduce the imaginary time variable $\tau := it$. The time integration in the exponent is then from 0 to β . The limits in the $[d\phi]$ -integration in (2.19) mean that the fields ϕ are subject to periodic boundary conditions over the interval $[0, \beta]$. Since the whole problem is independent of the absolute value of the time component, this is true for all times and the integration is in fact periodical. We will soon see that this results in a series in frequency space, the summation of the so-called *Matsubara frequencies*. In the imaginary time notation the periodicity means $\phi(\mathbf{x}, \mathbf{0}) = \phi(\mathbf{x}, \beta)$. Altogether, we can write

$$Z = \int [d\phi] \int_{\text{periodic}} [d\phi] \exp \left[\int_0^\beta d\tau \int d^3\mathbf{x} \left(i\pi \frac{\partial \phi}{\partial \tau} - \mathcal{H}(\pi, \phi) + \mu_i \mathcal{N}^i(\pi, \phi) \right) \right] \quad (2.20)$$

with the density of the conserved quantities \mathcal{N}^i . The i from (2.19) has disappeared due to the change of the integration variable and has reappeared in the term with modified time derivative.

Remarks on Imaginary Time

The switching to an imaginary time variable deserves some more explanation. In order to see how the change implies periodicity in the energy component in a natural way, we define the modified Heisenberg picture ([27], §7): With $\hat{K} = \hat{H} - \mu \hat{N}$ the grand canonical Hamiltonian, we switch from the Schrödinger picture to the Heisenberg picture in imaginary time. Analogously to quantum mechanics, the field operators obtain the time dependency of the Hamiltonian. For any Schrödinger operator \hat{O}_S we set

$$\hat{O}_K(\mathbf{x}\tau) = e^{\hat{K}\tau} \hat{O}_S(\mathbf{x}) e^{-\hat{K}\tau}.$$

Note that there is no i in the exponent any more. In a naive way we can already understand why the integration in the path integral has to become periodic: The generating functional requires the integration over field operators. In the discretized version, the fields themselves are the integration variables (leading to gaussian integrals, see below). If the fields are rewritten in the modified Heisenberg picture, the integration of the time variable has to be carried out along the imaginary axis. But the exp-function is $2\pi i$ -periodic.

We want to see this connection in a more precise way. The imaginary time 2-particle Greensfunction is defined by (we will define it again in the next subsection)

$$\mathcal{G}(\mathbf{x}\tau, \mathbf{x}'\tau') := -tr \left[\hat{\rho}_G T_\tau \left(\hat{\Psi}_K(\mathbf{x}\tau) \hat{\Psi}_K^\dagger(\mathbf{x}'\tau') \right) \right]$$

Here, all spin and isospin subscripts have been suppressed. The τ -ordered product is to be understood that the smallest value of τ stands on the right side. We set $\tau = 0$ and $|\tau' - \tau| < \beta$. The periodicity in the first time variable is then shown by

$$\begin{aligned}
\mathcal{G}(\mathbf{x}, 0; \mathbf{x}', \tau') &\stackrel{(1)}{=} -e^{\beta\Omega} \text{tr} \left(e^{-\beta\hat{K}} \hat{\Psi}_K^\dagger(\mathbf{x}', \tau') \hat{\Psi}_K(\mathbf{x}, 0) \right) \\
&\stackrel{(2)}{=} -e^{\beta\Omega} \text{tr} \left(\hat{\Psi}_K(\mathbf{x}, 0) e^{-\beta\hat{K}} \hat{\Psi}_K^\dagger(\mathbf{x}', \tau') \right) \\
&\stackrel{(3)}{=} -e^{\beta\Omega} \text{tr} \left(e^{-\beta\hat{K}} \hat{\Psi}_K(\mathbf{x}, \beta) \hat{\Psi}_K^\dagger(\mathbf{x}', \tau') \right) \\
&\stackrel{(4)}{=} +\mathcal{G}(\mathbf{x}, \beta; \mathbf{x}', \tau').
\end{aligned} \tag{2.21}$$

Here, (1) reflects that the boson field operators commute (no (-1) as there would be in the fermionic case). The second equality (2) follows from the cyclic property of the trace operation. In (3), the operator $\hat{\Psi}_K(\mathbf{x}, 0)$ has been shifted in the time component by multiplying with a negative and positive propagation exponential from the left and right side. The last equality (4) again reflects the commuting property of bosonic field operators in the modified Heisenberg picture.

In full analogy the periodicity in the second time argument can be shown.

2.3.2 Self Interacting Charged Bose gas

As an example how interactions can be incorporated perturbatively within the framework of finite temperature field theory, we consider a self interacting charged Bose gas (no neutral particles) which is described by the Lagrangian

$$\mathcal{L} = \partial_\mu \phi^\star \partial^\mu \phi - m^2 \phi^\star \phi - \underbrace{\lambda(\phi\phi^\star)^2}_{=:\mathcal{L}_{\text{int}}}. \tag{2.22}$$

From this, the conserved current

$$j_\mu = i(\phi^\star \partial_\mu \phi - \phi \partial_\mu \phi^\star) =: i \left(\phi^\star \overleftrightarrow{\partial}_\mu \phi \right)$$

follows which obeys $\partial_\mu j^\mu = 0$. (see A.2 in order to understand how to calculate conserved currents. About Noether's theorem consult [13], §2.2). The complex fields ϕ and ϕ^\star are decomposed in two real fields for convenience by

$$\phi = \frac{1}{\sqrt{2}}(\phi_1 + i\phi_2) \quad \text{and} \quad \phi^\star = \frac{1}{\sqrt{2}}(\phi_1 - i\phi_2).$$

In order to evaluate the Hamiltonian density we calculate the conjugate momenta

$$\pi_1 = \frac{\partial \phi_1}{\partial t} \quad \text{and} \quad \pi_2 = \frac{\partial \phi_2}{\partial t}$$

and therefore have

$$\mathcal{H} = \pi_1 \frac{\partial \phi_1}{\partial t} + \pi_2 \frac{\partial \phi_2}{\partial t} - \mathcal{L} = \frac{1}{2} [\pi_1^2 + \pi_2^2 + (\nabla \phi_1)^2 + (\nabla \phi_2)^2 + m^2(\phi_1^2 + \phi_2^2) + \frac{1}{4} \lambda (\phi_1^2 + \phi_2^2)^2].$$

The conserved charge in terms of the real fields and their conjugates is

$$Q = \int d^3\mathbf{x} j_0(\mathbf{x}) = \int d^3\mathbf{x} (\phi_2 \pi_1 - \phi_1 \pi_2).$$

We can rewrite the partition function (2.20) as

$$Z = \int [d\pi_1][d\pi_2] \int_{\text{periodic}} [d\phi_1][d\phi_2] \exp \left[\int_0^\beta d\tau \int d^3\mathbf{x} \left(i\pi_1 \frac{\partial \phi_1}{\partial \tau} + i\pi_2 \frac{\partial \phi_2}{\partial t} - \mathcal{H}(\pi_1, \pi_2, \phi_1, \phi_2) + \mu (\phi_2 \pi_1 - \phi_1 \pi_2) \right) \right] \quad (2.23)$$

where the chemical potential μ has been inserted which is associated with the conserved charge Q (see (2.20)). We observe that the momenta π_1 and π_2 occur at most quadratic in the exponent, whereas the fields appear in the 4th power. We can therefore perform the momentum integration directly using gaussian integration. For this we recall that the path integral is just the representation of the continuum limit $N \rightarrow \infty$ (see (A.9)). We return to the discretized version of the path integral (the resulting term is not denoted here). Then, the integration variables are the π_i .

The linear and quadratic terms in the exponent of the grand canonical partition function are completed to squares and the integrals (2.32) in the shifted variables are performed. The result is

$$Z = (N')^2 \int_{\text{periodic}} [d\phi_1][d\phi_2] \exp \left[-\frac{1}{2} \left(\frac{\partial \phi_1}{\partial \tau} - i\mu \phi_2 \right)^2 - \frac{1}{2} \left(\frac{\partial \phi_2}{\partial \tau} + i\mu \phi_1 \right)^2 - \frac{1}{2} (\nabla \phi_1)^2 - \frac{1}{2} (\nabla \phi_2)^2 - \frac{1}{2} m^2 (\phi_1^2 + \phi_2^2)^2 - \frac{1}{4} \lambda (\phi_1^2 + \phi_2^2)^2 \right]. \quad (2.24)$$

Naively, one would expect the argument of (2.24) to have the form

$$\mathcal{L}(\phi_1, \phi_2, \partial_\mu \phi_1, \partial_\mu \phi_2; \mu = 0) + \mu j_0(\phi_1, \phi_2, i \frac{\partial \phi_1}{\partial \tau}, i \frac{\partial \phi_2}{\partial \tau}).$$

But (2.24) differs by $\mu^2 \phi \phi^*$ from that. This is due to the momentum dependence of j_0 . In a fermionic theory for example, the conserved current does not contain any momentum dependency (even if it is gauged). There, the argument has the expected form. If there was no momentum dependency in (2.24), the chemical potential would be involved in the momentum integration only as a constant factor. This could never lead to a more than linear dependency of the result on μ .

Expression (2.24) cannot be evaluated in a closed form unless $\lambda = 0$. Then the functional integration becomes gaussian. In the following we set $\mu = 0$. This implies the assumption of an isotopically symmetric system at chemical equilibrium as it is the case in the charged pion gas. Furthermore, we ignore the infrared character of the Boson field. In [12] the infrared character, meaning the desire of bosons to accumulate in the condensate, is taken into account by introducing a mixing angle and a new parameter in the Fourier transform (2.25). This enables a clear distinction between thermal and condensate contributions in the grand canonical partition function. We are not interested in Bose–Einstein condensation. With the Fourier expansions

$$\begin{aligned} \phi_1 &= \sqrt{\frac{\beta}{V}} \sum_n \sum_{\mathbf{p}} e^{i(\mathbf{p}\mathbf{x} + \omega_n \tau)} \tilde{\phi}_{1;n}(\mathbf{p}) \\ \phi_2 &= \sqrt{\frac{\beta}{V}} \sum_n \sum_{\mathbf{p}} e^{i(\mathbf{p}\mathbf{x} + \omega_n \tau)} \tilde{\phi}_{2;n}(\mathbf{p}), \end{aligned} \quad (2.25)$$

and setting $\lambda = 0$ we obtain free result

$$Z_0 = (N') \left[\prod_n \prod_{\mathbf{p}} \int d\tilde{\phi}_{1;n}(\mathbf{p}) d\tilde{\phi}_{2;n}(\mathbf{p}) \right] e^{S_0} \quad (2.26)$$

with the action

$$S_0 = -\frac{1}{2}\beta^2 \sum_n \sum_{\mathbf{p}} (\omega_n^2 + \omega^2) [\tilde{\phi}_{1;-n}(-\mathbf{p})\tilde{\phi}_{1,n}(\mathbf{p}) + \tilde{\phi}_{2;-n}(-\mathbf{p})\tilde{\phi}_{2,n}(\mathbf{p})] \quad (2.27)$$

with $\omega^2 = \mathbf{p}^2 + m_\pi^2$ and $\omega_n = 2\pi i n T$ the Matsubara frequencies (for bosons). See also [12], (2.53) with $\mu = 0$. (Path integrals in euklidian space include the action S respectively S_0 as in (2.26) with a minus sign by convention.) The negative values in the arguments of the field operators in (2.27) arise since the property $\phi_{-n}(-\mathbf{p}) = \phi_n^*(\mathbf{p})$ of the Fourier terms of real fields has been used. The double product in (2.26) arises from the change of variables in the functional integration according to (2.25). Equation (2.27) follows directly from an integration by parts from (2.24).

2.3.3 Perturbation Series expansion

One way to solve for the partition function, e.g. (2.24), is to expand the interaction in powers of the coupling constant, which is equivalent to a perturbative treatment of the problem.

The grand canonical partition function is rewritten as

$$Z = (N')^2 \int [d\phi] e^S.$$

In the last section we decomposed the interacting charged boson field in a free and in an interacting part. We defined the free part of the exponent as S_0 and calculated it in momentum space with the real fields ϕ_1 and ϕ_2 . We already saw, that the 4th power in the interaction term did not allow functional integration. In order to gain further insight in the effects of the interaction we can expand the the part containing S_I of the exponential (where the exponential is $S = S_0 + S_I$). S_I is equal to an integral and product over \mathcal{L}_{int} . We therefore write

$$Z = (N')^2 \int [d\phi] e^{S_0} \sum_{r=0}^{\infty} \frac{1}{r!} S_I^r \quad (2.28)$$

Taking the logarithm on both sides leads to

$$\begin{aligned} \log Z &= \log \left((N')^2 \int [d\phi] e^{S_0} \right) + \log \left(\frac{1 + \sum_{r=1}^{\infty} \frac{1}{r!} \int [d\phi] e^{S_0} S_I^r}{\int [d\phi] e^{S_0}} \right) \\ &=: \log Z_0 + \log Z_I \end{aligned} \quad (2.29)$$

We return to our representation of the Z in terms of the complex fields ϕ and ϕ^* for a moment. In the first order ($r = 1$), (2.29) can be rewritten as

$$\log Z_1 = \frac{-\lambda \int_0^\beta d\tau \int d^3x \int [d\phi][d\phi^*] e^{S_0} (\phi^* \phi)^2}{\int [d\phi][d\phi^*] e^{S_0}} \quad (2.30)$$

with the free action S_0 from (2.27). Expressing this in terms of the real fields ϕ_1 and ϕ_2 and using (2.27), (2.30) can be rewritten as

$$\begin{aligned}
\log Z_1 = & -\lambda \int_0^\beta d\tau \int d^3\mathbf{x} \sum_{n_1, \dots, n_4} \sum_{\mathbf{p}_1, \dots, \mathbf{p}_4} \frac{\beta^2}{V^2} e^{i(\mathbf{p}_1 + \dots + \mathbf{p}_4)\mathbf{x}} e^{i(\omega_{n_1} + \dots + \omega_{n_4})\tau} \\
& \prod_j \prod_{\mathbf{q}} \int d\tilde{\phi}_{1,j}(\mathbf{q}) d\tilde{\phi}_{2,j}(\mathbf{q}) \exp\left[-\frac{1}{2}\beta^2(\omega_j^2 + \mathbf{q}^2 + m_\pi^2)[\tilde{\phi}_{1,-j}(-\mathbf{q})\tilde{\phi}_{1,j}(\mathbf{q}) + \tilde{\phi}_{2,-j}(-\mathbf{q})\tilde{\phi}_{2,j}(\mathbf{q})]\right] \\
& \frac{1}{4}(\tilde{\phi}_{1,n_1}(\mathbf{p}_1) + i\tilde{\phi}_{2,n_1}(\mathbf{p}_1))(\tilde{\phi}_{1,n_2}(\mathbf{p}_2) - i\tilde{\phi}_{2,n_2}(\mathbf{p}_2))(\tilde{\phi}_{1,n_3}(\mathbf{p}_3) + i\tilde{\phi}_{2,n_3}(\mathbf{p}_3))(\tilde{\phi}_{1,n_4}(\mathbf{p}_4) - i\tilde{\phi}_{2,n_4}(\mathbf{p}_4)) \\
& \times 1/\left(\prod_j \prod_{\mathbf{q}} \int d\tilde{\phi}_{1,j}(\mathbf{q}) d\tilde{\phi}_{2,j}(\mathbf{q}) \exp\left[-\frac{1}{2}\beta^2(\omega_j^2 + \mathbf{q}^2 + m_\pi^2)[\tilde{\phi}_{1,-j}(-\mathbf{q})\tilde{\phi}_{1,j}(\mathbf{q}) + \tilde{\phi}_{2,-j}(-\mathbf{q})\tilde{\phi}_{2,j}(\mathbf{q})]\right]\right)
\end{aligned} \tag{2.31}$$

Here, we associated the subscripts 1 and 3 with ϕ -fields and 2 and 4 with ϕ^* -fields. The third line contains S_0 , the fourth the interaction term $-\frac{1}{4}\lambda(\phi_1^2 + \phi_2^2)$ and the last line again contains S_0 from the denominator of (2.30).

We can solve the path integral similarly to the neutral scalar case in [12]. The integration over \mathbf{x} and τ yields a factor $\beta V \delta_{n_1 + \dots + n_4, 0} \delta_{\mathbf{p}_1 + \dots + \mathbf{p}_4, 0}$. We gain further constraints on the delta functions by applying symmetric integration. In (2.31) we have to integrate over a full set of fields. In fact we have a sum over many products in the numerator and a product of integrals in the denominator.

We investigate a term in the sum with fixed n_1, \dots, n_4 in the numerator. If $j \neq n_1, \dots, n_4$ and $\mathbf{q} \neq \mathbf{p}_1, \dots, \mathbf{p}_4$ then the product of the four fields from \mathcal{L}_{eff} is independent of the integration and the integral cancels the corresponding integral in the denominator. But at one point we face the case for example $j = n_1$ and $\mathbf{q} = \mathbf{p}_1$. We have then an integral of the form

$$\int_{-\infty}^{+\infty} dt t e^{-\frac{1}{2}at^2} = 0$$

unless it is for example $n_2 = -n_1$ and $\mathbf{p}_2 = -\mathbf{p}_1$. This is an integral over an even function which gives a non-vanishing contribution. In the same product, j also reaches the values of n_3 and n_4 and \mathbf{q} values of \mathbf{p}_3 and \mathbf{p}_4 . Using the same argument, we have the further constraint that not only $n_2 = -n_1$ and $\mathbf{p}_2 = -\mathbf{p}_1$ but also $n_4 = -n_3$ and $\mathbf{p}_4 = -\mathbf{p}_3$ to get a non-zero value.

From the analytical structure of the four fields in the numerator we can also combine n_1 with n_4 and n_2 with n_3 , momenta respectively. In our case of a charged scalar field the other combinations vanish — for example if $n_1 = -n_3$ we get two integrals that add up to 0. This means that only ϕ and ϕ^* can be combined but never ϕ and ϕ or ϕ^* and ϕ^* . This behavior expresses the conservation of charge (We omit the "˜" of the Fourier components from now on). By exploiting the real character of the fields ϕ_1 and ϕ_2

$$\phi_n^*(q) = \phi_{-n}(-q)$$

and $x^2 + y^2 \triangleq \phi_{1,n}^2(q) + \phi_{2,n}^2(q) = \phi_n \phi_n^*$ we have to solve integrals of the form

$$\frac{\int_{-\infty}^{+\infty} dx dy e^{-\frac{1}{2}a(x^2+y^2)} (x^2 + y^2)}{\int_{-\infty}^{+\infty} dx dy e^{-\frac{1}{2}a(x^2+y^2)}} = \frac{2}{a}. \tag{2.32}$$

This is a factor of 2 different from the neutral scalar case. Since this integral appears squared the additional factor cancels with the $1/4$ from the normalization of the real field transformation. Finally we obtain

$$\log Z_1 = -2\lambda\beta V \left(T \sum_n \int \frac{d^3\mathbf{p}}{(2\pi)^3} \mathcal{D}_0(\omega_n, \mathbf{p}) \right)^2 \quad (2.33)$$

with the propagator in frequency momentum space

$$\mathcal{D}_0(\omega_n, \mathbf{p}) := \frac{1}{\omega_n^2 + \mathbf{p}^2 + m_\pi^2}. \quad (2.34)$$

2.3.4 Diagrammatic Expansion

We calculated the first term in the expansion of the exponential of the interaction. This is correct as long as the interaction is small compared to the free gas case. We found that the correction Z_1 can be represented as the product of λ and two propagators from (2.34). Expression (2.33) can be visualized by the following vertex:

$$\lambda(\phi\phi^*)^2 : \left(\begin{array}{cc} \phi_{n_1}(\mathbf{p}_1) & \phi_{n_3}(\mathbf{p}_3) \\ \phi_{n_2}^*(\mathbf{p}_2) & \phi_{n_4}^*(\mathbf{p}_4) \end{array} \right) \quad (2.35)$$

We draw four legs since the perturbation contains 4 field operators. The directions of the arrows reflect the signs of momenta and frequencies. We obtained two constraints on the selection of momenta and frequency numbers: Either $n_2 = -n_1$ and $\mathbf{p}_2 = -\mathbf{p}_1$ or $n_4 = -n_3$ and $\mathbf{p}_4 = -\mathbf{p}_3$. Thus we connect the ends of (2.35) in pairs. We write the two pairings as

$$\log Z_1 = 2 \left(\text{Diagram of two connected loops} \right) \quad (2.36)$$

With each closed loop, we associate

$$T \sum_n \int \frac{d^3\mathbf{p}}{(2\pi)^3} \mathcal{D}_0(\omega_n, \mathbf{p}) \quad (2.37)$$

and with each vertex a factor of λ and the momentum conservation

$$\beta \delta_{\omega_{\text{in}}, \omega_{\text{out}}} V \delta_{\mathbf{p}_{\text{in}}, \mathbf{p}_{\text{out}}} \longrightarrow \beta \delta_{\omega_{\text{in}}, \omega_{\text{out}}} (2\pi)^3 \delta(\mathbf{p}_{\text{in}} - \mathbf{p}_{\text{out}}).$$

Since the arguments of the frequency (energy)–momentum conserving δ 's are zero, we get an overall factor of βV .

We have just evaluated the Feynman rules for the $\lambda(\phi\phi^*)^2$ –theory at finite temperature.

Thus, pictorially, (2.36) corresponds precisely with (2.33).

Our result is consistent with [12], where the simpler case of neutral bosons is considered.

In the next chapter we will evaluate the Feynman rules for an effective model, both in vacuum and finite temperature field theory. There we will show the full consistency of the definition of propagators

and Feynman rules in both theories. The combination of "–" and i 's always lead to the same coefficients in a given diagram in both theories.

In the next paragraph we want to give a short overview about the introduction of the self energy in our calculations. We can define the the propagator at finite temperature in position space as the correlation

$$\mathcal{D}(\mathbf{x}_1, \tau_1; \mathbf{x}_2, \tau_2) := \langle \phi^*(\mathbf{x}_1, \tau_1) \phi(\mathbf{x}_2, \tau_2) \rangle.$$

It can be understood as the amplitude of a particle to propagate from \mathbf{x}_2 at τ_2 to \mathbf{x}_1 at τ_1 . It corresponds to (2.34) in the lowest order. Though, \mathcal{D} contains all orders in the perturbation and can therefore not be determined analytically. In momentum space we have the relation

$$\mathcal{D}(\omega_n, \mathbf{p}) = \beta^2 \frac{\int [d\phi] e^S \phi_n(\mathbf{p}) \phi_{-n}(-\mathbf{p})}{\int [d\phi] e^S} = 2\mathcal{D}_0^2 \frac{\delta \log Z}{\delta \mathcal{D}_0}. \quad (2.38)$$

We can define a new quantity, the self energy $\Pi(\omega_n, \mathbf{p})$ by

$$\mathcal{D}(\omega_n, \mathbf{p}) = \frac{1}{\omega_n^2 + \mathbf{p}^2 + m^2 + \Pi(\omega_n, \mathbf{p})} = \frac{\mathcal{D}_0}{1 + \mathcal{D}_0 \Pi} \quad (2.39)$$

The self energy can be understood as a momentum dependent additional contribution to the mass m . Then, the self energy is expressed as the variational derivative of the grand canonical partition function:

$$\Pi \sim \left(\text{diagram with a dashed line and a loop} \right) = 2 \frac{\delta}{\delta \mathcal{D}_0} \left(\text{diagram with two loops and a cut} \right) \quad (2.40)$$

(The left side has some coefficients which are omitted here). This gives a good visualization of how the variational derivative works: It cuts the line to which it is applied. The factor of 2 occurs since the line can be cut at each of the two loops. The variational derivative was previously defined in (A.6) and (A.7). It is evaluated at a certain value of the integration range and returns the value of the integral kernel at this value. In (2.40) the role of the kernel is played by the cutted line. The derivative evaluates this line at a certain value, the external momentum of the ϕ -particle. This external momentum can be on-shell. As well, self energy diagrams can be subparts of larger diagrams and be off-shell. Then the external momentum can still carry an integration.

For details concerning this paragraph see [12], p. 37–39.

2.3.5 Evaluating Matsubara Sums

In finite temperature field theory one has to sum Matsubara frequencies. We already faced one example in the first order correction to the grand partition function in (2.33). We evaluate an even simpler example: the single loop on the left side of (2.40). It is the first correction to the self energy, contains only one sum instead of two (as it is the case on the right side of (2.40)) and reads

$$\Pi_1 = 8\lambda T \sum_{n=-\infty}^{\infty} \frac{d^3 \mathbf{p}}{(2\pi)^3} \frac{1}{\omega_n^2 + \omega^2} \quad (2.41)$$

with $\omega_n = 2\pi i n T$. The factor of 8 consists of the 2 from (2.38), the possibility to cut the line at two different positions and the two different possibilities to contract the ϕ 's and ϕ^* 's. We can solve this sum by applying

$$\sum_{n=-\infty}^{\infty} \frac{1}{(n-x)(n-y)} = \frac{\pi(\cot(\pi x) - \cot(\pi y))}{y-x}.$$

Since we will face analytically different terms to be summarized later on, it is convenient to find a general method how to sum the class of terms that will appear again and again in the calculation of self energies.

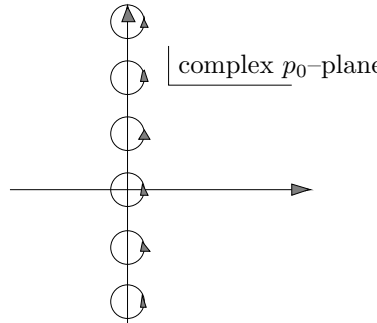
With p_0 the 0-component of the Minkowski four-vector ($p_0 = i\omega_n = 2\pi inT$) we can express the frequency sum

$$T \sum_{n=-\infty}^{+\infty} f(p_0 = i\omega_n = 2\pi inT)$$

as a contour integral

$$\frac{T}{2\pi i} \oint_C dp_0 f(p_0) \beta \frac{1}{2} \coth \left(\frac{1}{2} \beta p_0 \right) \quad (2.42)$$

where the (counter-clockwise) contour C is



(2.43)

The poles of $\frac{1}{2} \beta \coth \left(\frac{1}{2} \beta p_0 \right)$ at $p_0 = 2\pi nT i$ lie in the centers of the circular contours. We know that f has its poles on the real axis at positive finite values (in a one-loop calculation of a massive theory). Therefore f is a smooth function along the imaginary p_0 -axis. The poles of the hyperbolic cotangent are of first order and can therefore be evaluated using the residue theorem (5.15) and (5.16). We have with

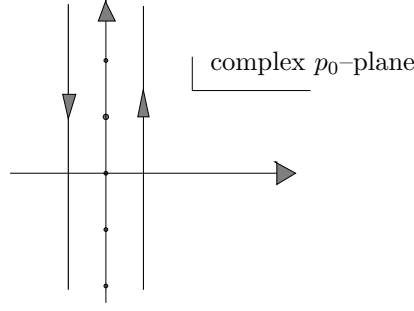
$$e^{\frac{1}{2} \beta p_0} - e^{-\frac{1}{2} \beta p_0} \sim \beta p_0$$

for small $|p_0|$ (and due to the periodicity of exp for all small $|p_0 - 2\pi inT|$)

$$\begin{aligned} \frac{T}{2\pi i} \oint_C dp_0 f(p_0) \beta \frac{1}{2} \coth \left(\frac{1}{2} \beta p_0 \right) &= \frac{T\beta}{2} \text{Res} \left[f(p_0) \frac{e^{\frac{1}{2} \beta p_0} + e^{-\frac{1}{2} \beta p_0}}{e^{\frac{1}{2} \beta p_0} - e^{-\frac{1}{2} \beta p_0}} \right] \\ &= \frac{T\beta}{2} \lim_{p_0 \rightarrow 2\pi inT} \left[f(p_0) \frac{2(p_0 - 2\pi inT)}{\beta(p_0 - 2\pi inT)} \right]. \end{aligned} \quad (2.44)$$

This corresponds exactly to the n th term in the sum (2.42). The contour can be deformed due to Cauchy's

theorem into



(2.45)

In the performance of the integration it is important to take a factor of (-1) (see (5.15)) into account due to the clockwise integration contour (closing the contour in the right half plane).

Rearranging the exponentials of the hyperbolic cotangent leads to

$$\begin{aligned}
 T \sum_{n=-\infty}^{+\infty} f(p_0 = i\omega_n) &= \underbrace{\frac{1}{2\pi i} \int_{-i\infty}^{i\infty} dp_0 \frac{1}{2} [f(p_0) + f(-p_0)]}_{\text{vacuum part}} \\
 &+ \underbrace{\frac{1}{2\pi i} \int_{-i\infty+\epsilon}^{i\infty+\epsilon} dp_0 [f(p_0) + f(-p_0)] \frac{1}{e^{\beta p_0} - 1}}_{\text{matter part}}. \quad (2.46)
 \end{aligned}$$

(Note that f must not have singularities along the imaginary axis.) The frequency sum naturally separates into a piece which is temperature independent (vacuum piece) and a piece containing the Bose–Einstein distribution (matter piece). We switched from the discrete variable in Minkowski ω_n space to the continuous p_0 . By evaluating the vacuum part of (2.41) directly and closing the integration contour in the right half plane for the matter part we finally arrive at

$$\begin{aligned}
 \Pi_1 &= \Pi_1^{\text{vac}} + \Pi_1^{\text{mat}} \\
 \Pi_1^{\text{vac}} &= 8\lambda \int \frac{d^4 p}{(2\pi^4)} \frac{1}{p_4^2 + \mathbf{p}^2 + m^2} \\
 \Pi_1^{\text{mat}} &= 8\lambda \int \frac{d^3 \mathbf{p}}{(2\pi)^3} \frac{1}{\omega} \underbrace{\frac{1}{e^{\beta\omega} - 1}}_{=: n[\omega]}. \quad (2.47)
 \end{aligned}$$

For Π_1^{vac} we defined $p_4 = ip_0$ and $d^4 p = dp_4 d^3 \mathbf{p}$ with p_4 integrated from $-\infty$ to $+\infty$.

The vacuum contribution of Π_1 is ultraviolet divergent. The regularization is performed by adding a mass term δm^2 to the Lagrangian. The cutoff parameter is then chosen in the standard way that the mass in the Lagrangian always stays the physical mass [12]. This can be achieved order by order in $\lambda(\phi^\star \phi)^2$.

For every Matsubara sum we get a matter part containing the Bose factor n . In two loop calculations we obtain terms with no n that are brought to zero, order by order, by expanding the counterterm δm^2 in every order in perturbation theory. Furthermore we get mixing of matter contributions and vacuum

contributions from different loop momenta. Those can all be cancelled by the boson renormalization constant of the vacuum (see [12], p. 74). Only the terms containing two Bose factors, contribute.

In the calculations of this thesis we do not have a simple $\lambda(\phi\phi^*)$ -theory but an effective theory involving derivative couplings and gauge fields. In principle we would have to undergo the whole procedure from the sections 2.3.2, 2.3.3 and 2.3.4 again in order to derive Feynman rules — integrating the momenta in the path integral, Fourier transform, splitting in free and interacting part and extracting vertices and propagators. Furthermore, the introduction of the photon fields leads to serious problems concerning the gauging. We will avoid this by deriving the Feynman rules in the canonical way by applying free waves as external particles. However, we will need the path integral again in order to see how coefficients change if one switches from zero-temperature formalism to the finite temperature formulation.

Analytic Continuation

So far, we have calculated the self energy in the imaginary time formalism. We defined the self energy *without* external propagators but *with* the vertices that attach a n -loop self energy bubble to the external lines. In a theory which does not contain derivative couplings all self energy diagrams which are connected to the two external propagators by only one vertex, do not carry any information about the external momentum. However, if the theory contains derivative couplings or if the external lines couple by two vertices to the self energy bubble, the external momentum q will explicitly appear in the self energy.

Then, the self energy is known for all (real) 3-momenta \mathbf{q} but only for the discrete set of imaginary values $q_0 = 2\pi i n T$ for the time component. In the theory of complex calculus, the theorem of analytic continuation reads that a function that is known on a subset of a compact area can be continued to all values in the area in a unique way. Additionally, the subset must have an accumulation point within the area. (That already implies that the subset has infinitely many points). In our case the area is neither compact nor have the values $q_0 = 2\pi i n T$ an accumulation point. We need to compactify the whole complex plane which can be achieved by including ∞ in the set of complex values. In the compactified complex plane (visualized by the number sphere), the q_0 have an accumulation point at $q_0 = \infty$. Additionally, the resulting self energy diagrams are limited and analytic in $q_0 = \infty$. In that framework, the existence of *exactly one* analytic continuation to all values of q_0 is ensured. See also Baym [26].

Nevertheless, branch cuts occur in self energy diagrams [27],[16]. Fortunately they only occur at real values of q_0 above threshold $|q_0|^2 > 2m^2$ symmetric to the origin. This reflects the physical property that the particles in a self energy diagram can be on-shell if the energy of the external particle is bigger than the rest mass of the particles it decays into in a self energy diagram. In particular, this means that we do not have to care about analyticity of the self energy in the static limit $q_0 = 0, \mathbf{q} \rightarrow 0$ as long as the produced particles are massive. See the later discussion of the properties of the static limit in 5.2.

We introduce the real time Greens function by [27]

$$i\overline{G}(\mathbf{x}t, \mathbf{x}'t') := \text{tr} \left(\hat{\rho}_G T \left[\hat{\Psi}_K(\mathbf{x}t) \hat{\Psi}_K^\dagger(\mathbf{x}'t') \right] \right)$$

with

$$\hat{\Psi}_K(\mathbf{x}t) := e^{i\hat{K}t} \hat{\Psi}(\mathbf{x}) e^{-i\hat{K}t}.$$

In analogy to the vacuum theory we can introduce advanced and retarded real time propagators which have the feature to be analytic in the upper (lower) half plane:

$$\overline{G}(\mathbf{k}, \omega_n) = \frac{1}{1 - e^{-\beta\omega}} \overline{G}^R + \frac{1}{1 - e^{\beta\omega}} \overline{G}^A.$$

(the step functions in the time variable are included in the definition of the retarded and advanced propagator, see [12]) We can additionally introduce the spectral function ρ associated with the real

time propagator. This spectral function determines the imaginary parts of the advanced and retarded propagators by

$$\text{Im } \overline{G}^R(\mathbf{q}, \omega) = -\frac{1}{2} \rho(\mathbf{q}, \omega) \quad \text{and} \quad \text{Im } \overline{G}^A(\mathbf{q}, \omega) = \frac{1}{2} \rho(\mathbf{q}, \omega).$$

We can regard this as the definition of the spectral function. With infinitesimal η we then have

$$\overline{G}^R(\mathbf{q}, \omega) = \Gamma(\mathbf{q}, \omega + i\eta) \quad \text{and} \quad \overline{G}^A(\mathbf{q}, \omega) = \Gamma(\mathbf{q}, \omega - i\eta)$$

with

$$\Gamma(\mathbf{q}, z) = \int_{-\infty}^{\infty} \frac{d\omega'}{2\pi} \frac{\rho(\mathbf{q}, \omega')}{z - \omega'}.$$

The connection between real and imaginary time propagator is then given by

$$\mathcal{G}(\mathbf{q}, \omega_n) = \Gamma(\mathbf{q}, i\omega_n).$$

That means the following: We obtain the real time propagator by continuing the imaginary time propagator towards the real axis. There, the function Γ has a discontinuity which determines the real time propagator.

The knowledge of the real time time propagator can be used in linear response theory in order to calculate correlation functions. The imaginary parts of the poles of the real time propagator determine the lifetime of the particle as in the vacuum theory. In finite temperature field theory, however, it is interesting to note that "lifetime" gets a new meaning [16]. It determines the *relaxation* time until chemical equilibrium is achieved.

Chapter 3

Effective Interaction

3.1 QCD Lagrangian

In the last chapter we prepared the tools of finite temperature field theory. We learned how to calculate the grand canonical partition function in the $\lambda(\phi\phi^*)$ -theory for bosons like the pion. As mentioned in 1.2 we need to calculate a different object though: the self energy of the photon in the hot pion gas. In the pion gas, the photon will show all types of self energy contributions in general. All known processes happen: E.g. the photon can decay in an electron and a positron which then recombine. All these processes are absorbed in the renormalized masses of the particles participating in the process. This is not only true for processes in which a photon is involved: For example we found that the vacuum contribution of the first correction to the self energy Π_1 in $\lambda(\phi\phi^*)^2$ -theory can be absorbed in the renormalization constant. The renormalization procedure can be performed in the way that the mass that appears in the pion propagator stays the physical mass.

The consequence of this is, that we only have to calculate the parts of Feynman diagrams that contain the maximum number of Bose factors $n[\dots]$. This number equals the number of loops involved in the diagram.

In order to calculate the photonic self energy, we have to find an interaction between photons and pions. This will be the gauged Lagrangian (2.22), the Lagrangian of scalar QED (sQED).

First, we want to extend our model, though. The pions themselves can undergo other interactions with particles present in the hot gas. We restrict ourselves to the influence of the ρ -meson and suppress the chiral partner of the ρ -meson, the a_1 -particle since its mass of $m_{a_1} = 1260 \text{ MeV}$ is almost twice as high as the $m_\rho = 770 \text{ MeV}$. The thermic influence of a particle is the stronger the lighter it is due to the Bose suppression (the mass appears in the exponential of the denominator). Even if both the masses of the a_1 - and the ρ -meson were equal, the influence of the a_1 were weaker since the a_1 always decays into three pions (directly or via an intermediate ρ -meson). Even in lowest order in perturbation theory we obtain diagrams with three pion loops. Then, the resulting three Bose factors result in a stronger high temperature suppression than the ρ -meson diagrams. At first order in the effective theory ($e^2 g^2$) the latter include at most two Bose factors.

The first task we want to undertake is the calculation of an interaction between pions and ρ -mesons. (Later on we will remove the ρ -meson from the heat bath in order to obtain a (simpler) effective theory. But this has nothing to do with the physics of the $\rho\pi\pi$ -coupling.)

For that we start with the Lagrangian of QCD and manipulate it until it has a form that is similar to (2.22). We will then gauge it in order to include the photonic interaction. After that we can apply a perturbative expansion in finite temperature field theory.

The train of thought for this section (up to (3.6)) follows the review of Weise [17] and summarizes

the parts needed in the final evaluation of the interaction Lagrangian (3.6).

3.1.1 Quantum Chromodynamics

Quantum Chromodynamics (QCD) is the gauge theory of quarks and gluons. The quarks fall into two distinct groups according to their masses — the light u -, d - and s -quarks and the heavy quarks (c , b and t). Each quark is characterized by its baryon number $B = 1/3$ while their electric charges are $2e/3$ for u , c and t , and $-e/3$ for d , s and b (where $e = 1$ is the magnitude for the electron charge). In addition, each of the quarks has three possible "color" charges by which it couples to the gluons, the set of eight gauge bosons which mediate the strong interactions. The conceptual basis of QCD is then local gauge invariance under changes of color, the gauge group being $SU(3)_c$.

We assume $N_f = 3$ flavors, the heavier particles frozen out. The quark fields are combined in the 3-component spinor

$$\Psi(x) = \begin{pmatrix} u(x) \\ d(x) \\ s(x) \end{pmatrix}$$

and the QCD Lagrangian is

$$\mathcal{L}_{\text{QCD}} = \bar{\Psi}[i\gamma_\mu D^\mu - m]\Psi - \frac{1}{4} G_{\mu\nu}G^{\mu\nu}. \quad (3.1)$$

It involves the $SU(3)_c$ couplings of quarks and gluons through the covariant derivative D_μ (containing the running coupling constant $\alpha_s(\mu)$ which depends on the energy scale μ) and the non-abelian gluon field tensor $G_{\mu\nu}$. The quark masses are grouped together in the mass matrix

$$m = \begin{pmatrix} m_u & 0 & 0 \\ 0 & m_d & 0 \\ 0 & 0 & m_s \end{pmatrix}.$$

Apart from the running coupling constant α_s , the only remaining parameters in the QCD Lagrangian are the quark masses. Since they are small compared to the hadronic scale like the proton mass it is meaningful to examine the limit $m_u = m_d = m_s = 0$. All other quarks are treated infinitely heavy and represent no degrees of freedom any more.

We split the quark field in a lefthanded and a righthanded part by

$$\Psi_{R,L} = \frac{1}{2} (1 \pm \gamma_5)\Psi$$

and introduce a global unitary transformation which is applied separately on these fields,

$$\Psi_R \rightarrow R\Psi_R = \exp\left[i\Theta_R^a \frac{\lambda_a}{2}\right]\Psi_R, \quad \text{and} \quad \Psi_L \rightarrow \Psi_L = \exp\left[i\Theta_L^a \frac{\lambda_a}{2}\right]\Psi_L$$

with $\lambda_1, \dots, \lambda_8$ the standard Gell-Mann $SU(3)$ matrices. This transformation leaves the QCD Lagrangian (3.1) invariant in the massless limit: right- and left-handed components of massless quarks do not communicate. The group of these transformations is called $SU(3)_R \times SU(3)_L$. Invariance under this group is referred to as the *Chiral Symmetry* of QCD. The linear combinations of the sixteen conserved currents that follow from the invariance of the Lagrangian under the (global) chiral transformation are called vector and axial currents which imply the conserved charges Q_a^V and Q_a^A .¹

If we compare the mass of the ρ -meson and its axial partner, the a_1 -meson, we found that the latter is almost twice as heavy as the ρ -meson. If the ground state of QCD were symmetric both conserved

¹The quark masses are small but not equal to zero. Therefore the currents are not conserved any more and show a small but finite divergence. This is called *explicit symmetry breaking*.

charges would annihilate the vacuum $Q_a^V|0\rangle = Q_a^A|0\rangle = 0$ and the spectra of vector and axial mesons should be identical.

From the big mass difference we conclude that still $Q_a^V|0\rangle = 0$ but $Q_a^A|0\rangle \neq 0$. The $SU(3)_R \times SU(3)_L$ symmetry is spontaneously broken down to $SU(3)_V$. This is the so called *Nambu–Goldstone* realization of chiral symmetry.

Goldstone’s theorem reads that for any broken global symmetry of a given Lagrangian there exists a massless mode, called Goldstone boson (see Adler, Dashen [18]).

In our case we have 8 massless Goldstone bosons. Their masses do not vanish though due to the explicit breaking of the chiral symmetry. Without this, they remain massless (as it is assumed from now on). They can be grouped together in an unitary matrix field $U(x) \in SU(3)$ ($U^\dagger U = 1$ and $\det U = 1$). This matrix transforms linearly under the chiral rotations $\Psi_R \rightarrow R\Psi_R$ and $\Psi_L \rightarrow L\Psi_L$ of the right- and lefthanded quarks: $U \rightarrow RUL^\dagger$. Explicitly, U can be denoted

$$U(x) = \exp\left(i \frac{\Phi(x)}{f}\right)$$

with f a constant and

$$\Phi(x) = \sqrt{2} \begin{pmatrix} \frac{\pi_0}{\sqrt{2}} + \frac{\eta}{\sqrt{6}} & \pi^+ & K^+ \\ \pi^- & -\frac{\pi_0}{\sqrt{2}} + \frac{\eta}{\sqrt{6}} & K^0 \\ K^- & \bar{K}^0 & -\frac{2\eta}{\sqrt{6}} \end{pmatrix}. \quad (3.2)$$

From (3.2) we see that the lightest of these particles, the pions, belong to a subgroup, called $SU(2)_R \times SU(2)_L$. For an deeper introduction into chiral symmetry, consult Koch [19]

3.1.2 Chiral Effective Models

Our aim is to replace the QCD Lagrangian (3.1) by an effective model that can be solved in the so called *chiral perturbation theory* (at sufficiently low energies). We want to reexpress the the QCD Lagrangian in terms of the 8 massless Goldstone bosons. The effective model incorporates all relevant symmetries of the underlying fundamental theory. We can then successively ignore the heavy η - and K -mesons.

In the following we restrict to two flavors, excluding the s -quark. This restricts the representation to the subgroup $SU(2)$ of $SU(3)$.

The most important constraints of QCD on the effective Lagrangian $\mathcal{L}_{\text{eff}} = \mathcal{L}_0 + \mathcal{L}_{\text{sb}}$, where the 0 denotes the symmetric part and sb the spontaneous symmetry breaking, are:

- \mathcal{L}_0 is symmetric under the chiral flavor group $SU(2)_R \times SU(2)_L$.
- The chiral symmetry is spontaneously broken. The ground state is symmetric only under $SU(2)_V$.
- The massless particles of the theory are the eight Goldstone bosons associated with spontaneous symmetry breaking.
- The axial currents are conserved.

A Lagrangian \mathcal{L}_{eff} has the same low-energy expansion as QCD itself. The low-energy expansion is performed in an ordering in powers of energy and momenta. The mass terms that break the chiral symmetry explicitly are so small that they can be handled perturbatively together with energy and momentum. The advantage of such a Lagrangian is that the Goldstone bosons do not interact with each other at *small* momenta.

The constraints and Lorentz invariance lead to an effective Lagrangian whose leading term in a generalized Taylor expansion is²

$$\mathcal{L}_{\text{eff}}^{(2)} = \frac{f^2}{4} \text{tr} [\partial^\mu U^\dagger \partial_\mu U]. \quad (3.3)$$

The next step is to include resonances. In the neighborhood of resonances, chiral perturbation theory will fail ("singularities in the S -matrix"). We therefore incorporate the vector ρ -meson and its strong coupling to the two-pion continuum. The ρ -meson is part of the vector meson nonet (ρ, ω, K^*, ϕ) which represent the dipole excitations of the QCD vacuum. There is a connection between the hadron electromagnetic current and the ρ -meson, showing a close analog to the coupling of the spin-1 photon to the conserved electromagnetic current in sQED. We include the ρ as the gauge field of the Goldstone bosons under flavor rotation. For an explicit example of a gauging procedure see A.2.

With

$$\tau_1 = \begin{pmatrix} 0 & 1 \\ 1 & 0 \end{pmatrix} \quad \tau_2 = \begin{pmatrix} 0 & -i \\ i & 0 \end{pmatrix} \quad \tau_3 = \begin{pmatrix} 1 & 0 \\ 0 & -1 \end{pmatrix}$$

the ρ -meson has the form

$$\rho_\mu = \tau_a \rho_\mu^a = \begin{pmatrix} \rho_\mu^3 & \rho_\mu^1 - i\rho_\mu^2 \\ \rho_\mu^1 + i\rho_\mu^2 & -\rho_\mu^3 \end{pmatrix} = \begin{pmatrix} \rho_\mu^0 & \sqrt{2}\rho_\mu^+ \\ \sqrt{2}\rho_\mu^- & -\rho_\mu^0 \end{pmatrix} \quad (3.4)$$

in $SU(2)$ -representation, where $\rho^+ = \frac{1}{\sqrt{2}}(\rho^1 - i\rho^2)$, $\rho^- = \frac{1}{\sqrt{2}}(\rho^1 + i\rho^2)$ and $\rho^0 = \rho^3$. Accordingly, the pion field can be written as

$$\pi = \begin{pmatrix} \pi^0 & \sqrt{2}\pi^+ \\ \sqrt{2}\pi^- & -\pi^0 \end{pmatrix}. \quad (3.5)$$

The Lagrangian of the ρ -field is

$$\mathcal{L}_\rho = -\frac{1}{8} \text{tr}(\rho_{\mu\nu} \rho^{\mu\nu}) + \frac{1}{4} m_\rho^2 \text{tr}(\rho_\mu \rho^\mu)$$

with the field tensor

$$\rho_{\mu\nu} = \partial_\mu \rho_\nu - \partial_\nu \rho_\mu - i \frac{g}{2} [\rho_\mu, \rho_\nu].$$

From the form of the Lagrangian it becomes clear that the ρ -meson can be understood as a massive photon. Showing the strong analog to the photon field $F^{\mu\nu}$, the field ρ -tensor additionally contains a term that involves the so-called universal coupling constant g . Therefore we introduce a covariant derivative by

$$D_\mu \Phi = \partial_\mu \Phi - \frac{ig}{2} [\rho_\mu, \Phi]$$

and replace the derivatives $\partial_\mu \Phi$ in (3.3) ($\Phi = \pi$ in $SU(2)$). To second order in the pion field, the resulting interaction terms are

$$\mathcal{L}_{\text{int}(\pi\rho)} = \frac{ig}{4} \text{tr}(\rho_\mu [\partial^\mu \pi, \pi]) - \frac{g^2}{16} \text{tr}([\rho_\mu, \pi]^2) \quad (3.6)$$

[17] for the $\rho\pi$ - interaction.

Introducing additionally the photon at this stage leads to $\gamma\pi$ - and $\gamma\rho$ -couplings. However, we want to follow another strategy meaning the construction of an effective Lagrangian which is gauged afterwards.

²The chiral constraints only allow a certain class of effective Lagrangian's: (3.3) as well as

$$(\text{tr} [\partial^\mu U^\dagger \partial_\mu U])^2, \quad \text{tr} [(\partial^\mu U^\dagger \partial_\mu U)^2], \quad \dots,$$

see [19].

Determination of the Universal Coupling Constant g

We can determine the strength of the universal coupling constant g from the $\rho \rightarrow \pi\pi$ -decay. We start with the integration over the two-body phase space of the general decay rate formula

$$d\Gamma = \frac{1}{2m_A} \left(\prod_f \frac{d^3 p_f}{(2\pi)^3} \frac{1}{2E_f} \right) |\mathcal{M}(m_A \rightarrow \{p_f\})|^2 (2\pi)^4 \delta^{(4)}(p_A - \sum p_f) \quad (3.7)$$

which describes the decay of the particle A in two ($f = 1, 2$) particles. All physics lies in the transition amplitude \mathcal{M} , the remaining terms are kinematic factors. In [13] a formalism for creation and annihilation of two-particle, non-relativistic bound states is derived. The spin-1 ρ -meson can be understood as such a bound system. Using quantum mechanics in the construction of the bound state, $|\mathcal{M}|$ can be calculated. From this, the formula for the $\rho \rightarrow \pi\pi$ -decay [17] follows:

$$\Gamma(q^2) = \frac{g^2}{48\pi} \frac{q^2}{m_\rho} \left(1 - \frac{4m_\pi^2}{q^2} \right)^{\frac{3}{2}} \Theta(q^2 - 4m_\pi^2). \quad (3.8)$$

The Θ -function contains the threshold for the pion production. Inserting the particle masses and using the experimental result $\Gamma(m_\rho^2) \simeq 150 \text{ MeV}$ leads to $g^2 \simeq 36.2$ and therefore $g \simeq 6$ which is the value used throughout this thesis.

The 3-vertex $\rho\pi\pi$ -coupling

The $\text{SU}(2)$ - representation of π and ρ in the term $\frac{ig}{4} \text{tr}(\rho_\mu [\partial^\mu \phi, \phi])$ can be transformed into an $\text{O}(3)$ representation.

Inserting the matrix- $\text{SU}(2)$ representations of the ρ - and the π -meson (3.4) and (3.5) in the first part of the Lagrangian (3.6) results in

$$\begin{aligned} \frac{4}{ig} \mathcal{L}_{\rho\pi\pi(1)} &= \text{tr}(\rho_\mu [\partial^\mu \pi, \pi]) \\ &= 2 \text{tr} \left[\begin{pmatrix} \rho_\mu^0 & \sqrt{2}\rho_\mu^+ \\ \sqrt{2}\rho_\mu^- & -\rho_\mu^0 \end{pmatrix} \begin{pmatrix} (\partial^\mu \pi^+) \pi^- - (\partial^\mu \pi^-) \pi^+ & \sqrt{2}[(\partial^\mu \pi^0) \pi^+ - (\partial^\mu \pi^+) \pi^0] \\ \sqrt{2}[(\partial^\mu \pi^-) \pi^0 - (\partial^\mu \pi^0) \pi^-] & (\partial^\mu \pi^-) \pi^+ - (\partial^\mu \pi^+) \pi^- \end{pmatrix} \right] \\ &= 4 [\rho_\mu^0 ((\partial^\mu \pi^+) \pi^- - (\partial^\mu \pi^-) \pi^+) + \rho_\mu^- ((\partial^\mu \pi^0) \pi^+ - (\partial^\mu \pi^+) \pi^0) + \rho_\mu^+ ((\partial^\mu \pi^-) \pi^0 - (\partial^\mu \pi^0) \pi^-)] \\ &= 4 \vec{\rho}_\mu (\partial^\mu \vec{\pi} \times \vec{\pi}). \end{aligned} \quad (3.9)$$

Terms that contain the same isospin component twice in a product cancel in the second line. Here,

$$\vec{\pi} = \begin{pmatrix} \pi^+ \\ \pi^- \\ \pi^0 \end{pmatrix}, \quad \vec{\rho}_\mu = \begin{pmatrix} \rho_\mu^+ \\ \rho_\mu^- \\ \rho_\mu^0 \end{pmatrix}.$$

The result is

$$\mathcal{L}_{\rho\pi\pi(1)} = ig \vec{\rho}_\mu \cdot (\partial^\mu \vec{\pi} \times \vec{\pi}). \quad (3.10)$$

The 3-component (ρ_0 -component) of this coupling shows the same structure as the scalar QED-coupling. There is one important thing to note about the cartesian product: Our notation is rather uncommon since it decrees to apply the cartesian product $(\mathbf{a} \times \mathbf{b})_i = \epsilon_{ijk} \mathbf{a}_j \mathbf{b}_k$ to a pair of vectors in *spherical* representation. We will soon gain more clarity about the cartesian and the spherical $\text{O}(3)$ -representation.

The structure of (3.10) reveals which processes happen at a $\rho\pi\pi$ -vertex: The cross product mixes charged and neutral pions. This happens in a way, that the ρ -meson carries the difference charge if a neutral pion is for example transformed into a positive pion. The fact that the interaction Lagrangian is a scalar (in isospin space) implies the conservation of charge. In (3.10) this achieved by the scalar triple product which results in a scalar value.

The 4-vertex $\rho\rho\pi\pi$ -Coupling

The second part of the Lagrangian (3.6) can be transformed as well:

$$\begin{aligned}
-\frac{16}{g^2}\mathcal{L}_{\rho\rho\pi\pi(2)} &= \text{tr} \left([\rho_\mu, \pi]^2 \right) \\
&= 4\text{tr} \left[\begin{pmatrix} \pi^- \rho_\mu^+ - \pi^+ \rho_\mu^- & \sqrt{2}(\pi^+ \rho_\mu^0 - \pi^0 \rho_\mu^+) \\ \sqrt{2}(\pi^0 \rho_\mu^- - \pi^- \rho_\mu^0) & \pi^+ \rho_\mu^- - \pi^- \rho_\mu^+ \end{pmatrix}^2 \right] \\
&= 8 \left[(\pi^+ \rho_\mu^- - \pi^- \rho_\mu^+)^2 + 2(\pi^+ \rho_\mu^0 - \pi^0 \rho_\mu^+)(\pi^0 \rho_\mu^- - \pi^- \rho_\mu^0) \right] \\
&= -8 \begin{pmatrix} \pi^+ \rho_\mu^0 - \pi^0 \rho_\mu^+ \\ \pi^0 \rho_\mu^- - \pi^- \rho_\mu^0 \\ \pi^- \rho_\mu^+ - \pi^+ \rho_\mu^- \end{pmatrix} \begin{pmatrix} \pi^- \rho_\mu^0 - \pi^0 \rho_\mu^- \\ \pi^0 \rho_\mu^+ - \pi^+ \rho_\mu^0 \\ \pi^+ \rho_\mu^- - \pi^- \rho_\mu^+ \end{pmatrix} \\
&= -8(\vec{\rho}_\mu \times \vec{\pi})(\vec{\rho}_\mu \times \vec{\pi})^* = -8|\vec{\rho}_\mu \times \vec{\pi}|^2,
\end{aligned} \tag{3.11}$$

since $\pi^{+\star} = \pi^-$, $\pi^{-\star} = \pi^+$ and $\pi^{0\star} = \pi^0$. The result is therefore

$$\mathcal{L}_{\rho\rho\pi\pi(2)} = \frac{g^2}{2} |\vec{\rho}_\mu \times \vec{\pi}|^2. \tag{3.12}$$

By using the Lagrange identity $(\vec{a} \times \vec{b})(\vec{c} \times \vec{d}) = (\vec{a}\vec{c})(\vec{b}\vec{d}) - (\vec{b}\vec{c})(\vec{a}\vec{d})$, this can be simplified to

$$\mathcal{L}_{\rho\rho\pi\pi(2)} = \frac{g^2}{2} |\vec{\rho}_\mu|^2 |\vec{\pi}|^2 - |\vec{\rho}_\mu \vec{\pi}^*|^2. \tag{3.13}$$

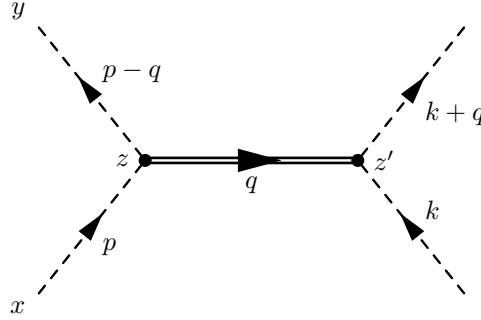
Our later goal will be the calculation of photon self energy diagrams in the order $e^2 g^2$. If we want to include this vertex as well, we have to close the ρ -line of this 4-vertex since no other order of g is available any more. In the high mass limit (see below) this vector meson loop shrinks into a single point leading to no new diagrams but only an effective mass shift of the π mass.

Some short calculations show that all occurring interaction Lagrangian's in this chapter are in fact hermitian. In order to show the hermiticity $\mathcal{L}_{\text{int}} = \mathcal{L}_{\text{int}}^\dagger$, one has to exploit the cyclic property of the trace in the $SU(2)$ -representation. In the $O(3)$ -representation one has to perform the vector product explicitly. Then, the fact that $\pi^+ = \pi^{-\dagger}$ and the neutral pion is its own adjoint, give the hermiticity.

3.2 The High Mass Limit

In the following chapters the simplification is made that the ρ -mass is large compared to its exchanged momentum. Typical diagrams with *finite* ρ mass are shown in Fig. 3.1, and in ⑤ and ⑥ of Fig. 6.10.

The transition of the ρ -mass to infinity corresponds to the exchange of a heavier and heavier particle between two pions – pion scattering with an exchange of a virtual particle (see Fig. 3.1). In space

Figure 3.1: Scattering of pions, exchange of ρ

coordinates this corresponds to a Yukawa potential with less and less range — or equivalently the stronger and stronger exponential suppression of the Coulomb potential by the increasing mass of the force carrying exchange boson. One can visualize the process by shrinking the ρ -line in a diagram into a point.

The scattering of Fig 3.1 is treated by squaring the $\rho\pi\pi$ part (3.10) of the interaction lagrangian (3.6). The complete term consists of three summands each corresponding to the exchange of a positive, neutral and negative charged ρ -meson. We only investigate the part with the neutral ρ meson here. This term enables the scattering of π^+ with π^+ , π^- with π^+ and π^- with π^- .

Let z be the left vertex, z' the right one. The amplitude reads

$$\begin{aligned}
 (ig)^2 \rho_\mu^0(z) \rho_\nu^0(z') & (+ \partial^\mu \pi^+(z) \pi^-(z) \partial^\nu \pi^+(z') \pi^-(z') \\
 & - \partial^\mu \pi^+(z) \pi^-(z) \partial^\nu \pi^-(z') \pi^+(z') \\
 & - \partial^\mu \pi^-(z) \pi^+(z) \partial^\nu \pi^+(z') \pi^-(z') \\
 & + \partial^\mu \pi^-(z) \pi^+(z) \partial^\nu \pi^-(z') \pi^+(z')).
 \end{aligned} \tag{3.14}$$

We assume the case that all pions are negative. Then the incoming pion fields are π^- -operators and the outgoing external pion fields are π^+ -operators. Consider the first line of (3.14).

The incoming negative pion operator π^- couples at the vertex at z and contracts into a propagator with the derivated field operator $\pi^+(z)$ from the interaction Lagrangian. The remaining $\pi^-(z)$ from the interaction Lagrangian can then be contracted with the "out"-field of the scattered pion $\pi^+(y)$ into another propagator. The same procedure applies for the pion at z' .

In the first contraction the derivative has not been taken into account yet. Applying it to the pion propagator, this results in a factor of $(+ip)$ at the vertex z in momentum space:

$$\overline{\pi^-(x) \partial^\mu(z) \pi^+(z)} = \partial^\mu(z) (D_F(x-z)) = \int \frac{d^4 p}{(2\pi)^4} \frac{i}{p^2 - m^2 + i\epsilon} (ip_\mu) e^{-ip_\mu(x-z)^\mu}. \tag{3.15}$$

Similarly, a derivative acting on a π^- results in a factor $(-ip)$:

$$\partial^\mu \overline{\pi^-(z) \pi^+(y)} = \partial^\mu(z) (D_F(z-y)) = \int \frac{d^4 p}{(2\pi)^4} \frac{i}{(p-q)^2 - m^2 + i\epsilon} (-i(p-q)_\mu) e^{-i(p-q)_\mu(z-y)^\mu}. \tag{3.16}$$

In the scattering diagram the two minus signs in (3.14) change therefore into a "+". In total, one has to put the quantity

$$f(p, k, q) = (ig)^2 i^2 (pk + p(k+q) + (p-q)k + (p-q)(k+q)) \tag{3.17}$$

in the numerator of the scattering amplitude in momentum space. The term (3.14) is invariant under the exchange of z and z' as one would expect.

The ρ -propagator simplifies in the high mass limit:

$$\rho^\mu(z)\rho^\nu{}^*(z') = \frac{-i}{k^2 - m_\rho^2} \left(g^{\mu\nu} - \frac{k^\mu k^\nu}{m_\rho^2} \right) \xrightarrow{m_\rho^2 \gg k^2} \frac{ig^{\mu\nu}}{m_\rho^2} \quad (3.18)$$

The second term in the brackets is suppressed now. The denominator $k^2 - m_\rho^2$ becomes a constant because the Boltzmann factors in finite temperature theory suppresses the region where k becomes as big as m_ρ . Remember: In a loop, k can reach all values since one has to integrate over it.

The ρ -propagator becomes the constant metric matrix. This is already an approach to compute Feynman rules and will be worked out later in greater detail.

3.2.1 Effective Interaction Lagrangian of the High Mass Limit

The effective Lagrangian in the order g^2 of the high mass limit can be expressed explicitly: To describe the scattering process in Fig. 3.1, one has to multiply the Lagrangian's.

In spherical representation, the propagator of the ρ -meson is

$$D^{\mu\nu} = \rho^\mu \rho^\nu{}^*.$$

Since the interaction Lagrangian is hermitian,

$$\begin{aligned} i\mathcal{L}_{\text{eff}} &\stackrel{!}{=} \frac{1}{2} (i\mathcal{L}_{\text{int}}) (i\mathcal{L}_{\text{int}})^* \\ &= \frac{ig^2}{2m_\rho^2} |\partial_\mu \vec{\pi} \times \vec{\pi}|_{\text{spherical}}^2. \end{aligned} \quad (3.19)$$

The factors of i are due to the expansion of the perturbation exponential. The factor of $(1/2)$ results from the fact that the scattering process via the ρ -meson in Fig. 3.1 is in second order in perturbation theory. We arrive at

$$\begin{aligned} \mathcal{L}_{\text{eff}} &= \frac{g^2}{2m_\rho^2} |\partial_\mu \vec{\pi} \times \vec{\pi}|_{\text{spherical}}^2 \\ &= \frac{g^2}{2m_\rho^2} ([\partial_\mu \vec{\pi} \partial^\mu \vec{\pi}^*][\vec{\pi} \vec{\pi}^*] - [\vec{\pi} \partial_\mu \vec{\pi}^*][\vec{\pi}^* \partial^\mu \vec{\pi}]) \end{aligned} \quad (3.20)$$

by using the Lagrange identity again. "Effective" from the dynamical point of view means that we do not care about the processes at short length scale (\sim exchange of high momentum). In addition, the ρ -meson is removed from the heat bath since $m_\rho \rightarrow \infty$. One can understand this in the way that the Bose suppression becomes stronger and stronger the heavier the particle is.

All underlying symmetries as the chiral symmetry and the character of the ρ -meson as the gauge field of the pion are obeyed in the form of the coefficients and the derivative couplings.

3.2.2 Gauging the π^4 Effective Lagrangian: Photon Field

Minimal Coupling: The Gauging Procedure and Complex Fields

The effective Lagrangian in spherical $O(3)$ -representation is

$$\mathcal{L} = (\partial_\mu \vec{\pi})(\partial^\mu \vec{\pi}^*) - m_\pi^2 \vec{\pi} \vec{\pi}^* + \frac{g^2}{2m_\rho^2} |\partial^\mu \vec{\pi} \times \vec{\pi}|^2. \quad (3.21)$$

For convenience we rewrite this in the $U(1) \otimes 1$ -representation (or often referred to as simply $U(1)$ -representation).

It is

$$\vec{\pi} = \begin{pmatrix} \pi^+ \\ \pi^- \\ \pi^0 \end{pmatrix} = \begin{pmatrix} \frac{1}{\sqrt{2}}(\phi_1 + i\phi_2) \\ \frac{1}{\sqrt{2}}(\phi_1 - i\phi_2) \\ \phi_3 \end{pmatrix} = \begin{pmatrix} \phi \\ \phi^* \\ \phi_0 \end{pmatrix} \rightarrow \begin{pmatrix} \phi \\ \phi^* \end{pmatrix} \otimes \phi_0.$$

First we express the spherical $O(3)$ -representation by the components of the (real) cartesian representation $\vec{\pi} = (\phi_1, \phi_2, \phi_3)$. (This is called the $O(2) \otimes 1$ -representation). We can write the first and second component as field ϕ and its complex conjugate ϕ^* . The first two components span a subspace under (complex) $U(1)$ rotations — the third component is another subspace so that we can represent the pion field by $U(1) \otimes 1$ in isospin space. The $U(1)$ rotations are rotations around the ϕ_0 -axis. (Isospin rotations in general include rotations around other isospin directions as well.)

With this replacement, (3.19) reads:

$$\begin{aligned} \mathcal{L}_{\text{eff}(\pi^4)} &= \frac{g^2}{2m_\rho^2} \left(-(\phi^* \overleftrightarrow{\partial}_\mu \phi)^2 + 2(\phi_0 \overleftrightarrow{\partial}_\mu \phi)(\phi_0 \overleftrightarrow{\partial}^\mu \phi^*) \right) \\ &= -\frac{g^2}{2m_\rho^2} \left(\frac{j_\mu}{i} \right)^2 + \frac{g^2}{m_\rho^2} \left(\frac{j_{0\phi\mu}}{i} \right) \left(\frac{j_{0\phi^*\mu}^\mu}{i} \right) \\ &= \frac{g^2}{2m_\rho^2} \left(j_\mu^2 - 2j_{0\phi\mu} j_{0\phi^*\mu}^\mu \right) \end{aligned} \quad (3.22)$$

where

$$j_\mu := i \left(\phi^* \overleftrightarrow{\partial}_\mu \phi \right), \quad j_{0\phi\mu} := i \left(\phi_0 \overleftrightarrow{\partial}_\mu \phi \right), \quad j_{0\phi^*\mu}^\mu := i \left(\phi_0 \overleftrightarrow{\partial}_\mu \phi^* \right)$$

have been introduced, with j_μ the conserved current of a global transformation of the Klein–Gordon–Lagrangian. Furthermore, there appear two new terms $j_{0\phi}^\mu$ and $j_{0\phi^*}^\mu$ from the mixing of the ϕ_0 -field with ϕ and ϕ^* . Since they have the formal structure of the conserved current j_μ , we assign the same symbol to them although they are no conserved quantities. Their definition is in analogy with the conserved current j_μ .

For clarity we write down the complete Lagrangian in $U(1) \otimes 1$ -representation:

$$\mathcal{L} = \frac{1}{2} (2(\partial_\mu \phi)(\partial^\mu \phi)^* + (\partial_\mu \phi_0)^2) - \frac{1}{2} m_\pi^2 (2\phi\phi^* + \phi_0^2) + \frac{g^2}{2m_\rho^2} \left(j_\mu^2 - 2j_{0\phi\mu} j_{0\phi^*}^\mu \right). \quad (3.23)$$

The neutral ϕ_0 -field obtains a factor of $(1/2)$ from the fact that the propagator $\mathcal{G} \sim 2\phi^*\phi + \phi_0^2$.

The Lagrangian (3.23) is invariant under a global $U(1)$ rotation. This implies the conservation of a current (Noether's theorem). If the $U(1)$ -transformation is made local, the Lagrangian is not invariant any more, in the sense that the equations of motion are not form invariant. The deviation from invariance can be obtained by computing the variation of the Lagrangian $\delta\mathcal{L}$. In order to cancel the non-vanishing variation, we have to couple the Lagrangian to a new field that compensates the deviation by obeying a certain transformation behavior under *local* $U(1)$ rotations. We will call it the photon field. The details of this calculation are found in A.2.

The result is:

$$\begin{aligned} \mathcal{L}_{(\rho)\phi\gamma} &= -\frac{1}{4} (F^{\mu\nu})^2 - m_\pi^2 \left(\phi\phi^* + \frac{1}{2} \phi_0^2 \right) + (D_\mu \phi)(D^\mu \phi)^* + \frac{1}{2} (\partial_\mu \phi_0)^2, \\ &- \frac{g^2}{2m_\rho^2} \underbrace{(\phi^* (D_\mu \phi) - \phi (D_\mu \phi)^*)^2}_{\text{no } \pi^0} + \frac{g^2}{m_\rho^2} \underbrace{(\phi_0 D_\mu \phi - \phi \partial_\mu \phi_0) (\phi_0 (D^\mu \phi)^* - \phi^* \partial^\mu \phi_0)}_{\pi^0 \text{ mixing}}. \end{aligned} \quad (3.24)$$

Comparing the result with (3.22) and (3.23), we see that the replacement

$$\partial_\mu \begin{pmatrix} \phi \\ \phi^\star \\ \phi_0 \end{pmatrix} \rightarrow (\partial_\mu \mathbf{1}_3 + ieA_\mu T_3) \begin{pmatrix} \phi \\ \phi^\star \\ \phi_0 \end{pmatrix}, \quad T_3 = \begin{pmatrix} 1 & 0 & 0 \\ 0 & -1 & 0 \\ 0 & 0 & 0 \end{pmatrix} \quad (3.25)$$

has taken place. Replacing the derivatives with *covariant* ones is the canonical procedure in order to gauge Lagrangian's.

3.3 Vacuum Feynman Rules from the $(\rho)\pi\gamma$ -Lagrangian — Processes without π^0

The covariant derivatives in the kinetic term of (3.24) lead to the vertices of sQED, the gauged effective ρ -interaction leads to the new structures of a $2\gamma 4\pi$ - and a $1\gamma 4\pi$ -vertex. For the π^0 there are different rules.

The technique in the canonical formalism to derive Feynman rules is the following (see Quigg [21], p. 48f): Draw a diagram that puts all lines of a vertex on-shell, meaning as external lines. Replace all field operators by free wave functions. Evaluate the expression in momentum space and omit all factors that arise from external lines as well as the free waves. The remaining term is the rule for the vertex. Special attention must be paid if external lines can be contracted with the operators of the vertex in different ways. One has to sum over all these possibilities. Only topologically different diagrams can lead to additional factors, which have to be taken into account. The possibility to exchange vertices (if there is more than one in a diagram) needs not to be taken into account in most cases since this symmetry factor is cancelled by the $1/n!$ in the perturbation series expansion. However, we will face one case where this does not hold.

3.3.1 Scalar QED Feynman Rules

Let us first consider the kinetic term $(D_\mu \phi)(D^\mu \phi)^\star$ in the Lagrangian (3.24). This term is the only one in case $g = 0$ and therefore sufficiently describes the gauging of a charged scalar field. The vertex rules derived from it are the ones of sQED. The substitution of the vertex field operators reads:

$$\phi_l \rightarrow S_l e^{-ip_l x}, \quad \phi_m^\star \rightarrow S_m e^{ip_m x}, \quad A_{\mu,n} \rightarrow \epsilon_\mu^\star(k_n) e^{ik_n x} \quad (3.26)$$

with the exponentials representing free waves and S and ϵ the factors that occur in the contraction with external fields. There might be more than one field operator ϕ, A_μ (ϕ^\star, A_μ) referring to an incoming (outgoing) line. Therefore additional subscripts l, m, n are used. Note that operator ϕ (ϕ^\star) can only be connected to an incoming (outgoing) state whereas A_μ can be connected to an incoming photon field as well as to an outgoing. The reason is that the photon does not carry charge (but the isospin 0 and 1). Furthermore a factor of i is included in every vertex. Then, all occurrence of i 's from the expansion of the imaginary perturbation exponential is already included in the vertex rule.

There is a term linear and a term quadratic in A_μ contributing to the scalar QED rules:

$$(D_\mu \phi)(D^\mu \phi)^\star \rightarrow ieA_\mu(\phi^\star \partial^\mu \phi - \phi \partial^\mu \phi^\star) + e^2 A_\mu A^\mu \phi^\star \phi.$$

The arrow indicates that we only have to keep terms containing both $\phi^{(*)}$ and A_μ . The replacement in the first term leads to

$$\begin{aligned} i\mathcal{L}_1 &\rightarrow eA_\mu(k) [\phi^\star(p_2) \partial^\mu \phi(p_1) - \phi(p_1) \partial^\mu \phi^\star(p_2)] \\ &\rightarrow \epsilon_\mu^\star(k) S_1 S_2 e^{i(p_2+k-p_1)x} (-ip_1 - ip_2)^\mu \\ &\rightarrow -ie(p_1 + p_2)^\mu \delta(p_2 + k - p_1). \end{aligned} \quad (3.27)$$

Including momentum conservation, the vertex rule reads

$$\longrightarrow -ie(p_1 + p_2)^\mu \delta(p_2 + k - p_1).$$

The replacement of the second term leads to

$$\begin{aligned} i\mathcal{L}_2 &\rightarrow ie^2 A_\mu A_\nu g^{\mu\nu} \phi^*(p_2) \phi(p_1) \\ &\rightarrow ie^2 g^{\mu\nu} [\epsilon_\mu^*(k_1) \epsilon_\nu^*(k_2) + \epsilon_m u^*(k_2) \epsilon_\nu^*(k_1)] e^{i(p_2 + k_1 + k_2 - p_1)x} \\ &\rightarrow 2ie^2 g^{\mu\nu}. \end{aligned} \quad (3.28)$$

The fact has been taken into account that the photon can be incoming as well as outgoing, meaning it can couple to A_μ respectively to A_ν . The vertex rule (including momentum conservation) therefore reads

$$\longrightarrow 2ie^2 g^{\mu\nu} \delta(p_2 + k_1 + k_2 - p_1).$$

In both diagrams the left side means the incoming side whereas the right the outgoing one. Note that this assignment is arbitrary since the rule is symmetric under exchange of incoming and outgoing side. No distinction between these cases needs to be done any more. In that sense the first rule of the 3-vertex simply says that momenta of the pion propagators have to be added at a vertex.

There is no electromagnetic coupling to neutral pions: In (3.24) the derivative at the neutral pion is not replaced by a covariant one.

3.3.2 Vertices Including the Effective Interaction

The covariant derivative in the $\rho\pi$ -interaction term leads to vertices with quadratic, linear and no derivative coupling. In order to investigate this further the square is expanded (note: The Lagrangian is multiplied with i which changes the coefficient $-\frac{g^2}{2m_\rho^2} \rightarrow -\frac{ig^2}{2m_\rho^2}$). Then the interaction Lagrangian $i\mathcal{L}_{\text{int}} = i j_D^2$ from (3.24) (without terms including π^0), where the D denotes the gauging, is multiplied with $-\frac{2m_\rho^2}{ig^2}$ in order to simplify the righthand side. This is cancelled in the last step):

$$\begin{aligned} -\frac{2m_\rho^2}{ig^2} i \mathcal{L}_{\text{int}(\rho)\pi\gamma} &= (\phi^*(D_\mu \phi) - \phi(D^\mu \phi^*))^2 \\ &\rightarrow \phi^* \phi^* (\partial_\mu \phi) (\partial^\mu \phi) - 2\phi^* \phi (\partial_\mu \phi^*) (\partial^\mu \phi) + \phi \phi (\partial_\mu \phi^*) (\partial^\mu \phi^*) \quad (\text{term 1-3}) \\ &+ 4ie A_\mu \phi^* \phi (\phi^* (\partial^\mu \phi) - \phi (\partial^\mu \phi^*)) \quad (\text{term 4}) \\ &- 4e^2 A_\mu A_\nu g^{\mu\nu} \phi^* \phi^* \phi \phi \quad (\text{term 5}). \end{aligned} \quad (3.29)$$

(term 1 – 3): 4π Coupling in the Order g^2

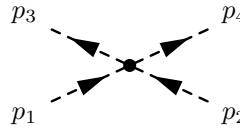
Let p_1 and p_2 be incoming momenta and p_3 and p_4 outgoing ones. Substituting the field operators in the terms 1 – 3 results in

$$\begin{aligned}
& \left[4S_3S_4(S_1S_2(-ip_1)(-ip_2)) - 2S_1S_3(S_2S_4(-ip_2)(ip_4)) - 2S_2S_3(S_1S_4(-ip_1)(ip_4)) \right. \\
& \quad \left. - 2S_1S_4(S_2S_3(-ip_2)(ip_3)) - 2S_2S_4(S_1S_3(-ip_1)(ip_3)) + 4S_1S_2(S_3S_4(ip_3)(ip_4)) \right] \\
& \quad e^{i(p_3+p_4-p_1-p_2)x} \\
& \rightarrow -2 \left[2p_1p_2 + p_2p_4 + p_1p_4 + p_2p_3 + p_1p_3 + 2p_3p_4 \right] \\
& = -2 \left[(p_1 + p_3)(p_2 + p_4) + (p_1 + p_4)(p_2 + p_3) \right] \\
& \rightarrow \frac{ig^2}{m_\rho^2} \left[(p_1 + p_3)(p_2 + p_4) + (p_1 + p_4)(p_2 + p_3) \right]. \tag{3.30}
\end{aligned}$$

In the first line, the first and last term term get an additional factor of four since there are 2·2 combinations to connect incoming (outgoing) lines to the field operators with (without) the derivatives. The same holds for the last term. In the middle term the different possibilities to contract operators lead to analytically different terms which are written down separately. For the assignment of momenta see the picture below.

The Feynman rule reads, that in the numerator there occurs a quadratic coupling which adds the possibilities of multiplying paired terms of incoming / outgoing momenta. The result is symmetric. This behavior originates from having a t -channel process as in Fig. 3.1 or an u -channel process. In both cases the resulting vertex is a 4-point interaction.

The Feynman rule for the 4-vertex is



$$\begin{aligned}
& \xrightarrow{\quad} \frac{ig^2}{m_\rho^2} \left[(p_1 + p_3)_\mu (p_2 + p_4)^\mu + (p_1 + p_4)_\mu (p_2 + p_3)^\mu \right] \\
& \quad \times \delta(p_3 + p_4 - p_1 - p_2)
\end{aligned}$$

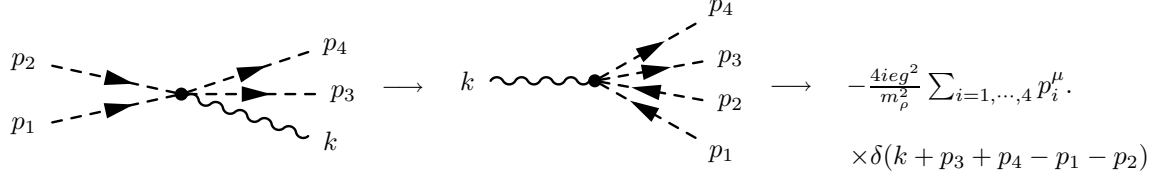
(term 4): $\gamma 4\pi$ Coupling in the Order eg^2

Substituting the field operators in term 4 results in

$$\begin{aligned}
& 4ie\epsilon_\mu^*(k) e^{i(k+p_3+p_4-p_1-p_2)x} [S_3S_1(S_4S_2(-i(p_2+p_4))) + S_3S_2(S_4S_1(-i(p_1+p_4))) \\
& + S_4S_1(S_3S_2(-i(p_2+p_3))) + S_4S_2(S_3S_1(-i(p_1+p_3)))] \\
& \rightarrow 4ie2(-ip_1 - ip_2 - ip_3 - ip_4) \\
& \rightarrow -\frac{4ieg^2}{m_\rho^2} \sum_{i=1,\dots,4} p_i^\mu. \tag{3.31}
\end{aligned}$$

For assignment of momenta see the picture below. There are two possibilities for every incoming line: it can be connected to the bracket in term 4 or couple to the appropriate operator outside the brackets, resulting in no derivative. Altogether there are four combinations in each of which two momenta are

added. The resulting rule is a sum over all pion momenta taking part in the process. The result is again symmetric in incoming / outgoing states:



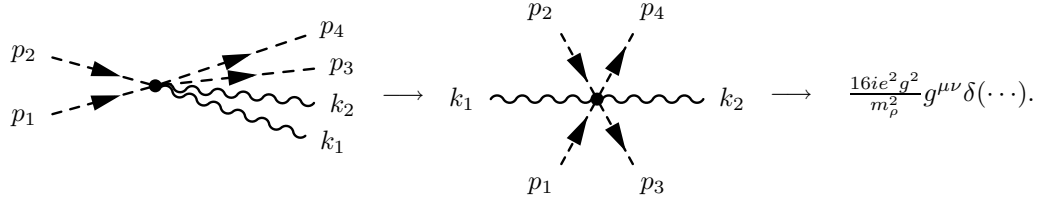
$$\begin{aligned} & \xrightarrow{\quad} k \text{ wavy line} \xrightarrow{\quad} -\frac{4ie^2g^2}{m_\rho^2} \sum_{i=1,\dots,4} p_i^\mu \cdot \\ & \times \delta(k + p_3 + p_4 - p_1 - p_2) \end{aligned}$$

(term 5): $2\gamma 4\pi$ Direct Coupling in the Order e^2g^2

Substituting the field operators in term 5 results in

$$\begin{aligned} & -4e^2g^{\mu\nu} (\epsilon_\mu^*(k_1)\epsilon_\nu^*(k_2) + \epsilon_\mu^*(k_2)\epsilon_\nu^*(k_1)) (2S_1S_2)(2S_3S_4)e^{i(k_1+k_2+p_3+p_4-p_1-p_2)x} \\ & \rightarrow \frac{16ie^2g^2}{m_\rho^2}g^{\mu\nu}. \end{aligned} \quad (3.32)$$

For the assignment of the momenta see the picture below. Note, that the sum for different coupling possibilities is written down explicitly only for the photon. Since there are two incoming and two outgoing scalar field operators now, for every incoming / outgoing line one finds two possibilities each to couple to a field operator. This has been taken into account by the two factors of 2 (which each represent a sum of two terms as written down for the photon.) The Feynman rule for this vertex is therefore



$$\xrightarrow{\quad} k_1 \text{ wavy line} \xrightarrow{\quad} \frac{16ie^2g^2}{m_\rho^2}g^{\mu\nu}\delta(\dots).$$

3.3.3 Vacuum Feynman Rules including π^0

The Feynman rules for the 4π -, the $\gamma 4\pi$ - and the $2\gamma 4\pi$ -vertex involving neutral pions are very similar to those we just calculated. In appendix A.3 the rules are evaluated. The only difference results from the somewhat different analytical form of the interaction Lagrangian and the fact that the ϕ_0 can be contracted with an incoming as well as with an outgoing field.

3.4 Feynman Rules at Finite Temperature

In the derivation of the vacuum rules almost all work is done for the derivation of the finite temperature rules. There is only one major difference: In the vacuum case we always obtained an i in each order in perturbation theory. This was due to the occurrence of an i in the exponential of the perturbation series. The crucial fact at the finite temperature level is that this i is missing.

In the derivation of the rules in the $\lambda(\phi\phi)^* = \mathcal{L}_{\text{int}}$ -theory we find that the overall factor $-\lambda$ of the interaction Lagrangian goes through the whole calculation without change, leading to the vertex rule $-\lambda$

(plus momentum conservation of the 3-momenta and the Matsubara frequencies and an overall factor of βV). The only thing to be done is to find out how the derivative couplings work in the finite temperature case. The only \mathbf{x} - and τ -dependency in (2.31) is found in the Fourier exponentials

$$e^{i(\mathbf{p}_1+\dots+\mathbf{p}_4)\cdot\mathbf{x}} e^{i(\omega_{n_1}+\dots+\omega_{n_4})\tau}.$$

From this we see that we obtain the very same factors ($\pm ip^\mu$) if a derivative is applied to a $\phi^{(*)}$ in the interaction Lagrangian. We conclude the following replacement scheme in order to obtain Feynman rules at finite temperature from the vacuum case:

$$\text{rule}_{\text{temperature}} = \left(\frac{1}{i} \right) \text{rule}_{\text{vacuum}}$$

and for the propagator

$$\frac{i}{p^2 - m_\pi^2} \rightarrow -\frac{1}{p_0^2 - \omega^2}$$

with $\omega^2 = \mathbf{p}^2 + m_\pi^2$ the relativistic dispersion relation and $p_0 = 2\pi i n T$ the Matsubara frequencies from.

3.4.1 Summary of Feynman Rules in the order $e^2 g^2$

The Feynman rules to calculate Self Energy diagrams in the order $e^2 g^2$ are:

- Choose a combination from the set of vertices so that their orders in the coupling constant add up to $e^2 g^2$. The vacuum vertex rules are:

Vertex	π^\pm -Interaction	π^0 - π^\pm -Interaction
$\gamma 2\pi$	$-ie(p_1 + p_2)^\mu$	0
$2\gamma 2\pi$	$2ie^2 g^{\mu\nu}$	0
4π	$\frac{ig^2}{m_\rho^2} [(p_1 + p_3)_\mu (p_2 + p_4)^\mu + (p_1 + p_4)_\mu (p_2 + p_3)^\mu]$	$\frac{ig^2}{m_\rho^2} [2p_2 p_4 - p_1 p_4 + p_3 p_4 + p_1 p_2 - p_2 p_3 + 2p_1 p_3]$
$\gamma 4\pi$	$-\frac{4ie g^2}{m_\rho^2} \sum_{i=1,\dots,4} p_i^\mu$	$-\frac{2ie g^2}{m_\rho^2} (p_\phi + p_{\phi^*})^\mu$
$2\gamma 4\pi$	$\frac{16ie^2 g^2}{m_\rho^2} g^{\mu\nu}$	$\frac{4ie^2 g^2}{m_\rho^2} g^{\mu\nu}$

Appropriate momenta conserving δ -functions have to be attached.

- Connect the vertices by boson propagators in all possible ways. The momenta at all vertices must be preserved. The self energy is defined without the external photon lines. Therefore do not assign photon propagators to them as well as no external polarization vectors.
- Integrate / sum over all undetermined loops. (There is no additional factor of (-1) in the bosonic case as in fermionic loops). Assign a phase space factor of $1/(2\pi)^3$ with every integration. There is a factor of (-1) in each summation of Matsubara frequencies due to the counter clockwise integration contour.
- Determine symmetry factors.
- Introduce the neutral pion and apply the Feynman rules and the other steps above. Note that only certain combinations are allowed. A sQED vertex will always exclude neutral pions.

Chapter 4

Charge Fluctuations and Self Energy

In order to derive the connection between charge fluctuations and self energy diagrams the ensemble average of the derivative of the charge density needs to be calculated. The fermionic case is shown in [12], p. 93. In this thesis, however, the more complicated case of bosons including the effective ρ -interaction is treated.

The charge density has to be derivated with respect to the chemical potential in order to equal the charge fluctuations. The charge density will then be expressed in terms of single 1- and 2-particle propagators. A mathematical trick (4.15) enables us to extend the single propagator up to fully dressed self energy diagrams. This expansion requires to establish Ward identities in the effective theory for 1- and 2-particle functions.

As a first step we calculate the conserved current of the gauged Lagrangian (3.24) without π^0 -mixing.

4.0.2 Conserved Current of the Gauged $(\rho)\pi\pi$ -Lagrangian

The rest of the chapter excludes neutral pions. No Ward identities for neutral pions are shown. Therefore the subsequent results are only valid for processes without involving π^0 . However, we will later calculate the influence of the neutral pion on the self energy assuming that Ward identities are obeyed (see 5.3.1). Furthermore, the rest of this chapter will be written in the vacuum definitions for vertices and propagators. The generalization to finite temperature is easy as we saw in the last chapter.

So far, the conserved current for the charged scalar field $j^\mu = i(\phi^* \partial^\mu \phi - \phi \partial^\mu \phi^*)$ and for the charged scalar field including the effective $\rho\pi$ -Lagrangian J^μ has been calculated. The gauged Lagrangian (3.24) leads to the conserved current

$$\begin{aligned} J_D^\mu &= i \left(\phi^* \frac{\partial \mathcal{L}}{\partial(\partial_\mu \phi^*)} - \phi \frac{\partial \mathcal{L}}{\partial(\partial_\mu \phi)} \right) \\ &= j_D^\mu \left(1 + b \phi \phi^* + \frac{b}{2} \phi_0^2 \right), \quad b = \frac{2g^2}{m_\rho^2} \end{aligned} \quad (4.1)$$

where j_D^μ means the conserved current of the charged scalar field in which the minimal coupling prescription $\partial^\mu \rightarrow D^\mu$ of (3.25) has been applied. We easily find that the conserved current of the gauged charged scalar field without effective interaction is not j^μ any more but

$$j_D^\mu = i \left(\phi^* D^\mu \phi - \phi (D^\mu \phi)^* \right).$$

Note further, that the electromagnetic field explicitly appears in the conserved current as soon as the Lagrangian is gauged because the bosonic current contains derivatives. In contrast, the conserved currents of the gauged and the ungauged Lagrangian of the (fermionic) QED are the same.

In A.6 it is shown that J_D^μ (without π^0 -mixing) is indeed the conserved current of the gauged Lagrangian. Furthermore the new equations of motion can be found there.

4.1 Charge Fluctuations and Charge Density

We establish the connection between charge fluctuations and the derivative of the charge density. Later on, we connect the latter to self energy diagrams.

The fluctuations of a conserved quantity in a grand canonical ensemble can be expressed as the derivative of the ensemble average of this quantity with respect to its chemical potential (Lifschitz [14], p. 382) In our notation, we repeat the steps of the proof for $\mu = \mu_Q$.

It is (at constant temperature)

$$\frac{\partial}{\partial \mu} \langle \hat{Q} \rangle = \frac{\partial}{\partial \mu} \frac{\text{Tr}(\hat{\rho}_G \hat{Q})}{\text{Tr} \hat{\rho}_G}$$

with the grand canonical statistical operator. Therefore,

$$\begin{aligned} \frac{\partial}{\partial \mu} \langle \hat{Q} \rangle &= \frac{\partial}{\partial \mu} \left[e^{\beta \Omega} \text{Tr}(e^{\beta(-\hat{H} + \mu \hat{Q})} \hat{Q}) \right] \\ &= \beta \frac{\partial \Omega}{\partial \mu} e^{\beta \Omega} \text{Tr}(e^{\beta(-\hat{H} + \mu \hat{Q})} \hat{Q}) + e^{\beta \Omega} \text{Tr}(e^{\beta(-\hat{H} + \mu \hat{Q})} \hat{Q}^2) \\ &= -\beta \langle \hat{Q} \rangle \langle \hat{Q} \rangle + \beta \langle \hat{Q}^2 \rangle = \frac{1}{T} \langle \delta \hat{Q}^2 \rangle \end{aligned} \quad (4.2)$$

because from the representation of the grand canonical potential $\Omega = E - TS - \mu Q$ follows $\partial \Omega / (\partial \mu) = -Q (= -\langle \hat{Q} \rangle)$.

The charge fluctuations are proportional to the volume. (Later on, the *ratio* present in the quantity D will remove the explicit volume dependency). In a unit volume and at spatial homogeneity it is $Q = \int d^3x j_0 = V j_0$, the 0-component of the conserved current. This is the quantity we want to deal with. The actual charge fluctuation is $e^2 \langle \delta \hat{Q}^2 \rangle$ so that the quantity under investigation is

$$e^2 T \frac{\partial}{\partial \mu} \langle j_0 \rangle.$$

4.2 Charge Density and Self Energy Diagrams

4.2.1 Charge Density as Imaginary Time Propagator

The charge density can be expressed as the trace over field operators:

$$\begin{aligned} \langle j_0 \rangle &= \langle J_D^0 \rangle = \frac{\text{Tr}[\hat{\rho}_G \mathcal{J}^0]}{\text{Tr} \hat{\rho}_G} = e^{\beta \Omega} \sum_{\alpha} \text{Tr}[e^{-\beta \hat{K}} \mathcal{J}^0] \\ &= e^{\beta \Omega} \sum_{\alpha} \text{Tr} \left[e^{-\beta \hat{K}} i(1 + b \phi \phi^*) \left[\phi^* (\partial^0 + i e A^0) \phi - \phi (\partial^{0'} - i e A^0) \phi^* \right] \right] \\ &= e^{\beta \Omega} \sum_{\alpha} \text{Tr} \left[e^{-\beta \hat{K}} \left(\overbrace{(\partial + \partial')^0} - 2eA^0 \right) (\phi^* \phi) \left(1 + b(\phi^* \phi) \right) \right] \\ &= e^{\beta \Omega} \left(\overbrace{(\partial + \partial')^0} - 2eA^0 \right) \sum_{\alpha} \text{Tr} \left[e^{-\beta \hat{K}} \left(\overbrace{\phi^* \phi} \right) \right] \end{aligned}$$

$$+ e^{\beta\Omega} \left(\overbrace{(\partial + \partial')^0} - 2eA^0 \right) \sum_{\alpha} \text{Tr} \left[e^{-\beta\hat{K}} \left(b(\phi^{\star}\phi)(\phi^{\star}\phi) \right) \right]. \quad (4.3)$$

In order to exploit the cyclic property of the trace, the statistical operator has been replaced by its definition. The term $(\partial + \partial')^0$ leads to factors of $(p + p')^0$ in momentum representation¹.

Furthermore, the summation over isospin subscripts has been written down explicitly (α) as a reminder that we deal with an average. This summation reduces to two terms concerning the $\phi^{(*)-}$ and the ϕ^0 -term since we are working in the U(1) representation. In the case of fermions one has to do a summation over spin indices.

The lines still indicate in which respect the derivative has to be executed. A separation according to the number of field operators has been carried out. This will lead to 1- respectively 2-particle functions.

To gain the connection to diagrammatic techniques we investigate the imaginary time propagator. The 1-particle or 2-point Greens function in finite field theory in the modified Heisenberg picture is defined as

$$\mathcal{G}_{\alpha\beta}(\mathbf{x}\tau; \mathbf{x}'\tau') := -\text{Tr}[\hat{\rho}_G T_{\tau}(\phi_{K\alpha}(\mathbf{x}\tau)\phi_{K\beta}^{\dagger}(\mathbf{x}'\tau'))],$$

where T_{τ} denotes the τ -ordered product. Note the minus sign in the case of bosons, which is chosen in the convention of [27], see (23.1)–(23.8).

For the terms linear in $\phi^{\star}\phi$ in (4.3) we have, using the cyclic property of the trace,

$$\begin{aligned} e^{\beta\Omega} \sum_{\alpha} \text{Tr} \left[e^{-\beta\hat{K}} \phi^{\star}(\mathbf{x})\phi(\mathbf{x}) \right] &= e^{\beta\Omega} \sum_{\alpha} \text{Tr} \left[e^{-\beta\hat{K}} e^{\hat{K}\tau} \phi^{\star}(\mathbf{x})\phi(\mathbf{x}) e^{-\hat{K}\tau} \right] \\ &\stackrel{(*)}{=} \sum_{\alpha} \text{Tr} \left[\hat{\rho}_G \phi_K^{\star}(\mathbf{x}\tau)\phi_K(\mathbf{x}, \tau + \epsilon) \right] \\ &= - \sum_{\alpha} \mathcal{G}_{\alpha\alpha}(\mathbf{x}\tau, \mathbf{x}\tau + \epsilon) = -\text{Tr} \mathcal{G}(\mathbf{x}\tau, \mathbf{x}\tau^+) \\ &\rightarrow -\mathcal{G}(\mathbf{x}\tau, \mathbf{x}\tau^+), \end{aligned} \quad (4.4)$$

where ϵ and τ^+ are reminders to take the limit approaching from higher values of τ (due to the τ -ordered product in the definition of \mathcal{G}). Note that all unitary transformations between the field operators cancel and only the uttermost survive. The " \rightarrow " in the last line indicates that \mathcal{G} is propagator for ϕ^{\star} , ϕ and ϕ^0 -field.

For convenience and in order to arrive at the momentum space representation of the self energy, a Fourier transformation in the spatial components and a Fourier series in the imaginary time component is performed, where $\tau = 0$ and $\tau^+ > 0$:

$$\mathcal{G}_{\alpha\beta}(\mathbf{x}\mathbf{x}'\tau^+) = \frac{1}{\beta} \int \frac{d^3\mathbf{p}}{(2\pi)^3} e^{i\mathbf{p}(\mathbf{x}-\mathbf{x}')} \sum_{n=-\infty}^{\infty} e^{-i\omega_n\tau} \mathcal{G}_{\alpha\beta}(\mathbf{p}, \omega_n)$$

¹We are now working with a fully dressed propagator at finite temperature. The transition $(\partial + \partial')^0 \rightarrow (p + p')^0$ is common for us from the derivation of the Feynman rules. Here, we have to use the explicit form of the fully dressed bosonic propagator at finite temperature

$$\mathcal{G}(\mathbf{x}\mathbf{x}; \tau\tau^+) \rightarrow \mathcal{G}(\mathbf{x}; \tau) = \frac{1}{\beta} \int \frac{d^3\mathbf{p}}{(2\pi)^3} \sum_{p_0=-\infty}^{\infty} e^{-ip_0\tau} e^{-\mathbf{x}\mathbf{p}} \frac{1}{-p_0^2 + \mathbf{p}^2 + m_{\pi}^2 + \Pi(p_0, \mathbf{p})}$$

and apply the derivative with respect to the 0-component of the space coordinate inside the integral. Here Π denotes the self energy of the bosonic propagator \mathcal{G} (not to be mixed up with the photon self energy $\Pi^{\mu\nu}$). As one can see, the factor $(p + p')^0$ does not depend on the bosonic form of the self energy in momentum space but originates from the Fourier exponential.

$$\rightarrow T \sum_{n=-\infty}^{\infty} \int \frac{d^3 \mathbf{p}}{(2\pi)^3} \mathcal{G}_{\alpha\beta}(\mathbf{p}, \omega_n) \quad \text{for } \mathbf{x}' \rightarrow \mathbf{x}, \tau^+ \rightarrow 0. \quad (4.5)$$

(see [27], (25.12), p. 244 for the time component and (25.23), p. 246 for the complete transformation). Here, $\omega_n = 2\pi i n T$. Note that this form of a Fourier transformation with dependency only on $\tau^+ - \tau$ and $\mathbf{x} - \mathbf{x}'$ is only true in a static and spatially homogeneous system which is assumed here. Note further that only in this scenario the exponential $e^{i\mathbf{p}(\mathbf{x}-\mathbf{x}')}$ disappears in the limit $\mathbf{x} \rightarrow \mathbf{x}'$.

Besides the linear terms we have the quadratic occurrence in $\phi^* \phi$ resulting from the effective Lagrangian term that describes the exchange of the ρ -meson in the high mass limit. Therefore we define a 2-particle or 4-point Greens function by

$$\mathcal{G}_{\alpha\beta; \gamma\delta}^{(2)}(\mathbf{x}_1 \tau_1, \mathbf{x}_2 \tau_2; \mathbf{x}'_1 \tau'_1, \mathbf{x}'_2 \tau'_2) := Tr \left[\hat{\rho}_G T_\tau [\phi_{K\alpha}(\mathbf{x}_1 \tau_1) \phi_{K\beta}(\mathbf{x}_2 \tau_2) \phi_{K\delta}^*(\mathbf{x}'_2 \tau'_2) \phi_{K\gamma}^*(\mathbf{x}'_1 \tau'_1)] \right]$$

(see [27], p. 253).

Then, the above calculation reads

$$\begin{aligned} e^{\beta\Omega} \sum_{\alpha} Tr \left[e^{\beta\hat{K}} (\phi^*(\mathbf{x}) \phi(\mathbf{x}))^2 \right] &= e^{\beta\Omega} \sum_{\alpha} Tr \left[e^{-\beta\hat{K}} e^{\hat{K}\tau} \phi^*(\mathbf{x}) \phi(\mathbf{x}) \phi^*(\mathbf{x}) \phi(\mathbf{x}) \right] \\ &\rightarrow \mathcal{G}(\mathbf{x}\tau \mathbf{x}\tau; \mathbf{x}\tau^+ \mathbf{x}\tau^+) \\ &= T^2 \sum_{n=-\infty}^{\infty} \int \frac{d^3 \mathbf{p}}{(2\pi)^3} \mathcal{G}^{(2)}(\mathbf{p}, \omega_n), \end{aligned} \quad (4.6)$$

with the Fourier frequencies ω_i and a new factor of $(1/\beta^2)$ from the periodicity interval of the energy component. The static and spatial invariance of the system has been used in the last line.

The derivative of the charge density can now be rewritten as

$$\begin{aligned} e^2 T \left(\frac{\partial \langle \hat{j}_0 \rangle}{\partial \mu} \right)_T &= -e^2 T \frac{\partial}{\partial \mu} T \sum_{\omega_n=-\infty}^{\infty} \int \frac{d^3 \mathbf{p}}{(2\pi)^3} \lim_{\epsilon \rightarrow 0} \left([(p + (p + \epsilon))^0 - 2eA^0] \mathcal{G}(\mathbf{p}, \omega_n) \right) \\ &\quad + be^2 T \frac{\partial}{\partial \mu} T^2 \sum_{\omega_n=-\infty}^{\infty} \int \frac{d^3 \mathbf{p}}{(2\pi)^3} \lim_{\epsilon \rightarrow 0} \left([(p + (p + \epsilon))^0 - 2eA^0] \mathcal{G}^{(2)}(\mathbf{p}, \omega_n) \right). \end{aligned} \quad (4.7)$$

Note that the ϵ simply indicates that the derivative originates from two different propagators. In the calculation ϵ might be set to 0 without any hesitation. We have just kept it to show the formal analogy to the sQED 3-vertex. There, the bosons have different momenta p and p' . In the calculation of the self energy diagrams we are working in the static limit, however, where $p = p'$ and the photon momentum equals zero.

In the next sections self energy diagrams will be constructed. In the derivation we have to relate fully dressed propagators to dressed vertices. This means that we have to find Ward identities in different formulations. We do this in three steps: First we derive the WI for sQED and face the new feature of insertion possibilities in contrast to the fermionic case. Then we get insight in WI's for 2-particle functions by treating $\lambda(\phi^* \phi)^2$. Considering the complication of derivative couplings we finally obtain knowledge about Ward identities for 1- and 2-particle functions in the effective theory.

4.3 Ward–Takahashi Identity (WTI) for sQED

$$\sum_{\text{insertion points}} k_\mu \left(\text{Diagram with } n \text{ fermion lines } p_1 \dots p_n \text{ and } n \text{ boson lines } q_1 \dots q_n \text{ meeting at a vertex, with a wavy line labeled } k_\mu \text{ attached to the vertex} \right) = e \sum_i \left(\text{Diagram with } n \text{ fermion lines } p_1 \dots p_n \text{ and } n \text{ boson lines } q_1 \dots (q_i - k) \dots q_n \text{ meeting at a vertex} - \text{Diagram with } n \text{ fermion lines } p_1 \dots (p_i + k) \dots p_n \text{ and } n \text{ boson lines } q_1 \dots q_n \text{ meeting at a vertex} \right) \quad (4.8)$$

The Ward-Takahashi identity for fermions applies in the bosonic case as well. Though, we have to take insertions into account which transform 3-vertices of the original diagrams into 4-vertex direct couplings (definitions, proof and concise explanations are found in A.4.1).

We formulate the WTI in a diagrammatic way (for alternative formulations see A.4.1). The statement depicted in (4.8) means: The sum over all insertion points of a given amplitude \mathcal{M}^μ equals the sum over the difference on the right side (the diagram contributing to an amplitude \mathcal{M}_0), where the incoming / outgoing momenta of all n throughgoing propagators are successively increased / decreased by a momentum of k . In analytic terms this reads:

$$k_\mu \mathcal{M}^\mu(k; p_1, \dots, p_n; q_1, \dots, q_n) = e \sum_i \left[\mathcal{M}_0(p_1, \dots, p_n; q_1, \dots, (q_i - k), \dots, q_n) - \mathcal{M}_0(p_1, \dots, (p_i + k), \dots, p_n; q_1, \dots, q_n) \right]. \quad (4.9)$$

See [13] for the fermionic case.

From an analysis of the propagators and vertices involved in the proof of this WTI and the subsequent ones, it turns out that all identities hold in finite temperature field theory as well. Although the analytical form of propagators and vertices change at finite temperature, as we found out in the last chapter, the identities are untouched by that.

4.3.1 The Ward Identity

The next task is to formulate the Ward identity (WI) using (A.27) respectively (4.9). We restrict ourselves to the special case $n = 1$ in (4.8) and no external photon of \mathcal{M}_0 (no photon lines on the righthand side of the interaction region in (4.8) — often referred to as Ward identity. Then the summation over the insertion points of the three-point function reads diagrammatically (The sum in (4.9) has shrunk to one term):

$$k_\mu \cdot \left(\text{Diagram: a circle vertex with a wavy line labeled } k_\mu \text{ attached to its left, and two fermion lines labeled } p \text{ and } p+k \text{ attached to its top and bottom} \right) = e \left(\text{Diagram: a circle vertex with two fermion lines labeled } p \text{ attached to its top and bottom} - \text{Diagram: a circle vertex with two fermion lines labeled } p+k \text{ attached to its top and bottom} \right). \quad (4.10)$$

Here, the shaded circles with the additional photon mean the complicated interaction region of the diagram. It represents the sum over all insertion points over all diagrams contributing to \mathcal{M}_0 and should be denoted more precisely as

$$(4.11)$$

We call the the first $2ie^2\Gamma_{(4)}^\mu$ and second vertex $-ie\Gamma_{(3)}^\mu$ in order to keep consistency with common fermionic case notation in [13], p. 185. Note that in the diagram of $2ie^2\Gamma_{(4)}^\mu$ the photon line from the vertex to the region of interaction belongs to \mathcal{M}_0 and is not part of the inserted photon line.

The terms on the right side of (4.10) are fully dressed propagators. Multiplying the equation (4.10) from both sides with $S^{-1}(p+k)$ and $S^{-1}(p)$ cuts the external legs of the vertex. Then the Ward identity reads

$$ik_\mu (-\Gamma_{(3)}^\mu(p, p+k) + 2e\Gamma_{(4)}^\mu(p, p+k)) = S^{-1}(p+k) - S^{-1}(p). \quad (4.12)$$

This can be rewritten in the infrared limit as

$$\frac{\partial S^{-1}(p)}{\partial p^\nu} = i(-\Gamma_{(3)}^\nu(p, p+\epsilon) + 2e\Gamma_{(4)}^\nu(p, p+\epsilon)). \quad (4.13)$$

This step deserves an explanation: We can't naively divide both sides of 4.12 by k^μ , since the k_μ on the left side includes a summation over μ . Instead of that we first have to perform the limit $k_\zeta \rightarrow 0$ for for all (three) $\zeta \in [1, \dots, 4]$, $\zeta \neq \nu$. Then the summation vanishes but the ν -component. Now we can divide by k_ν and take the limit $k_\nu \rightarrow 0$ of the difference equation on the right side in order to obtain the derivative. (see also A.8 where this is displayed explicitly). We explicitly introduce the sum over all vertex diagrams *including* external legs in order to simplify further calculations by

$$V^\mu(p, p+k) = -ie\Gamma_{(3)}^\mu(p, p+k) + 2ie^2\Gamma_{(4)}^\mu(p, p+k)$$

and can express the Ward identity as

$$e \frac{\partial S^{-1}}{\partial p_\mu} = V^\mu. \quad (4.14)$$

4.3.2 The Ward Identity in Different Orders

The Ward identity is a non-perturbative statement but can be expanded in different orders in perturbation theory. In the order e we have a single 3-vertex insertion on the lefthand side of (4.10) and bare propagators on the righthand side. The resulting vertex is $\Gamma_{(3)}^{\mu(1)} = (2p+k)^\mu$ as expected. The first non-trivial contribution is shown in Fig. 4.1. The resulting vertex is of order e^3 .

The possible insertion points in Fig. 4.1 are indicated by arrows. The insertions outside the loop lead to the righthand side of (A.27) and an additional error, which is partially cancelled by the insertion point inside the loop. The remaining error is then cancelled by the two $3 \rightarrow 4$ -insertions at the 3-vertices.

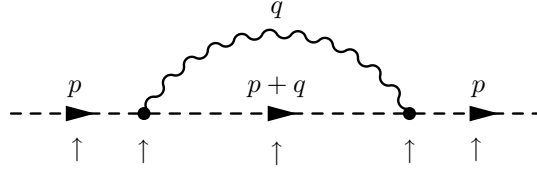


Figure 4.1: Insertion points of the photon $\gamma(k)$ in the first non-trivial order correction for the boson vertex

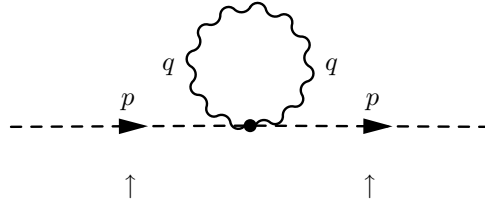


Figure 4.2: Insertion points of the photon $\gamma(k)$ in the first non-trivial order correction for the boson vertex – the direct coupling

Note that there is another contribution to the propagator in the same order in form of a 4-vertex attached photon, displayed in Fig. 4.2 — but this contribution is trivial and analytically almost as simple as the bare case.

4.4 Applying the WTI in the Construction of Self Energy Diagrams in sQED

We are now switching off the effective interaction in (4.7). The second term in (4.7) vanishes and there is no $\mathcal{G}^{(2)}$ any more. We are dealing with sQED. First, we are deriving a trick in order to apply the WI:

$$\frac{\partial}{\partial p_0} \mathcal{G} = \frac{\partial}{\partial p_0} (\mathcal{G} \mathcal{G}^{-1} \mathcal{G}) = 2 \frac{\partial}{\partial p_0} \mathcal{G} + \mathcal{G} \left(\frac{\partial}{\partial p_0} \mathcal{G}^{-1} \right) \mathcal{G}$$

which leads to

$$\frac{\partial}{\partial p_0} \mathcal{G} = -\mathcal{G} \left(\frac{\partial}{\partial p_0} \mathcal{G}^{-1} \right) \mathcal{G}. \quad (4.15)$$

The derivative with respect to μ has to be applied to the propagator as well as to the coefficient in (4.7).

For the latter case we recall the definition of μ . The chemical potential is the free enthalpy per particle (see(2.17)). In case of an external field this depends on the coupling of this particle to the external field and its strength. Here, the charge is the preserved quantity and the electric potential is the 0-component of the electromagnetic 4-vector. Therefore

$$\mu = eA^0.$$

A second question arises: How does the derivative with respect to the chemical potential act on the single particle operator

$$\mathcal{G}(\mathbf{p}, \omega_n) = Tr(\hat{\rho}_G \phi_K^* \phi_K)?$$

From this representation we gather that the dependency of μ lies in the statistical operator and the transformation of the field operators in the modified Heisenberg picture. Both depend on $\hat{K} = \hat{H} - \mu \hat{Q}$

(the statistical operator depends on \hat{K} directly as well as through the grand canonical ensemble Ω). We can therefore rewrite the dependency of the propagator more precisely as $\mathcal{G}(p) \rightarrow \mathcal{G}(p_0 - \mu, \mathbf{p})$ so that

$$\frac{\partial}{\partial \mu} \mathcal{G}(p_0 - \mu) = -\frac{\partial}{\partial p_0} \mathcal{G}(p_0 - \mu).$$

From this, (4.7) in the sQED case can be modified:

$$\begin{aligned} e^2 T \left(\frac{\partial \langle \hat{j}_0 \rangle}{\partial \mu} \right)_T &= -e^2 T \frac{\partial}{\partial \mu} T \sum_{\omega_n=-\infty}^{\infty} \int \frac{d^3 \mathbf{p}}{(2\pi)^3} 2(p^0 - \mu) \mathcal{G}(\mathbf{p}, \omega_n) \\ &\stackrel{\mu \rightarrow 0}{=} -e^2 T \sum_{\omega_n=-\infty}^{\infty} T \int \frac{d^3 \mathbf{p}}{(2\pi)^3} \left(-2\mathcal{G}(\mathbf{p}, \omega_n) - 2p^0 \frac{\partial}{\partial p_0} \mathcal{G}(\mathbf{p}, \omega_n) \right) \\ &= T^2 \sum_{\omega_n=-\infty}^{\infty} \int \frac{d^3 \mathbf{p}}{(2\pi)^3} (2e^2 \mathcal{G}(\mathbf{p}, \omega_n) - e(2p^0) \mathcal{G}(\mathbf{p}, \omega_n) \Gamma(\mathbf{p}, \omega_n) \mathcal{G}(\mathbf{p}, \omega_n)) \\ &= T (\Pi_D^{00} \text{mat}(k_0 = 0, \mathbf{k} \rightarrow \mathbf{0}) + \Pi_B^{00} \text{mat}(k_0 = 0, \mathbf{k} \rightarrow \mathbf{0})) \quad (\text{matter}) \\ &= \frac{T^2}{i} \sum_{\omega_n=-\infty}^{\infty} \int \frac{d^3 \mathbf{p}}{(2\pi)^3} (2ie^2 \mathcal{G}(\mathbf{p}, \omega_n) - ie(2p^0) \mathcal{G}(\mathbf{p}, \omega_n) \Gamma(\mathbf{p}, \omega_n) \mathcal{G}(\mathbf{p}, \omega_n)) \\ &= \frac{T}{i} (i\Pi_D^{00}(k_0 = 0, \mathbf{k} \rightarrow \mathbf{0}) + i\Pi_B^{00}(k_0 = 0, \mathbf{k} \rightarrow \mathbf{0})) \quad (\text{vacuum}). \end{aligned} \quad (4.16)$$

The subscripts D denotes the case of the direct coupling as depicted in Fig. 4.4 and B the self energy bubble of Fig. 4.3.

The expression indicated with *(matter)* is clearly real, since we found in the determination of the Feynman rules, that all propagators and vertices at finite temperature are indeed real. The last two lines refer to the conventional definition of the self energy $i\Pi$ in the vacuum case.

The vacuum self energy is real as well because the energy integration over the 0-component in the vacuum always produces an additional factor of i . This can be seen in the explicit evaluation of Fig. 4.10 and Fig. 4.9 in dimensional regularization with the final result (A.46).

The calculation (4.16) provides the important result

$$\boxed{\langle \delta \hat{Q}^2 \rangle = TV \left(\Pi_D^{00} \text{mat}(k_0 = 0, \mathbf{k} \rightarrow \mathbf{0}) + \Pi_B^{00} \text{mat}(k_0 = 0, \mathbf{k} \rightarrow \mathbf{0}) \right)}. \quad (4.17)$$

Why do we not need a fully dressed vertex in Fig. 4.4 respectively a fully dressed left vertex in Fig. 4.3 in order to represent the full self energy? All vertex dressings in both cases are already contained in the propagator in case of Fig 4.4 respectively in the right vertex in case of Fig. 4.3. All additional photons and pions from the dressing can be shifted towards the bare vertices.

4.5 The WTI for $\lambda(\phi^\star \phi)^2$ -theory

In analogy to the sQED case we need to find a similar WTI for the theory that includes the effective ρ -coupling. Then we can use (4.15) again in order to construct self energy diagrams. A new WTI for the 4-point function $\mathcal{G}^{(2)}$ in (4.7) must be derived.

However, we have to deal with complicated quadratic derivative couplings (see Feynman rules). Not only this — there is also the possibility of photon insertions at the 4-vertex leading to the $1, 2\gamma 4\pi$ -vertices. In order to gain quick insight into the structure of 4-point functions we consider the (simpler) $\lambda(\phi^\star \phi)^2$ -theory of a charged scalar field.

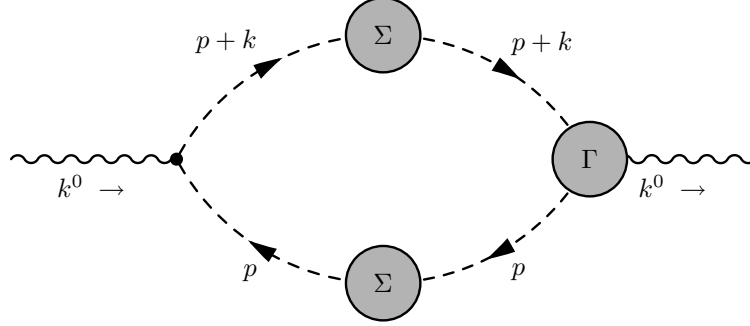


Figure 4.3: Photon Self Energy $\Pi^{00}(k)$ – The bubble part with fully dressed propagators and the full vertex

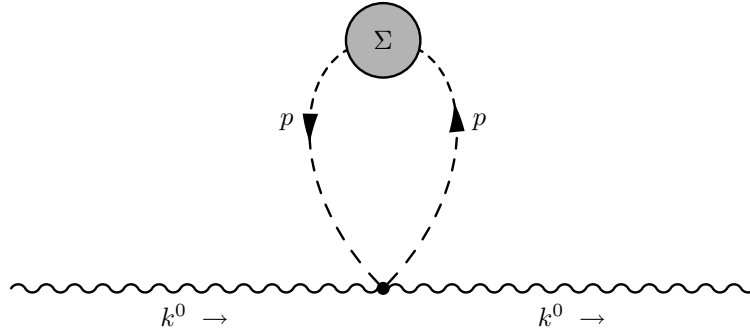


Figure 4.4: Photon Self Energy $\Pi^{00}(k)$ – The tadpole part with the fully dressed propagator and the bare direct vertex.

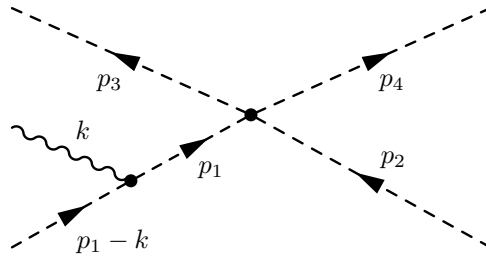


Figure 4.5: The simplest non-trivial 4-point function containing the direct $\lambda(\phi\phi^*)^2$ 4-vertex coupling. Also shown is one of the four possible photon insertions.

Gauging the $\lambda(\phi\phi^*)^2$ -theory would mean that we have to follow the steps of the gauging of the effective theory in (A.2) in principle. The interaction term

$$-i\lambda(\phi\phi^*)^2$$

is invariant under local and global $U(1)$ -transformations. Since from the interaction term no variation of the Lagrangian can arise we are left with the sQED case, and there we know how to proceed: Replace the partial derivatives by covariant ones. We end up with the well known 3- and 4-vertices (3.25). No insertion of a photon is possible at the $(\phi\phi^*)^2$ -vertex.

The question arises what the derivative of the 2-particle function $\mathcal{G}^{(2)}(p)$ means. We consider the simplest non-trivial 4-point function in Fig. 4.5.

We exploit

$$\frac{\partial}{\partial p_1^\mu} \mathcal{G}^{(2)}(p_1, \dots, p_4) + \dots + \frac{\partial}{\partial p_4^\mu} \mathcal{G}^{(2)}(p_1, \dots, p_4) \longrightarrow \frac{\partial}{\partial p^\mu} \mathcal{G}^{(2)}(p) \quad \text{for } p_1, \dots, p_4 \rightarrow p. \quad (4.18)$$

The identity enables us to restrict to photon insertions with only one of the four legs of the 4-point functions affected and then sum over all legs. To achieve a Ward identity we have to construct differences of propagators as in the sQED case. We investigate a 3-vertex insertion at the boson line with momentum p_1 and k flowing out of the diagram (not passing the 4-vertex). The result of the insertion is a new diagram as shown in Fig. 4.5 with the amplitude

$$(\epsilon_\mu^{(*)}(k))(-ie(2p_1 - k)^\mu) \frac{i}{(p_1 - k)^2 - m_\pi^2} \frac{i}{p_1^2 - m_\pi^2} f(p_2, p_3, p_4),$$

where f consists of the propagators of the three unchanged momenta and $\delta(p_1 + p_2 - p_3 - p_4)$ from the λ -vertex. ϵ_μ contains the polarization information of the external photon. If we replace it with the photon momentum k_μ and apply the trick to complete the square and cancel terms as in (A.24), we end up with

$$e(G_{(2)}(p_1 - k, p_2, p_3, p_4) - G_{(2)}(p_1, p_2, p_3, p_4)) \rightarrow -e \frac{\partial G_{(2)}(p_1, p_2, p_3, p_4)}{\partial p_1}.$$

Here, $G_{(2)}$ denotes the bare 4-point function. For the three other insertion points we get expressions like this, but the partial derivative in respect to the other momenta. After adding all diagrams and exploiting the rule (4.18) we obtain

$$\Gamma_{\text{full}}^\mu(p) = -e \frac{\partial G_{(2)}}{\partial p_\mu}, \quad (4.19)$$

where Γ_{full} denotes the sum of all insertion diagrams *with* external legs. The cutting of the external legs as in (4.12) does not work any more for the obvious reason that we are dealing with a 4-point function now. But with the new definitions in mind, the new formulation of the WI is equivalent to the canonical one. In fact we do not need more than (4.19) for further calculations.

4.5.1 Proof to all Orders

Fig. 4.6 shows the next-to-leading order contribution in λ^2 . There are six possible insertion points. Only the two insertions within the loop are shown. If there are two momenta assignments in Fig. 4.6, the one in brackets refers to the photon insertion from below. The absence of derivative couplings enables us to replace the four external pion lines by photons. Then we have a new diagram that equals the old one up to a factor of $(2ie^2)/(-i\lambda)^2$ since the seagull vertex in sQED does not contain derivatives either. The two insertions within the loop represent all insertions in a sQED loop and we have already shown that loop insertions vanish.

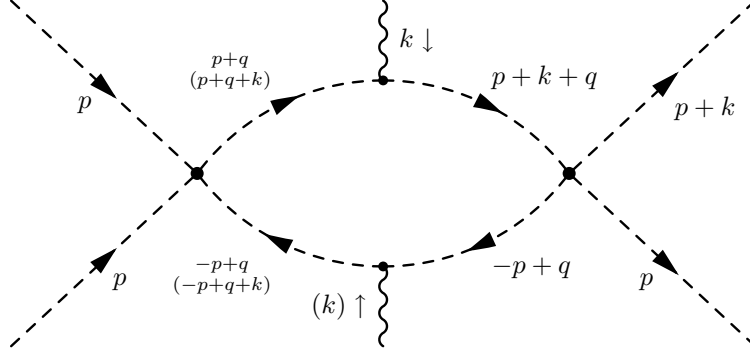


Figure 4.6: The 4-point function containing two direct $\lambda(\phi\phi^*)^2$ 4-vertex couplings. Also shown are two intermediate insertions. For further description see text.

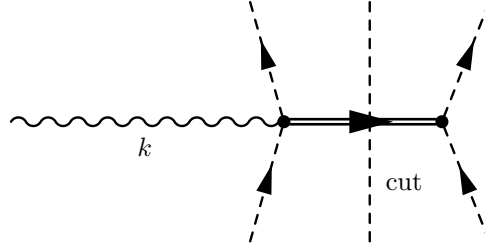


Figure 4.7: The diagram that leads to the $\gamma 4\pi$ -vertex in the effective coupling theory.

In the treatment of the next-to-leading order contribution in Fig. 4.6 we understood why only intermediate insertions are relevant. We can now proceed to higher orders, add another bubble to Fig. 4.6 and repeat the considerations. Then, equation (4.19) holds in all orders and is a true Ward identity.

4.6 The WTI for 4-point Functions in Effective ρ -Coupling

In the case of the effective ρ -coupling, the bare 4-point function as in Fig. 4.5 contains derivative couplings quadratically. We try to apply a similar trick as in the proof in the last paragraph, i.e mapping the problem into the known sQED case. For this we recall the calculation of the Feynman rules of the 4π -vertex as well as for the $\gamma 4\pi$ -vertex.

The first contains the factors $(p_1 + p_3)(p_2 + p_4) + (p_1 + p_4)(p_2 + p_3)$. The first part corresponds to the t -channel as in Fig 3.1, the second to the u -channel, where the upper pion legs in 3.1 switch their external points. See also [13], p. 156-158 for Mandelstam variables and instructive diagrams.

An inspection of the operators present in the $\gamma 4\pi$ -vertex shows that this vertex originates from diagram 4.7. The ρ -meson in this diagram shrinks to a point resulting in the effective vertex.

Cutting the ρ -lines in Fig. 3.1 and 4.7 then corresponds to cutting the effective vertices in the way that every piece contains two pion lines. The remaining halves behave like throughgoing pion lines with a ρ coupled in a $\pi\pi\rho$ - respectively $\gamma\pi\pi\rho$ -vertex. Since those vertices are very similar to photon 3- respectively 4-vertices in sQED, we can apply the WTI identity for sQED and are done. This idea is

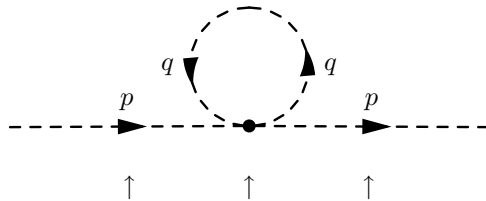


Figure 4.8: Insertion points of the photon $\gamma(k)$ in the first non-trivial order correction for the boson vertex — effective theory

worked out in full detail in A.4.3. The result is a new WI for 4-point functions and reads

$$\Gamma_{\text{full}}^{\mu}(p) = -2e \frac{\partial}{\partial p_{\mu}} G^{(2)}(p). \quad (4.20)$$

This is as well the WI for fully dressed 4-point functions in the effective theory because we found a linear mapping. The vertex function Γ_{full} is defined in the way as in (4.19) from the $\lambda(\phi^* \phi)^2$ -case: It includes all external legs.

4.7 Ward Identity for 2-point Functions in the Effective Coupling

We found the Ward identity for 4-point functions in the effective coupling. The last step is the derivation of a Ward identity for the 2-point functions of this theory in (4.7). This is easily achieved by using the results of the last section. We find very similar identities as I_1 to I_5 for the 2-point function (see (A.31) and (A.32)). We are dealing with only one throughgoing boson line now. This implies that the expansion (A.34) is not necessary any more, and the factor of 2 in (4.20) vanishes. We obtain again (4.13) and (4.14), except that this time the propagator also contains effective 4-, 5- and 6-fold interactions. We need diagrams in the order $e^2 g^2$ in the next section. This means that we have to apply the WI for a propagator as depicted in Fig. 4.8. The possible insertion points are indicated by arrows.

4.8 Construction of Self Energy Diagrams in the Effective Theory

Finally we are ready to construct self energy diagrams in the effective theory starting from the derivative of the conserved current with respect to the chemical potential as in (4.7). Furthermore, we are able to do this in a current conserving way since we found Ward identities for the 1- and 2-particle propagator in (4.7).

The self energy diagrams have to be constructed following the procedure of section 4.4 where we found the diagrams of sQED. This can be done in a straightforward way. Instead of writing down the steps we describe them in words, since they do not contain any new concept compared to section 4.4. It is not necessary to apply (4.15) again as in (4.16). We formulated the WI for the effective 2- and 4-point function in the way that external legs of the vertex are still included. In our effective WI not the inverse of the propagator appears in the derivative but the propagator itself. The trick (4.15) only has to be applied if the WI is formulated with the inverse propagator.

This time, we can close the boson lines directly. The result of this procedure is that we obtain the self energy diagrams for (4.7) in the following way:

The derivative with respect to μ in (4.7) is first applied to the coefficient $(2p - 2\mu)$ in both sums. The results are 2- and 4-point functions whose external legs can be closed. The external photon then couples either via a sQED 4-vertex or a $2\gamma 4\pi$ -vertex since those are the only ones carrying no derivative coupling.

If one applies the derivative with respect to μ to the propagators themselves, the (first order) derivative coupling in the coefficients stays. Again, $\partial/(\partial\mu) = -\partial/(\partial p_0)$ and the WI's (4.20) for the 4-point function respectively (4.20) without the factor of two for the 2-point function can be applied (with a slight change since the 4-point Ward identities assume 4 identical momenta at the effective $\gamma 4\pi$ -vertex).

The result should automatically satisfy the Ward identity. Again, the output consists of fully dressed diagrams as in Fig. 4.3 and Fig. 4.4, with the generalization that dressed effective 4π -vertices are allowed as well. Both terms of (4.7) contribute to the new class of diagrams.

In the order $e^2 g^2$, five topologically different diagrams arise. They are:

$$\begin{aligned}
 \Pi^{00}(k_0 = 0, \mathbf{k} \rightarrow 0) = & \text{Diagram 1} + \text{Diagram 2} \\
 & + \text{Diagram 3} + \text{Diagram 4} \\
 & + \text{Diagram 5}
 \end{aligned} \tag{4.21}$$

We will show later on that this set of diagrams indeed satisfies the Ward identity.

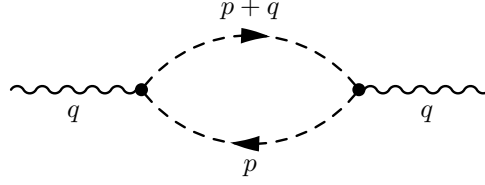
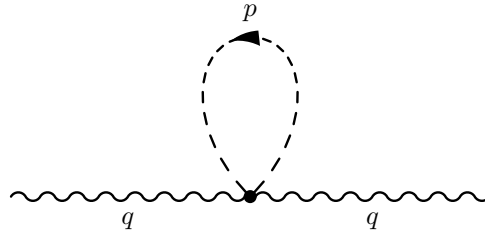
4.9 The Transversality of Diagrams in a Simple Example

The remaining task in the framework of current conservation is to show the transversality of the set of diagrams in (4.21). This is postponed until we are more familiar with them and after they are evaluated in the static limit.

Instead, the simplest example of self energy diagrams in the sQED theory is investigated in order to demonstrate calculation techniques.

In order to check current conservation in e^2 , the Ward identity

$$q_\mu \Pi^{\mu\nu}(q) = 0 \quad \forall \quad \nu = 0, \dots, 3$$


 Figure 4.9: Photon Self Energy in the order e^2 : The Bubble Diagram

 Figure 4.10: Photon Self Energy in the order e^2 : The Tadpole Diagram

([13], p. 245) has to be fulfilled where $\Pi^{\mu\nu}$ is the sum of all possible diagrams in e^2 . These are the diagrams in Fig 4.9 and Fig. 4.10.

The amplitude of the diagram in Fig. 4.9 is

$$\begin{aligned} \Pi_{\text{Fig.4.9}}^{\mu\nu}(p_0, \mathbf{p}, q_0, \mathbf{q}) &= T \sum_{p_0=-\infty, \infty} \int \frac{d^3 \mathbf{p}}{(2\pi)^3} (-e(2p^\mu + q^\mu)) (-e(2p^\nu + q^\nu)) \frac{1}{p_0^2 - \eta^2} \frac{1}{(p_0 + q_0)^2 - \eta'^2} \\ &= e^2 T \sum_{p_0=-\infty, \infty} \int \frac{d^3 \mathbf{p}}{(2\pi)^3} \frac{(2p^\mu + q^\mu)(2p^\nu + q^\nu)}{(p_0^2 - \eta^2)((p_0 + q_0)^2 - \eta'^2)}. \end{aligned} \quad (4.22)$$

with $\eta^2 = \mathbf{p}^2 + m_\pi^2$ and $\eta'^2 = (\mathbf{p} + \mathbf{q})^2 + m_\pi^2$.

The corresponding amplitude of Fig. 4.10 is

$$\begin{aligned} \Pi_{\text{Fig.4.10}}^{\mu\nu}(k_0, \mathbf{k}) &= -T \sum_{p_0=-\infty \dots +\infty} \int \frac{d^3 p}{(2\pi)^3} (2e^2) g^{\mu\nu} \frac{1}{p_0^2 - \eta^2} \\ &= -2e^2 T g^{\mu\nu} \sum_{p_0=-\infty \dots +\infty} \int \frac{d^3 p}{(2\pi)^3} \frac{1}{p_0^2 - \eta^2}. \end{aligned} \quad (4.23)$$

4.9.1 Matter Part of $q_\mu \Pi^{\mu\nu}$, $\nu = 1, 2, 3$

This subsection explicitly shows how to manipulate frequency sums in order to show the WI. In general, it is, however, easier to apply the mapping technique, developed in section 5.5. It has the advantage that both the vacuum and the matter case of the WI can be proven simultaneously.

By using the matter part of (2.46) one can rewrite (4.23) as

$$\Pi_{\text{Fig.4.10}}^{\mu\nu}(q) = -4e^2 g^{\mu\nu} \int \frac{d^3 \mathbf{p}}{(2\pi)^3} \frac{1}{2\pi i} \int_{-i\infty+\epsilon}^{i\infty+\epsilon} dp_0 \frac{1}{p_0^2 - \eta^2} n(p_0). \quad (4.24)$$

In comparison to (4.23) there is the additional factor of 2 from the $f(p_0) + f(-p_0) -$ term in (2.46).

Expressing the Matsubara series as an integral as well, the matter part of (4.22) reads

$$\begin{aligned} \Pi_{\text{Fig.4.9}}^{\mu\nu}(q) &= e^2 \int \frac{d^3\mathbf{p}}{(2\pi)^3} \frac{1}{2\pi i} \int_{-i\infty+\epsilon}^{+i\infty+\epsilon} dp_0 n(p_0) \\ &\quad \left(\frac{(2p^\mu + q^\mu)(2p^\nu + q^\nu)}{(p_0^2 - \eta^2)((p_0 + q_0)^2 - \eta'^2)} + \frac{(2p^\mu + q^\mu)(2p^\nu + q^\nu)}{((p_0^2 - \eta^2)((-p_0 + q_0)^2 - \eta'^2)} \right). \end{aligned} \quad (4.25)$$

This results in

$$\begin{aligned} q_\mu \Pi_{\text{Fig.4.9}}^{\mu\nu} &= -e^2 \int \frac{d^3\mathbf{p}}{(2\pi)^3} \frac{1}{2\pi i} \int_{-i\infty+\epsilon}^{+i\infty+\epsilon} dp_0 n(p_0) (2p^\nu + q^\nu) \\ &\quad \left[\underbrace{\frac{1}{(p_0 - q_0)^2 - \eta'^2}}_1 + \underbrace{\frac{1}{(p_0 + q_0)^2 - \eta'^2}}_2 - \underbrace{\frac{2}{p_0^2 - \eta^2}}_3 \right]. \end{aligned} \quad (4.26)$$

By switching the vector integration variable to $\mathbf{l} = \mathbf{p} + \mathbf{q}$, $d^3\mathbf{l} = d^3\mathbf{p}$, the terms 1 and 2 in the brackets become symmetric in \mathbf{l} and

$$(2\mathbf{p} + \mathbf{q}) \rightarrow 2\mathbf{l} - \mathbf{q}.$$

The integration over the terms with $2\mathbf{l}$ disappears due to the antisymmetry of the integrand. In term 3 we replace

$$(2\mathbf{p} + \mathbf{q}) \rightarrow +\mathbf{q}$$

by using the same argument.

The result of the multiplication of q_μ with $\Pi_{\text{Fig.4.10}}^{\mu\nu}$, $\nu = 1, 2, 3$ is

$$-4e^2 \int \frac{d^3\mathbf{p}}{(2\pi)^3} \frac{1}{2\pi i} \int_{-i\infty+\epsilon}^{+i\infty+\epsilon} dp_0 n(p_0) \frac{q_\nu}{p_0^2 - \eta^2}. \quad (4.27)$$

Adding both terms of Fig. 4.9 and of Fig. 4.10 leads to

$$\begin{aligned} q_\mu \Pi_{\text{Fig.4.9+Fig.4.10}}^{\mu\nu}(q) &= e^2 q^\nu \int \frac{d^3\mathbf{p}}{(2\pi)^3} \frac{1}{2\pi i} \int_{-i\infty+\epsilon}^{+i\infty+\epsilon} dp_0 n(p_0) \\ &\quad \left[\frac{1}{(p_0 - q_0)^2 - \eta'^2} + \frac{1}{(p_0 + q_0)^2 - \eta'^2} - \frac{2}{p_0^2 - \eta^2} \right]. \end{aligned} \quad (4.28)$$

The poles of this expressions with respect to p_0 in the right p_0 -half plain are at $p_0 = \eta$, $p_0 = \eta' + q_0$ and $p_0 = \eta' - q_0$. This is due to the fact that η and η' are always positive and $q_0 = 2\pi i n T$ is purely imaginary. All poles are of first order and can be calculated by using (5.16). In (4.28), all poles originate from different summands. After summation one is left with

$$\begin{aligned} q_\mu \Pi_{\text{Fig.4.9+Fig.4.10}}^{\mu\nu}(q) &= 2e^2 q^\nu \int \frac{d^3\mathbf{p}}{(2\pi)^3} \\ &\quad \left[-\frac{n(\eta)}{\eta} + \frac{n(\eta' + q_0)}{2\eta'} + \frac{n(\eta' - q_0)}{2\eta'} \right]. \end{aligned} \quad (4.29)$$

Shifting the integration by the constant value \mathbf{q} from η' to η in the second and third term and recalling $q_0 = 2\pi i n T$ (T cancels β in the exponent of the Bose factor), this is 0.

In the appendix A.4.4 the transversality in the vacuum is shown, once in dimensional regularization and once by shifting the integrand.

Chapter 5

Self Energy in the High Mass Limit

In the last chapter, the charge fluctuations were related to the self energy in the static limit by (4.17). The self energy can be expanded in a perturbative series, leading to the set of diagrams in (4.21) in the order $e^2 g^2$. In this chapter we will evaluate the five diagrams and then express them in simple terms of the self energy in e^2 .

In section 5.3.1 processes including neutral pions are introduced assuming that the Ward identities are satisfied for diagrams including π^0 . This will change the results only by constants.

At the end of this chapter the transversality of the five diagrams (without π^0 -processes) will be shown.

In the following we restrict ourselves to present only the evaluation of the *Duck* diagram. The calculations for the other diagrams are found in the appendix A.5.

5.0.2 The Bubble and the Tadpole Diagram in e^2

In order to rewrite the diagrams of the order $e^2 g^2$ in terms of the π -self energy in the order e^2 (see Fig. 4.9, Fig. 4.10), the latter are calculated.

From the amplitude (4.22) of the bubble in Fig. 4.9, we obtain

$$\begin{aligned}\Pi^{00}(q_0, \mathbf{q})_{\text{Fig. 4.9}} &= (-1)^2 T \sum_{p_0=-\infty}^{\infty} \int \frac{d^3 \mathbf{p}}{(2\pi)^3} (-e(2p_0 + q_0))^2 \frac{1}{p_0^2 - \eta^2} \frac{1}{(p_0 + q_0)^2 - \eta'^2} \\ &\rightarrow 4e^2 T \sum_{p_0=-\infty}^{\infty} \int \frac{d^3 \mathbf{p}}{(2\pi)^3} \frac{p_0^2}{(p_0^2 - \eta^2)(p_0^2 - \eta'^2)}\end{aligned}\quad (5.1)$$

for $q_0 = 0$. The result is:

$$\Pi_{\text{Fig. 4.9}}^{00}(q_0 = 0, \mathbf{q} \rightarrow 0) = e^2 C, \quad (5.2)$$

where

$$C = -\frac{1}{\pi^2} \int_0^\infty dp p^2 \left[\frac{n(\eta)}{\eta} + n'[\eta] \right] = \frac{1}{\pi^2} \int_{m_\pi}^\infty d\eta \frac{\eta^2}{p} n(\eta) = \frac{1}{\pi^2} \int_0^\infty dp \eta n(\eta). \quad (5.3)$$

The amplitude (4.23) of Fig. 4.10 leads to the self energy

$$\Pi_{\text{Fig. 4.10}}^{\mu\nu}(k_0, \mathbf{k}) = 2e^2 g^{\mu\nu} \int \frac{d^3 \mathbf{p}}{(2\pi)^3} \frac{n(\eta)}{\eta} = \frac{e^2 g^{\mu\nu}}{\pi^2} \int_0^\infty dp p^2 \frac{n(\eta)}{\eta} = \frac{e^2 g^{\mu\nu}}{\pi^2} \int_{m_\pi}^\infty d\eta p n(\eta) \quad (5.4)$$

The 00-component of (5.4) is rewritten as

$$\Pi^{00}(q_0, \mathbf{q} \rightarrow 0)_{\text{Fig. 4.10}} = e^2 D, \quad (5.5)$$

where

$$D = \frac{1}{\pi^2} \int_0^\infty dp p^2 \frac{n(\eta)}{\eta} = \int_{m_\pi}^\infty d\eta p n(\eta). \quad (5.6)$$

Furthermore, we obtain the relation

$$C = D + \frac{m_\pi^2}{\pi^2} \int_0^\infty dp \frac{n(\eta)}{\eta}. \quad (5.7)$$

5.1 The *Duck* Diagram

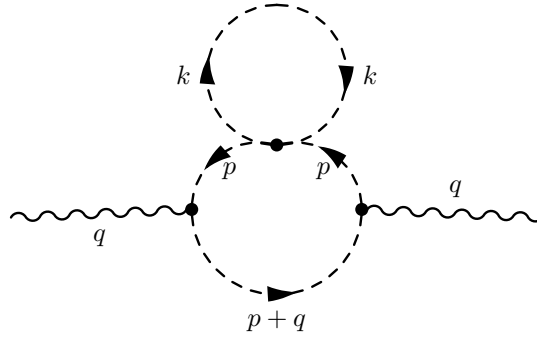


Figure 5.1: Simplification of ⑥ of Fig. 6.10: The *Duck* diagram

In the high mass limit, the diagram ⑥ in Fig. 6.10 simplifies to the one in Fig. 5.1, one of the set from (4.21).

Let us first consider the subdiagram consisting of the k -loop. The scattering amplitude with the vertex (3.30) is

$$\left(\frac{g^2}{m_\rho^2} \right) [(p+k)^2 + 4pk] \left(-\frac{1}{k^2 - m_\pi^2} \right).$$

At finite temperature, we set

$$g(p_0, \mathbf{p}) = \text{diagram} = -\frac{g^2}{m_\rho^2} \int \frac{d^3 k}{(2\pi)^3} T \sum_{k_0=-\infty}^{\infty} \frac{(p_0 + k_0)^2 - (\mathbf{p} + \mathbf{k})^2 + 4k_0 p_0 - 4\mathbf{k}\mathbf{p}}{k_0^2 - \mathbf{k}^2 - m_\pi^2}. \quad (5.8)$$

In the appendix A.5.1 this amplitude is investigated.

The vacuum contribution of the amplitude is regularized in a euclidian 4-dim integral. Another result of the analysis of (5.8) is (see A.5.1), that the angular integration over mixed momenta $\mathbf{p}\mathbf{k}$ in

the numerator vanishes if the rest of the integral only depends on \mathbf{p}^2 respectively \mathbf{k}^2 . Secondly, the Matsubara sum over terms linear in p_0 respectively k_0 vanishes as well. This can be directly concluded from (2.46). Terms linear in $p_0 k_0$ disappear as well.

The disappearance of the integral containing mixed $\mathbf{k}\mathbf{p}$ term implies the factorization of the diagram. The effective interaction in the limit $|m_\rho| \gg |k|$ provides a substantial simplification of two-loop diagrams. If there is no factorization in a two loop diagram as it is the case at finite ρ -mass, several problems arise. In the last chapter of this thesis, methods are described how to handle non-factorizing self energy diagrams.

The result of the k -loop is

$$g_{\text{matter},k\text{-loop}}(p_0, \mathbf{p}) = \text{Diagram} = a(p_0^2 - \mathbf{p}^2 + m_\pi^2), \quad a = \frac{2g^2}{m_\rho^2} \int_0^\infty \frac{dk}{(2\pi)^2} k^2 \frac{n(\omega)}{\omega}. \quad (5.9)$$

" a " can be rewritten as

$$a = \frac{2g^2}{m_\rho^2} \int_{m_\pi}^\infty \frac{d\omega}{(2\pi)^2} \sqrt{\omega^2 - m_\pi^2} n(\omega).$$

5.1.1 Complete Self Energy of the *Duck* Diagram

Symmetry Factors

In order to construct Fig. 5.1 we have to contract the pion field operators

$$A^\mu \phi_l^\star \overleftrightarrow{\partial} \phi_l (\phi_v^\star \overleftrightarrow{\partial} \phi_v)(\phi_v^\star \overleftrightarrow{\partial} \phi_v) \phi_r^\star \overleftrightarrow{\partial} \phi_r A^\nu \quad (5.10)$$

in all possible ways. In section A.5.1 this is denoted representatively for all other calculations.

Although Fig. 5.1 is in first order in the effective coupling g^2 , it originates from the third order in perturbation theory. The vertices have to be chosen from the cubed $\mathcal{L}_{\text{int}}^3$ (without π^0 -mixing). There are three possibilities to choose two 3-vertices from the cubed interaction Lagrangian which results in an overall factor of 3 for the *Duck* diagram. Furthermore, there are two possibilities to connect the two different external photons to the two sQED 2-vertices. Both factors together cancel the $1/3!$ from the perturbation series expansion. In order to determine the symmetry factor, one has to do explicit contractions in (5.10), following the rule that exactly one ϕ^\star from a 3-vertex has to be connected with a ϕ from the other 3-vertex. Doing every contraction carefully, one finds that there is an overall factor of 2 for the *Duck* diagram (see appendix A.5.1). In Fig. 5.1 we can visualize this new possibility by inserting the effective pion loop into the lower line of the bubble. In the contraction scheme this is reflected by the two possibilities to connect the two sQED 3-vertices by one contraction.

The Infrared Limit

See Fig. 5.1 for the assignment of momenta. For every photon-pion vertex, there is a factor of $-e(p+p')^\mu$. In the case of the 00-component of $\Pi^{\mu\nu}(q_0, \mathbf{q})$ this means a factor of $(e(2p_0 + q_0))^2$. The amplitude reads

$$\begin{aligned} \Pi^{00}(q_0, \mathbf{q}) &= -2ae^2 T \sum_{p_0=-\infty}^\infty \int \frac{d^3\mathbf{p}}{(2\pi)^3} \left(-\frac{1}{p_0^2 - \eta^2} \right)^2 \frac{(2p_0 + q_0)^2 (p_0^2 - \mathbf{p}^2 + m_\pi^2)}{(p_0 + q_0)^2 - \eta'^2} \\ &= -2ae^2 T \sum_{p_0=-\infty}^\infty \int \frac{d^3\mathbf{p}}{(2\pi)^3} \frac{(p_0^2 - \mathbf{p}^2 + m_\pi^2)(2p_0 + q_0)^2}{(p_0^2 - \eta^2)^2 ((p_0 + q_0)^2 - \eta'^2)} \end{aligned} \quad (5.11)$$

where $\eta = \sqrt{\mathbf{p}^2 + m_\pi^2}$ and $\eta' = \sqrt{(\mathbf{p} + \mathbf{q})^2 + m_\pi^2}$. The question arises in which order summation, integration and the infrared limits $q_0 = 0$ and $\mathbf{q} \rightarrow 0$ have to be performed. The calculations in section 4.4 clearly prescribe to perform first the limits and then integration and summation. However, all operations are freely interchangeable as it will be shown in the next section. We can therefore rewrite (5.11) in the static limit as

$$\begin{aligned}
& \Pi_{\text{Duck}}^{00}(q_0 = 0, \mathbf{q} \rightarrow \mathbf{0}) \\
&= -8ae^2 \int \frac{d^3\mathbf{p}}{(2\pi)^3} T \sum_{p_0=-\infty}^{\infty} \frac{p_0^2 (p_0^2 - \mathbf{p}^2 + m_\pi^2)}{(p_0^2 - \eta^2)^3} \\
&\stackrel{(2.46)}{\rightarrow} \\
&\stackrel{(5.15)}{\rightarrow} \\
&\stackrel{(5.16)}{=} -8ae^2 \int \frac{d^3\mathbf{p}}{(2\pi)^3} n[\Gamma] \frac{1}{2!} \lim_{p_0 \rightarrow \eta} \left[\frac{\partial^2}{\partial p_0^2} (p_0 - \eta)^3 2 \frac{p_0^2 (p_0^2 - \mathbf{p}^2 + m_\pi^2)}{(p_0^2 - \eta^2)^3} n[p_0] \right] \\
&\stackrel{n[\Gamma]=-1}{=} 8e^2 \int \frac{d^3\mathbf{p}}{(2\pi)^3} \frac{1}{4\eta^3} \left[(2\eta^2 - m_\pi^2)n[\eta] + \eta(3\eta^2 - m_\pi^2)n'[\eta] + m_\pi^2\eta^2 n''[\eta] \right] \\
&= \frac{ae^2}{\pi^2} \int_{m_\pi}^{\infty} d\eta \frac{\sqrt{\eta^2 - m_\pi^2}}{\eta^2} \left[(2\eta^2 - m_\pi^2)n[\eta] + \eta(3\eta^2 - m_\pi^2)n'[\eta] + m_\pi^2\eta^2 n''[\eta] \right] \quad (5.12)
\end{aligned}$$

where we have written the integration in favor of η as integration variable. An integration by parts of the second term removes the derivative from $n'[\eta]$. We obtain

$$\Pi_{\text{Duck}}^{00}(q_0 = 0, \mathbf{q} \rightarrow \mathbf{0}) = \frac{ae^2}{\pi^2} \int_{m_\pi}^{\infty} d\eta \left(m_\pi^2 n''(\eta) \sqrt{\eta^2 - m_\pi^2} - \frac{(m_\pi^2 + 2\eta^2)n(\eta)}{\sqrt{\eta^2 - m_\pi^2}} \right).$$

It is possible to shift derivatives $n''[\eta] \rightarrow n'[\eta]$ by

$$\int_{m_\pi}^{\infty} d\eta n''(\eta) p = \underbrace{[n'[\eta]p]_{m_\pi}^{\infty}}_{=0} - \int_{m_\pi}^{\infty} d\eta n'(\eta) \frac{\eta}{p} = - \int_0^{\infty} dp n'(\eta).$$

There is a new difficulty. Another integration by parts is not possible since p occurs in the denominator.

A way out is to use the definition of $n(\eta) = \frac{1}{e^{\beta\eta} - 1}$, the identity

$$\beta \frac{\partial}{\partial \beta} n(\beta, \eta) = \eta \frac{\partial}{\partial \eta} n(\beta, \eta)$$

and rewrite the integral as

$$- \int_0^{\infty} dp n'(\eta) = -\beta \frac{\partial}{\partial \beta} \int_0^{\infty} dp \frac{n(\eta)}{\eta}.$$

The pion loop insertion a can be rewritten as

$$a = \frac{g^2}{2m_\rho^2} D.$$

This reflects the formal analogy of the pion loop insertion and the sQED tadpole (both are $\sim D$).

Combining all terms and using the definition of a , the result is:

$$\Pi_{\text{Fig. 5.1}}^{00}(q_0 = 0, \mathbf{q} \rightarrow 0) = \frac{e^2 g^2}{2m_\rho^2} D \left(-\beta \frac{\partial}{\partial \beta} (C - D) - 3C + 2D \right). \quad (5.13)$$

The self energy of the *Duck* diagram is expressed in terms of the simple bubble and tadpole diagram in Fig. 4.9 and Fig. 4.10.

Fortunately, the remaining diagrams can be directly expressed in terms of C and D and require no derivative with respect to β . The evaluation of the remaining diagrams (*Specs*, *Propeller*, *Mouse*, *Snowman*) is performed in A.5 of the appendix. In principle, all calculation work the same although the determination of the symmetry factors involves some subtleties. In particular, a resummation based on the *Specs* diagram is performed in A.5.

5.2 Moving the Limit

Numerical and analytical investigations have shown that the summation and the static limit $q_0 = 0$, $\mathbf{q} \rightarrow 0$ can be exchanged in the evaluation of *Duck* diagram.

Why is allowed to move the limit freely and even split it in two parts? This question is of major interest since there is some confusion in the literature. Although from the calculations in [12] and from section 4.4 it is clear that the limit infrared limit has to be applied *before* summation and integration, the notation $\Pi(k_0 = 0, \mathbf{k} \rightarrow \mathbf{0})$ of [12] rather evokes the insinuation to perform the limit *after* summation and integration.

We investigate the exchange of limit and summation at the amplitude

$$\cdots \left(\frac{1}{p_0^2 - \eta^2} \right)^m \frac{1}{(p_0 + q_0)^2 - \eta'^2} \cdots \quad (5.14)$$

where the integration / summation runs over \mathbf{p} respectively p_0 . Again, $\eta^2 = \mathbf{p}^2 + m_\pi^2$ and $\eta'^2 = (\mathbf{p} + \mathbf{q})^2 + m_\pi^2$. This amplitude refers e.g. to the central structure of Fig. 4.9 for $m = 1$ and to Fig. 5.1 for $m = 2$.

In this section we assume $q_0 = 0$ and perform the integration after limit and summation. In fact we are comparing terms inside the momentum integral and do not integrate at all in momentum space.

In the evaluation of contour integrals, the residue theorem

$$\frac{1}{2\pi i} \oint_{\Gamma} f(\xi) d\xi = \sum_i n_i(\Gamma) \text{Res} f(z)|_{z=z_i}, \quad (5.15)$$

is usually applied where Γ is a closed path (with no singularities on it) and $n(\Gamma)$ is the number of circulations of Γ around the pole at $z = z_i$. In our case we always have to integrate from $-i\infty + \epsilon$ to $+i\infty + \epsilon$ and close the contour in the right half plane. This single clockwise path always has $n(\Gamma) = -1$ (counterclockwise $\rightarrow n(\Gamma) = +1$). See Fig. 5.2¹.

A convenient formula to calculate residues is

$$\text{Res} f(z)|_{z=z_0} = \lim_{z \rightarrow z_0} \frac{1}{(m-1)!} \frac{d^{m-1}}{dz^{m-1}} [f(z)(z - z_0)^m] \quad (5.16)$$

for a pole at $z = z_0$ of the order m [22].

We assume now $m = 1$.

There are two poles in the right p_0 -plane of (5.14), both of first order at $p_0 = \eta'$ and at $p_0 = \eta$. See Fig. 5.2. Let

¹In the summation of a two-loop diagram there usually appears a dependency of the pole η or η' on the 0-component of the external momentum k_0 . Therefore the location of the pole is not fixed any more. Fortunately, k_0 is a Matsubara frequency itself and therefore purely imaginary (at zero chemical potential). Hence the movement of the pole is restricted to the vertical direction in the p_0 -plane. This is indicated with the vertical arrows in Fig. 5.2.

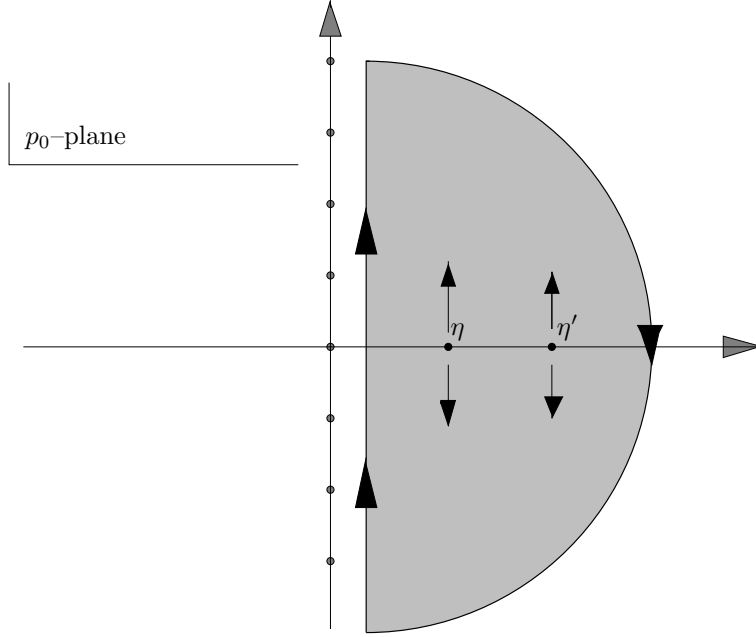


Figure 5.2: Integration path for the evaluation of Matsubara series

$$f(p_0) = \frac{1}{p_0^2 - \eta^2} \frac{1}{p_0^2 - \eta'^2}.$$

Then, the integration according to the matter part of (2.46)

$$\frac{1}{2\pi i} \int_{\Gamma} \underbrace{(f(p_0) + f(-p_0))n(p_0)}_{=:g_1(p_0)}$$

with an arbitrary smooth function n and Γ as in Fig. 5.2 equals

$$(-1)(\text{Res}(g_1(p_0); \eta) + \text{Res}(g_1(p_0); \eta')) = (-1) \left(\lim_{p_0 \rightarrow \eta} [(p_0 - \eta)g_1(p_0)] + \lim_{p_0 \rightarrow \eta'} [(p_0 - \eta')g_1(p_0)] \right).$$

This results in

$$(-1) \left[\left(\frac{1}{\eta} \frac{1}{\eta^2 - \eta'^2} n(\eta) \right) + \left(\frac{1}{\eta'^2 - \eta^2} \frac{1}{\eta'} n(\eta') \right) \right] = \frac{\eta n(\eta') - \eta' n(\eta)}{\eta \eta' (\eta^2 - \eta'^2)}.$$

The existence of the limit $\eta' \rightarrow \eta$ in this expression is not obvious. The right side is in fact a derivate in the limit $\eta' \rightarrow \eta$. In order to take the limit $\eta' \rightarrow \eta$, $n(\eta')$ is expanded up to the linear term by $n(\eta') = n(\eta) + (\eta' - \eta)n'(\eta)$, which leads to

$$\frac{n(\eta) - \eta n'(\eta)}{\eta \eta' (\eta + \eta')} \longrightarrow \frac{n(\eta) - \eta n'(\eta)}{2\eta^3}.$$

The Taylor expansion is useful because it expresses the unknown $n[\eta']$ in terms of $n[\eta]$.

What is the result, if the limit $\mathbf{k} \rightarrow 0$ is taken before summation? Let

$$g_2(p_0) := 2 \left(\frac{1}{p_0^2 - \eta^2} \right)^2 n(p_0)$$

and the integration over Γ (with the factor $\frac{1}{2\pi i}$) equals

$$(-1)\text{Res}(g_2(p_0); \eta) = (-1) \lim_{p_0 \rightarrow \eta} \frac{d}{dp_0} ((p_0 - \eta)^2 g_2(p_0)) = -2 \lim_{p_0 \rightarrow \eta} \frac{d}{dp_0} \left(\frac{n(p_0)}{(p_0 + \eta)^2} \right),$$

which equals

$$-2 \frac{n'(p_0)(p_0 + \eta)^2 - n(p_0)2(p_0 + \eta)}{(p_0 + \eta)^4} \rightarrow \frac{n(\eta) - \eta n'(\eta)}{2\eta^3}.$$

The derivative which we obtained in the calculation with g_1 resulted from the Taylor expansion and equals the derivative which now originates from the application of (5.16).

If both poles of (5.14) are of the order 1 ($m = 1$) for any analytical function n the limit can be performed before summation.

Let $m = 2$ now. Then

$$g_3(p_0) := 2 \left(\frac{1}{p_0^2 - \eta^2} \right)^2 \frac{1}{p_0^2 - \eta'^2} n(p_0) \quad (\text{pole of order 2, pole of order 1}). \quad (5.17)$$

The contributions of the pole at $p_0 = \eta'$ plus the pole at $p_0 = \eta$ evaluate the contour integration over $\frac{1}{2\pi i} g_3(p_0)$ as

$$\frac{3(n(\eta) - \eta n'(\eta)) + \eta^2 n''(\eta)}{8\eta^5}.$$

Here, the limit is taken after summation. Furthermore, a Taylor expansion has been applied up to the quadratic order for to express $n[\eta']$ as a function of η . It has been shown (see B.1) shown that the order after which we can cancel the expansion depends on the order of the pole. In general, the previous examples have shown, that the highest order of the Taylor expansion and the order m of the pole have to be equal. Taking the limit before summation leads to the new g_4

$$g_4(p_0) := \frac{2n(p_0)}{(p_0^2 - \eta^2)^3} \quad (\text{pole of order 3}). \quad (5.18)$$

The result of the integration is

$$\frac{3(n(\eta) - \eta n'(\eta)) + \eta^2 n''(\eta)}{8\eta^5}$$

as well. We see that it is necessary to keep the quadratic term in the Taylor expansion.

Finally, the validity of the our algebraic computation of contour integrals is successfully tested numerically (details in A.5.7).

5.2.1 Further Exchanges of Summation and Limits

In the last section it has been shown that the limit $q \rightarrow 0$ can be taken before summation or after ($\int \lim \sum \Leftrightarrow \int \sum \lim$) (up to amplitudes in the order $e^2 g^2$ as an inspection of the structure of the diagrams in (4.21) shows). In all considerations the 3-dim momentum integral has not been taken into account so far. We want to make up for what we have missed and investigate "lim ($\sum \leftrightarrow \int$)", meaning the limit is performed as the last operation. In the following section the full dependency of the simple π -bubble on the external momentum is calculated (Fig. 4.9).

First, we try to calculate in the the order " $\lim_{\mathbf{q} \rightarrow 0} \int(d\theta) \sum$ ", then we perform " $\lim_{\mathbf{q} \rightarrow 0} \sum \int(d\theta)$ ". Here, the argument of the integral indicates, that it only refers to the θ -integration over the relative angle between \mathbf{p} and \mathbf{q} . This is a crucial integration since it might lead to the occurrence of a $\log(\cdot)$ function with non-analytical behavior as $\mathbf{q} \rightarrow 0$. See also [16], where this behavior is studied for a *massless* theory without derivative couplings.

It is

$$\begin{aligned}
& \Pi_{\text{Fig. 4.9}}^{00}(q_0, \mathbf{q}) \\
&= e^2 \int \frac{d^3 \mathbf{p}}{(2\pi)^3} T \sum_{p_0=-\infty}^{\infty} \frac{(2p_0 + q_0)^2}{(p_0^2 - \eta^2)((p_0 + q_0)^2 - \eta'^2)} \\
&\rightarrow \int \frac{d^3 \mathbf{p}}{(2\pi)^3} \frac{1}{2\pi i} \int_{-i\infty+\epsilon}^{+i\infty+\epsilon} \left(\frac{(2p_0 + q_0)^2}{((p_0 + q_0)^2 - \eta'^2)(p_0^2 - \eta^2)} + \frac{(2p_0 - q_0)^2}{((p_0 - q_0)^2 - \eta'^2)(p_0^2 - \eta^2)} \right) n[p_0].
\end{aligned} \tag{5.19}$$

The matter part of the sum has been transformed into an integral according to (2.46).

Performing the θ -integration (recall $\eta' = \sqrt{m_\pi^2 + p^2 + q^2 + 2pq \cos(\theta)}$) first, leads to considerable difficulties: Not only that that the integration would be ultraviolet divergent and needed to be regularized: The result

$$-\frac{(2p_0 + q_0)^2 \log \left[\frac{m_\pi^2 + (p+q)^2 - (p_0+q_0)^2}{m_\pi^2 + (p-q)^2 - (p_0+q_0)^2} \right]}{2 p q (p_0^2 - \eta^2)}.$$

leads to a major problem.

This result has to be used as the f in the transformation rule (2.46) into a contour integral. The contour has to be closed in the right half plane. Then the residues in the right half plane contribute to the integral. But since there occurs a logarithm, a branch cut has to be applied. This branch cut can be shaped in an arbitrary (not self-intersecting) path as long as it starts at the branching point (where the log-argument is 0) and tends to infinity — the complex p_0 -plane is cut in an onefold connected area. Thus, it is not possible to find a closed integration contour that does not intersect with the branch cut².

Performing the summation first is therefore the way of choice. There are three different poles in the right half plane, which result from the η -term (one singularity) and the η' -term (two singularities resulting from the form of (2.46)). The angle integration (at finite q_0 and q) results in terms that contain logarithms, squareroots and logarithms of squareroots:

$$\Pi_{\text{Fig. 4.9}}^{00}(q_0, q = |\mathbf{q}|) = -e^2 \frac{(2\pi)}{(2\pi)^3} \int_0^\infty dp p^2 [\eta\text{-term} + \sqrt{\text{-term}} + \log\text{-term}] \tag{5.20}$$

²If there was a squareroot-type singularity, this would still be possible: The Riemann surface in this case consists of 2 sheets that intersect at the branch cut, and a closed path from the lower to the upper plane and back to the lower surface can be drawn, that circumscribes the singularity. In the logarithmic case, the Riemann surface has the shape of an infinite spiral and the path cannot be closed any more.

where the minus sign originates from the clockwise integration contour. The result (5.20) for the bubble diagram C in Fig. 4.9 is identical with the results of Gale/Kapusta [23] and Song [24] (only the static limit is derived in [24], though). Since we express all diagrams in terms of the basic diagrams C and D consistency with the literature is absolutely crucial at this point. There is a phase space factor and the coefficient (2π) from the longitudinal angle integration. The terms are

$$\begin{aligned}
\eta\text{-term} &= \frac{n[\eta]}{4 p q \eta} \left((q_0 - 2\eta)^2 \log \left[\frac{m_\pi^2 + (p - q)^2 - (q_0 - \eta)^2}{m_\pi^2 + (p + q)^2 - (q_0 - \eta)^2} \right] \right. \\
&\quad \left. + (q_0 + 2\eta)^2 \log \left[\frac{m_\pi^2 + (p - q)^2 - (q_0 + \eta)^2}{m_\pi^2 + (p + q)^2 - (q_0 + \eta)^2} \right] \right) \\
\sqrt{\text{-term}} &= \frac{4}{p q} \left(\left[-\sqrt{m_\pi^2 + (p - q)^2} + \sqrt{m_\pi^2 + (p + q)^2} \right] n[\eta] \right. \\
&\quad \left. + \left[2 p q + \eta \left(\sqrt{m_\pi^2 + (p - q)^2} - \sqrt{m_\pi^2 + (p + q)^2} \right) \right] n'[\eta] \right) \\
\log\text{-term} &= \frac{1}{4 p q \eta} \left((q_0 - 2\eta)^2 \log \left[\frac{\sqrt{m_\pi^2 + (p - q)^2} + q_0 - \eta}{\sqrt{m_\pi^2 + (p + q)^2} + q_0 - \eta} \right] \right. \\
&\quad + (q_0 + 2\eta)^2 \log \left[\frac{\sqrt{m_\pi^2 + (p + q)^2} - q_0 - \eta}{\sqrt{m_\pi^2 + (p - q)^2} - q_0 - \eta} \right] (n[\eta] + q_0 n'[\eta]) \\
&\quad + (q_0 - 2\eta)^2 \log \left[\frac{\sqrt{m_\pi^2 + (p - q)^2} - q_0 + \eta}{\sqrt{m_\pi^2 + (p + q)^2} - q_0 + \eta} \right] (n[\eta] + (q_0 - 2\eta) n'[\eta]) \\
&\quad \left. + (q_0 + 2\eta)^2 \log \left[\frac{\sqrt{m_\pi^2 + (p + q)^2} + q_0 + \eta}{\sqrt{m_\pi^2 + (p - q)^2} + q_0 + \eta} \right] (-n[\eta] + (q_0 + 2\eta) n'[\eta]) \right). \quad (5.21)
\end{aligned}$$

There are several noteworthy facts about this formula: First of all, the limit $q \rightarrow 0$ *exists*. This is not obvious from the analytical form of the terms but must be shown by using the limit rule of de L'Hôpital.

The derivative of the statistical factor n is more precisely denoted as $n'[\eta] = \frac{\partial}{\partial \eta} \frac{1}{e^{\beta \eta} - 1}$. This derivative originates from a Taylor expansion in order to express $n[\eta']$ in terms of η . Without doing this, the statistical factor would contain $\cos(\theta)$ and could not be integrated analytically any more.

In addition, all squareroots possess real values in all possible combinations of the variables inside. In contrast, the logarithm is not always defined for certain combinations. There must be absolute value brackets $|\dots|$ for the argument of the logarithms which have been left out here for simplicity. The p -integration over singularities of logarithmic type have to be understood as Cauchy principal values (which always exist in the logarithmic case, but not in general for singularities of order higher than three as we will see in the last chapter of this thesis).

The result (5.20) has the full dependency on the external photon momentum – the complexity of the expression, even for the simple diagram 4.9 reveals that it is crucial for us to take the static limit *before* integration.

The canonical procedure would now be the following: In order remove the derivative of the statistical factor, the integration would be switched from p to η and then an integration by parts would free the the n -factor of the derivative. However, the remaining "bare" p -factors would have to be substituted as well and the resulting terms would be awkwardly complicated. Also, there is no reason of dealing with that whole lot of information in the term since it is only linearly exact in q after we performed the Taylor expansion of the Bose factor.

Regarding all this, the way of choice is a Taylor expansion of all logarithms, squareroots and square-roots in logarithms at $q = 0$. The result in each single case is, that the constant term vanishes. Then the linear term can cancel the "bare" factor of q in the denominator in (5.20). The quadratic expansion term

vanishes as well and the error by the remaining series is therefore $\mathcal{O}(q^3)$. This shows that the self energy is smooth around $q = 0$ in a massive theory. When the smoke clears after the insertion of all expansions in (5.20), the result is stunningly simple:

$$(5.20) = e^2 \frac{1}{4\pi^2} \int_0^\infty dp p^2 \left(\frac{8n[\eta]}{\eta} - \frac{6n[\eta]}{\eta} + \frac{2n[\eta]}{\eta} \right),$$

which reproduces exactly the result for C (5.3). In the evaluation of C the limit was taken *before* summation and *before* integration.

This shows that, in contrast to the situation of Weldon's investigations [16], limits can be moved freely. This is due to the massive character of the pions. The branch cut in the pionic self energy diagrams lies at values of $p_0^2 > 2m_\pi^2$ and $p_0^2 < -2m_\pi^2$ (see also section 2.3.5). In a more recent paper [25] of Weldon, further properties of the infrared limit of the self energy is discussed, unfortunately partly in the real time formalism which we have not introduced here.

5.3 Classifications of Diagrams and Result

The contributions of the diagrams have been calculated in a way similar to the *Duck* diagram (details in A.5).

All diagrams have been expressed in terms of C and D with the result

Name	Contribution $\Pi^{00}(q_0 = 0, \mathbf{q} \rightarrow 0)$	Reference
<i>Duck</i>	$\frac{e^2 g^2}{2m_\rho^2} D \left(-\beta \frac{\partial}{\partial \beta} (C - D) - 3C + 2D \right)$	(5.13)
<i>Specs</i>	$\frac{3e^2 g^2}{2m_\rho^2} C^2$	(A.53)
<i>Snowman</i>	$-\frac{e^2 g^2}{2m_\rho^2} D(2D - C)$	(A.59)
<i>Mouse</i>	$\frac{4e^2 g^2}{m_\rho^2} CD$	(A.63)
<i>Propeller</i>	$-\frac{4e^2 g^2}{m_\rho^2} D^2$	(A.66)

Adding up all contributions results in

$$\Pi^{00}(q_0 = 0, \mathbf{q} \rightarrow 0) = \frac{e^2 g^2}{2m_\rho^2} \left[D \left(-\beta \frac{\partial}{\partial \beta} [C - D] - 8D \right) + 3(C^2 + 2CD) \right]. \quad (5.22)$$

5.3.1 The contribution of neutral pions

The inclusion of the neutral pion is easy. Already, we found the Feynman rules for π^0 -mixing. Those were identical with the ones of pure π^\pm -interaction. The effective π^0 -4-vertex (A.20), though, showed a different behavior. The special case (A.21) was evaluated. There, the assumption was made that the exiting π^0 forms a closed loop with the incoming π^0 . Still, this rule differs from the effective π^\pm -4-vertex as in Fig. 5.1 or Fig. A.7. The only structural difference, though, is the occurrence of mixed terms kp in the π^\pm -interaction (see the corresponding amplitudes). From our calculations we know that products of this form never contribute and can therefore be omitted. If we rewrite (3.30) with the loop-constraint $p_1 = p_4 = p$ and $p_2 = p_3 = k$ and omit the linear terms, the rule reads $\frac{g^2}{m_\rho^2} (p^2 + k^2)$. This equals (A.21).

Hence, the remaining task is, to rewrite (5.22) with different coefficients. For the *Specs* diagram there is the additional constraint that all legs of the effective 4-vertex are directly connected to sQED 3-vertices. Therefore, no process including neutral pions can take place.

From the above we conclude that both the contributions of the *Snowman* and the *Duck* diagram are enhanced by a factor of 2.

For the *Mouse* diagram in π^0 -mixing, an isospin symmetry factor of $(1/2)$ applies to the rule: There are not two distinguishable external ϕ^0 -fields any more. Furthermore, we found another symmetry factor of 2 for the *Mouse* diagram: It resulted from the possibility for the photon to couple either to the head or the body of the *Mouse*. In the π^0 -mixing it can only couple to the charged body of the *Mouse*. The comparison of the π^0 - and the π^\pm -rule shows, that the *Mouse* diagram is enhanced by a factor of $(1/16)$.

The *Propeller* diagram undergoes a change by a symmetry factor of $(1/2)$ in the π^0 -mixing as well as it did in the π^\pm -process, since there are not two distinguishable external ϕ^0 -fields any more. Comparing the vertex rules for the charged and uncharged interaction, the *Propeller* Diagram is enhanced by a factor of $(1/4)$.

The sum of the self energy diagrams therefore changes to

$$\sum_{i=1}^5 \Pi_i(q_0 = 0, \mathbf{q} \rightarrow \mathbf{0}) = \frac{e^2 g^2}{m_\rho^2} \left[D \left(-\beta \frac{\partial}{\partial \beta} [C - D] - 5D \right) + C \left(\frac{9}{4} D + \frac{3}{2} C \right) \right]. \quad (5.23)$$

5.4 The Ward Identity in $\lambda(\phi\phi^\star)^2$ -theory (Vacuum)

Not only have we constructed the diagrams using the Ward identity but also gauged the Lagrangian in a covariant way. Therefore the set of diagrams in (4.21) are supposed to fulfill the Ward identity. However, in order to obtain numerical results for screening or enhancement of the charge fluctuations in the hadronic phase, the relative signs and coefficients of the self energies in the high mass limit have to be correct. Therefore we will sum all amplitudes and explicitly check the transversality of the photon

$$\boxed{k_\mu \Pi^{\mu\nu}(k), \quad \nu = 0, \dots, 3} \quad (5.24)$$

in all four components of ν and *full* momentum dependency of the self energy on the external photon momentum k .

In order to get started, we check the transversality in the somewhat simpler $\lambda(\phi\phi^\star)^2$ -theory. We already found a WI for this theory in 4.5. The set of diagrams in the order $e^2\lambda$ from Fig. 5.3 shows a close relation to the *Specs*, *Duck* and *Snowman* diagrams of the effective theory apart from that the 4π -vertices carry no derivative couplings any more. Instead they carry a $(-\lambda)$.

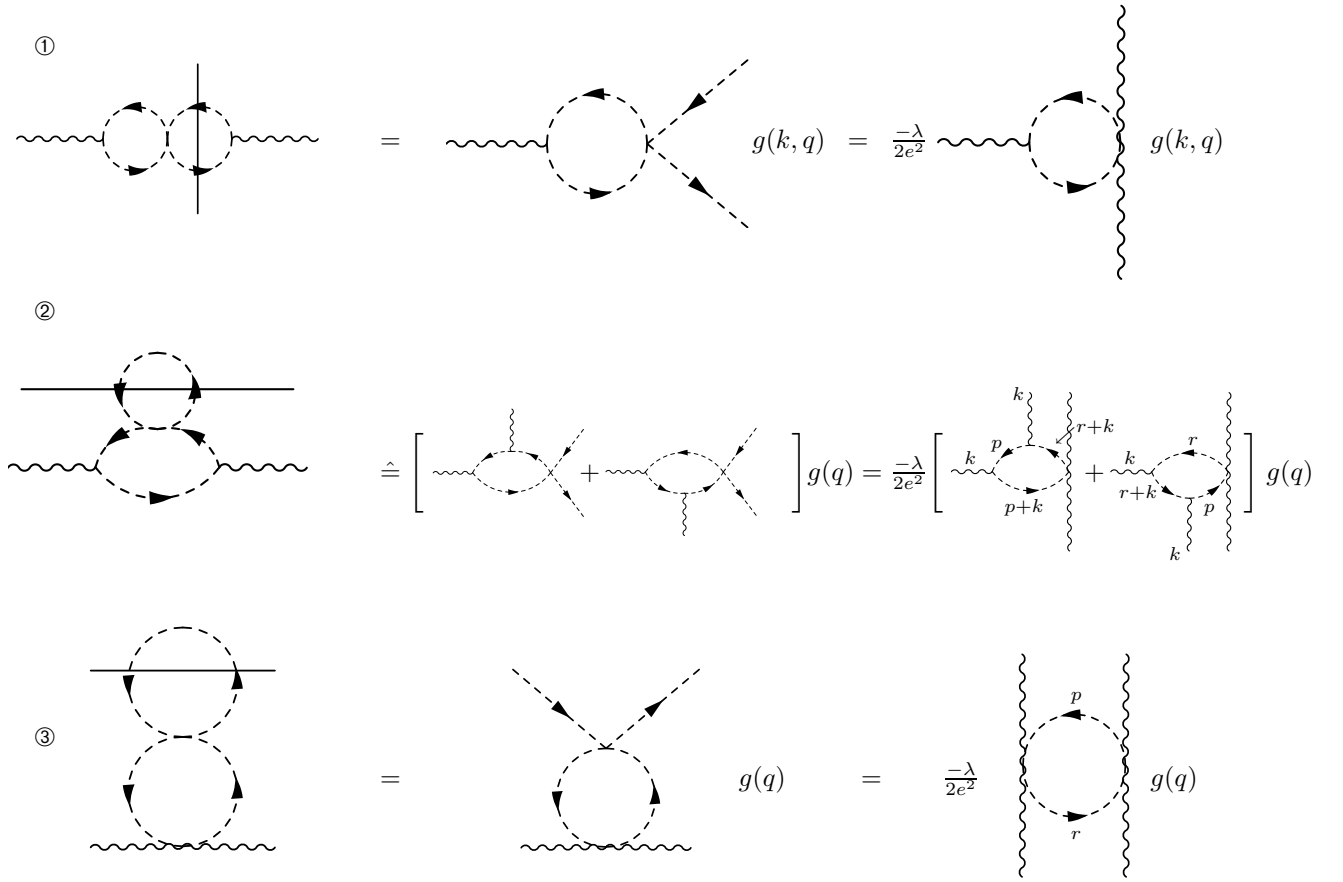
At first, the three diagrams in Fig. 5.3 undergo a cut. (In the second and third diagram this would not even be necessary, but we applied the cut anyways to show the close analogy to the first diagram). Then, the cut diagrams equal the original diagrams apart from factorizing integrations over other momenta, subsummed in the function g . In the last step the fact is used, that the direct coupling $-\lambda g^{\mu\nu}$ equals the seagull vertex of sQED $2e^2 g^{\mu\nu}$ up to a constant.

We expect diagram 2 and 3 being somehow related since they correspond to the two sQED diagrams in e^2 with an additional pion loop insertion.

Indeed, without calculations we can identify the first diagram with a saturated loop diagram. The insertion of this diagram has already been performed (photon from the left side). Since loop insertions vanish (see A.4.2) if multiplied by the external momentum, diagram ① cancels.

We want to understand this behavior terms of the amplitude. The amplitude of ①, multiplied with k_μ can be rewritten as

$$k_\mu (2p + k)^\mu \frac{1}{p^2 - m_\pi^2} \frac{1}{(p + k)^2 - m_\pi^2} g(k, q)$$


 Figure 5.3: Mapping the Diagrams in λe^2 to sQED

with the function g that contains coefficients and the part of the amplitude that is independent of p . By completing the square in the numerator we arrive at

$$\left(\frac{1}{p^2 - m_\pi^2} - \frac{1}{(p+k)^2 - m_\pi^2} \right) g(k, q). \quad (5.25)$$

If we shift the second term by k , the function f is not altered and the result is 0.

The remaining two diagrams ② and ③ need each other in order to cancel. The mapping of diagram ② requires some explanation. As we saw in the calculation of the *Duck* diagram, it has an explicit symmetry factor of 2. This is due to the fact that the pion loop insertion can be attached at the lower pion line as well. This quality is used to rewrite the diagram as the sum of two diagrams in sQED on the right side. Recall from the proof of the Ward identity, that insertions of photons into diagrams were performed disregarding any symmetry effects. Every insertion diagram counts as one. Therefore, we can use the symmetry of the diagram in the effective theory to denote *two* diagrams in sQED. Furthermore, the convention of the momentum flow of k (along the closed line in a counter clockwise direction) is precisely the same as in the proof of section A.4.2.

It is clear now that the three diagrams in sQED on the right sides of ② and ③ represent all possible insertion diagrams into a body diagram. (This body diagram accidentally is the one on the right side of ①). Transversality is proven.

Direct Proof of the Transversality (Vacuum)

It would be reassuring to have a direct proof of the transversality of the diagrams ② and ③ as we found it for diagram ① in (5.25). Since we perform the proof of the WI in the effective theory in the matter case, we want to present the $\lambda(\phi\phi)^*$ -case in the vacuum formulation here.

It is not clear that the two sQED diagrams on the right side of ② with the special momentum assignment as in Fig. 5.3 are equal.

We denote corresponding amplitudes:

$$\begin{aligned} & (-ie(2r+k)^\mu) \frac{i}{(r+k)^2 - m_\pi^2} (-ie(r+k+p)^\nu) \frac{i}{p^2 - m_\pi^2} \delta(r-p) \frac{i}{r^2 - m_\pi^2} g(q) \\ + & (-ie(2p+k)^\mu) \frac{i}{(p+k)^2 - m_\pi^2} \delta(r-p) \frac{i}{(r+k)^2 - m_\pi^2} (-ie(r+p+k)^\nu) \frac{i}{p^2 - m_\pi^2} g(q). \end{aligned} \quad (5.26)$$

There appears the function $g(q)$ in (5.26) that contains the q -dependency of the pion loop insertion, λ and coefficients.

We have inserted a δ -function that prescribes the momentum conservation at the $\lambda(\phi\phi^*)^2$ -vertex. Therefore we could split the square of the p -propagator by introducing a new momentum r . The first line of (5.26) clearly has the amplitude of the diagram on the left side of ②.

It has to be shown that the second line is identical with the first one. The prescription for transforming the second line into the first reads:

- Exchange the variable names $p \leftrightarrow r$.
- Substitute $r \rightarrow r - k$ and $p \rightarrow p - k$. Both procedures together will leave the δ function unchanged.
- Reverse the direction of momentum flow between the direct connection of the two photons by substituting $r \rightarrow -r$ and furthermore $p \rightarrow -p$.

All these transformation leave the integral over the second line of (5.26) unchanged. The manipulations can be easily visualized in Fig. 5.3 by turning the arrows around. (it should be clear that our transformation works since Feynman diagrams better are independent of the particular momentum assignment.)

The next task is to calculate the product of (5.26) with k_μ . If we complete the square in both terms and cancel the appropriate terms, we find out that the introduction of the δ -function has paid off: we have a very similar term structure as in the proof of the WTI for sQED in section A.4.2. Two of the four terms cancel in full analogy to the proof of WTI and we are left with

$$(-ie)^2 i^3 (r + p + k)^\nu \delta(r - p) \left(\frac{1}{r^2 - m_\pi^2} \frac{1}{p^2 - m_\pi^2} - \frac{1}{(r + k)^2 - m_\pi^2} \frac{1}{(p + k)^2 - m_\pi^2} \right) g(q).$$

Shifting the second term in the brackets by $p \rightarrow p - k$ and $r \rightarrow r - k$ changes the remaining derivative coupling in the numerator and the final result is

$$\frac{2ie^2 k^\nu}{(r^2 - m_\pi^2)(p^2 - m_\pi^2)} \delta(r - p) g(q).$$

By writing down the amplitude of the right side of ③, we see that this term will precisely cancel without any further calculation necessary.

Assigning the momenta in a set of diagrams so that they follow the conventions of the proof of the WI in sQED, and splitting the amplitudes, is always the way of choice in order to proof the WI.

5.5 The Ward Identity in the Order $e^2 g^2$

Since in the last chapters the WI has been proven in the order e^2 of sQED and in $\lambda(\phi\phi^*)^2$ -theory, many tricks and shortcuts have shown up which enable the proof in the somewhat more complicated case in the order $e^2 g^2$. Instead of two diagrams as in e^2 in sQED respectively three diagrams in $\lambda(\phi\phi^*)^2$ -theory, there is a couple of new diagrams.

There are three different possibilities to proof the transversality of the sum of all diagrams. First, we could write down all diagrams in dimensional regularization and shape the amplitudes according to (A.37). But we notice that already in the order e^2 this results in rather lengthy terms.

Second, we could write down the amplitudes and use the methods of shifting the integration variable as it has been done in the abbreviation of the proof of the transversality in e^2 in section A.4.4. This is indeed possible. In the last section we performed this for a scalar coupling. Analytical terms become awkwardly lengthy, though, if one tries to do the same in the effective theory (Extended tries have been undertaken to work directly with amplitudes but no manageable shortcut has been found).

Instead, we invent something similar to the the last section when we showed the transversality of all diagrams in the order $e^2 \lambda$. This time, it will be more complicated.

We use a procedure in which we first map all diagrams in sQED theory, extract the body diagrams from the result and identify all diagrams with insertion diagrams of the body diagrams. Furthermore, there are no subgroups of diagrams now, that cancel separately as in the $\lambda(\phi\phi^*)^2$ -case. Only taking all diagrams into account simultaneously returns the transversality.

5.5.1 Mapping the problem (Matter)

This time, we perform the proof at finite temperature. The vacuum case is shown analogously, a slightly different value of α being the only difference ($\alpha \rightarrow -i\alpha$, see below).

Recall the Ward Identity (4.20) for the effective theory. In its proof, we found a linear function to map [(A.31) and (A.32)] all occurring diagrams into sQED diagrams. Since this function is the same for all diagrams we concluded that the effective theory and sQED obey the same type of WI (up to a factor of 2 in (4.20)).

We define

$$\alpha \stackrel{\text{def}}{=} \frac{\left(\frac{q^2}{m_\rho^2}\right)}{(-e)^2} \left(-\frac{q^2}{1}\right) = \frac{\left(\frac{-4eg^2}{m_\rho^2}\right)}{2(2e^2)(-e)} \left(-\frac{q^2}{1}\right).$$

The first expression reflects the structure of mapping the effective 4-vertex, the second shows the factors in case of the $4\pi\gamma$ -vertex (see below).

By denoting the amplitudes we find a couple of mappings:

$$\begin{aligned}
 & \text{Diagram 1} = \alpha \left(\text{Diagram 2} + \text{Diagram 3} \right), \\
 & \text{Diagram 1: A bubble diagram with two vertices. The left vertex has incoming momentum k and outgoing momentum $p+k$. The right vertex has incoming momentum r and outgoing momentum $r+k$. The internal lines are dashed with arrows. The bottom-left internal line is labeled p , and the bottom-right internal line is labeled r . } \\
 & \text{Diagram 2: Similar to Diagram 1, but the internal lines are labeled p and r at the bottom, and q in the middle. } \\
 & \text{Diagram 3: A bubble diagram with two vertices. The left vertex has incoming momentum k and outgoing momentum $p+k$. The right vertex has incoming momentum r and outgoing momentum $r+k$. The internal lines are dashed with arrows. The bottom-left internal line is labeled p , and the bottom-right internal line is labeled r . The middle internal line is labeled q . } \\
 \end{aligned} \tag{5.27}$$

$$\begin{aligned}
 & \text{Diagram 1} = 2 \alpha \left(\text{Diagram 2} + \text{Diagram 3} \right), \\
 & \text{Diagram 1: A bubble diagram with two vertices. The left vertex has incoming momentum k and outgoing momentum $p+k$. The right vertex has incoming momentum r and outgoing momentum r . The internal lines are dashed with arrows. The bottom-left internal line is labeled p , and the bottom-right internal line is labeled p . } \\
 & \text{Diagram 2: Similar to Diagram 1, but the internal lines are labeled p and p at the bottom, and q in the middle. } \\
 & \text{Diagram 3: A bubble diagram with two vertices. The left vertex has incoming momentum k and outgoing momentum $p+k$. The right vertex has incoming momentum r and outgoing momentum r . The internal lines are dashed with arrows. The bottom-left internal line is labeled p , and the bottom-right internal line is labeled p . The middle internal line is labeled q . } \\
 \end{aligned} \tag{5.28}$$

$$\begin{aligned}
 & \text{Diagram 1} = \alpha \left(\text{Diagram 2} + \text{Diagram 3} \right), \\
 & \text{Diagram 1: A bubble diagram with two vertices. The left vertex has incoming momentum k and outgoing momentum k . The right vertex has incoming momentum p and outgoing momentum p . The internal lines are dashed with arrows. The bottom-left internal line is labeled r , and the bottom-right internal line is labeled r . } \\
 & \text{Diagram 2: Similar to Diagram 1, but the internal lines are labeled r and r at the bottom, and q in the middle. } \\
 & \text{Diagram 3: A bubble diagram with two vertices. The left vertex has incoming momentum k and outgoing momentum k . The right vertex has incoming momentum p and outgoing momentum p . The internal lines are dashed with arrows. The bottom-left internal line is labeled r , and the bottom-right internal line is labeled r . The middle internal line is labeled q . } \\
 \end{aligned} \tag{5.29}$$

$$\begin{aligned}
 & \text{Diagram 1} = 2 \alpha \left(\text{Diagram 2} + \text{Diagram 3} \right), \\
 & \text{Diagram 1: A bubble diagram with two vertices. The left vertex has incoming momentum k and outgoing momentum k . The right vertex has incoming momentum p and outgoing momentum $p+k$. The internal lines are dashed with arrows. The bottom-left internal line is labeled r , and the bottom-right internal line is labeled r . } \\
 & \text{Diagram 2: Similar to Diagram 1, but the internal lines are labeled r and r at the bottom, and q in the middle. } \\
 & \text{Diagram 3: A bubble diagram with two vertices. The left vertex has incoming momentum k and outgoing momentum k . The right vertex has incoming momentum p and outgoing momentum $p+k$. The internal lines are dashed with arrows. The bottom-left internal line is labeled r , and the bottom-right internal line is labeled r . The middle internal line is labeled q . } \\
 \end{aligned}$$

$$\begin{aligned}
 & + \left(\text{Diagram 1} + \text{Diagram 2} \right), \\
 & \text{Diagram 1: A wavy line with momentum } k \text{ enters from the left, splits into two wavy lines with momenta } q \text{ and } p+k \text{, which then recombine into a wavy line with momentum } k \text{ exiting to the right. A dashed loop with momenta } p \text{ and } p+k \text{ connects the two vertices.} \\
 & \text{Diagram 2: A wavy line with momentum } k \text{ enters from the left, splits into two wavy lines with momenta } p+k \text{ and } p \text{, which then recombine into a wavy line with momentum } k \text{ exiting to the right. A dashed loop with momenta } q \text{ and } p \text{ connects the two vertices.}
 \end{aligned} \tag{5.30}$$

and

$$\begin{aligned}
 & \text{Diagram 3} = 2\alpha \left(\text{Diagram 4} + \text{Diagram 5} \right). \\
 & \text{Diagram 3: A wavy line with momentum } k \text{ enters from the left, splits into two wavy lines with momenta } k \text{ and } k \text{, which then recombine into a wavy line with momentum } k \text{ exiting to the right. A dashed loop with momenta } p \text{ and } r \text{ connects the two vertices.} \\
 & \text{Diagram 4: A wavy line with momentum } k \text{ enters from the left, splits into two wavy lines with momenta } k \text{ and } q \text{, which then recombine into a wavy line with momentum } k \text{ exiting to the right. Two dashed loops with momenta } p \text{ and } r \text{ connect the two vertices.} \\
 & \text{Diagram 5: A wavy line with momentum } k \text{ enters from the left, splits into two wavy lines with momenta } k \text{ and } k \text{, which then recombine into a wavy line with momentum } k \text{ exiting to the right. A dashed loop with momenta } p \text{ and } r \text{ connects the two vertices.}
 \end{aligned} \tag{5.31}$$

The left side shows all diagrams of the effective theory in $e^2 g^2$ including all symmetry factors. The right sides are diagrams in sQED. They do *not* contain multiplicities and symmetry factors. They represent the amplitudes one obtains by denoting propagators and Feynman rules. In the proof of the WI for sQED the same meaning of a diagram is employed. (see also last section.)

From the results on the right side of the identities, four body diagrams are extracted:

$$\begin{aligned}
 & \text{Diagram 1} \quad \text{Diagram 2} \\
 & \text{Diagram 1: A wavy line with momentum } k \text{ enters from the left, splits into two wavy lines with momenta } k \text{ and } k \text{, which then recombine into a wavy line with momentum } k \text{ exiting to the right. A dashed loop with momenta } p \text{ and } r \text{ connects the two vertices.} \\
 & \text{Diagram 2: A wavy line with momentum } k \text{ enters from the left, splits into two wavy lines with momenta } k \text{ and } k \text{, which then recombine into a wavy line with momentum } k \text{ exiting to the right. A dashed loop with momenta } p \text{ and } r \text{ connects the two vertices.}
 \end{aligned} \tag{5.32}$$

and

$$(5.33)$$

It is obvious that the diagrams on the righthand side of the identities are insertion diagrams of these four body diagrams. This is demonstrated in an example: Consider **1** of (5.32).

- If we insert a photon on the righthand side we have the second term of (5.27).
- If we insert the photon at the endpoints of the intermediate photon we transform the 3-vertices into 4-vertices. We obtain the third plus fourth diagram of (5.30). Note, however, the multiplicity of 2 in front of (5.30). Therefore we have only identified *the half* of this term so far.
- If we insert the photon at the 3-vertex of the external photon of **1**, we gain the second term on the righthand side of (5.29)
- There are only two possible insertion points missing, to the left and to right of the 3-vertex of the external photon in **1**. Fortunately, we have a double contribution of (5.28) due to the multiplicity 2α .
- The insertion process of **1** is completed. We know that the sum over these insertion point diagrams vanishes. But so far we have only used the half of term 3 and 4 of (5.30). Furthermore, the second term of (5.31) is not identified so far.
- Inserting photons in the *second* diagram **2** shows that both leftovers are identified with the possible insertions.

The reader is urged make sure that the first terms of the identities (5.27) to (5.31) are insertion diagrams of the two non-1PI diagrams **3** and **4**.

We have shown that the sum of all diagrams of the effective theory in the order $e^2 g^2$ is proportional to the sum over the insertion diagrams of four body diagrams. From the proof of the Ward Identity we know that the sum over insertion diagrams of a loop body diagram vanishes if multiplied by the external photon momentum k_μ .

We have proven that the set of diagrams we use to calculate the charge fluctuations in the order $e^2 g^2$ is charge conserving.

The other way round, the method of mapping the effective diagrams into sQED provides a helpful tool in order to construct higher order sets of self energy diagrams which are automatically charge conserving! Just draw a set of body diagrams and insert photons in every possible way, then translate the diagrams back by shrinking the appropriate photon lines into effective interactions. In particular, the method might be applied in problems concerning the charge conservation in resummations.

The Mouse and the Propeller Diagrams

Our proof is valid in full extend, but we want at least show the cancellation behavior of the *Mouse* and the *Propeller* diagram in the amplitudes directly.

For the *Propeller* diagram in Fig. A.9 follows the amplitude (A.64) which is multiplied by the external momentum:

$$\begin{aligned}
 q_\mu \Pi^{\mu\nu} &= q_\mu \frac{8e^2 g^2}{m_\rho^2} g^{\mu\nu} \int \frac{d^4 k}{(2\pi)^4} \frac{d^4 p}{(2\pi)^4} \frac{1}{k^2 - m_\pi^2} \frac{1}{p^2 - m_\pi^2} \\
 &= \frac{8e^2 g^2}{m_\rho^2} \int \frac{d^4 k}{(2\pi)^4} \frac{d^4 p}{(2\pi)^4} \frac{q^\nu}{(k^2 - m_\pi^2)(p^2 - m_\pi^2)}.
 \end{aligned} \tag{5.34}$$

For the *Mouse* diagram in Fig. A.8 the amplitude (A.60) follows which is multiplied by the external momentum:

$$\begin{aligned}
 q_\mu \Pi^{\mu\nu} &= -\frac{8e^2 g^2}{m_\rho^2} \int \frac{d^4 k}{(2\pi)^4} \frac{d^4 p}{(2\pi)^4} \frac{q(2k + 2p + q)(2p + q)^\nu}{(k^2 - m_\pi^2)(p^2 - m_\pi^2)((p + q)^2 - m_\pi^2)} \\
 &= -\frac{8e^2 g^2}{m_\rho^2} \int \frac{d^4 k}{(2\pi)^4} \frac{d^4 p}{(2\pi)^4} \left(\frac{(2p + q)^\nu}{(k^2 - m_\pi^2)(p^2 - m_\pi^2)} - \frac{(2p + q)^\nu}{(k^2 - m_\pi^2)((p + q)^2 - m_\pi^2)} \right) \\
 &= -\frac{16e^2 g^2}{m_\rho^2} \int \frac{d^4 k}{(2\pi)^4} \frac{d^4 p}{(2\pi)^4} \frac{q^\nu}{(k^2 - m_\pi^2)(p^2 - m_\pi^2)}.
 \end{aligned} \tag{5.35}$$

The half of the result of the *Mouse* diagram cancels the *Propeller* diagram. This is exactly the way we have argued above, when we split the *Mouse* diagram between the second body diagrams of (5.32) respectively (5.33).

Chapter 6

Numerical Results and Outlook

6.1 Entropy in g^2

The entropy for a free Bose Gas has been readily evaluated with the result (2.11) (where the result (2.11) has to be multiplied by three in a Boson gas). The remaining task is to calculate corrections to the entropy. It is sufficient to expand the entropy in terms of the strong coupling g . The leading order term is the 8-shaped diagram of Fig. 2.36, with an effective 4-pion-interaction vertex.

The amplitude of Fig. 2.36 is

$$\log Z_1 = \frac{g^2}{m_\rho^2} \beta V T^2 \sum_{\substack{p_0=-\infty, \dots, +\infty \\ k_0=-\infty, \dots, +\infty}} \int \frac{d^3 \mathbf{p}}{(2\pi)^3} \frac{d^3 \mathbf{k}}{(2\pi)^3} \left(-\frac{1}{p_0^2 - \eta^2} \right) [(4p_0 k_0) - (4\mathbf{p}\mathbf{k}) + (p_0 + k_0)^2 - (\mathbf{p} + \mathbf{k})^2] \left(-\frac{1}{k_0^2 - \omega^2} \right). \quad (6.1)$$

If we take into account that several angle integrations and sums over terms linear in p_0 or k_0 vanish (see (A.49) and (2.46)) this is equal to

$$\log Z_1 = 2 \frac{g^2}{m_\rho^2} \beta V \left(T \sum_{p_0=-\infty}^{\infty} \frac{d^3 \mathbf{p}}{(2\pi)^3} \frac{p_0^2 - \mathbf{p}^2}{p_0^2 - \eta^2} \right) \left(T \sum_{k_0=-\infty, \dots, +\infty} \int \frac{d^3 \mathbf{k}}{(2\pi)^3} \frac{1}{k_0^2 - \omega^2} \right). \quad (6.2)$$

Obviously we have a convergence problem here. It is therefore necessary to introduce a convergence preserving exponential that equals 1 in the limit. This limit is then taken after the summation, leading to the same result as if we had calculated carelessly. Compare Fetter–Walecka [27], (25.32) – (25.35).

The solution of this is, clockwise integration taken into account,

$$\log Z_1 = \frac{1}{2} \left(\frac{m_\pi}{m_\rho} \right)^2 \beta V g^2 D^2. \quad (6.3)$$

Using the definition of D , (2.10) and integrating by parts leads to

$$S_1(\beta) = \beta V \left(\frac{m_\pi}{m_\rho} \right)^2 g^2 D(C + D). \quad (6.4)$$

6.2 Numerical Results for the Charge Fluctuations per Entropy

The proof of the Ward identity in the last chapter for the high mass limit in the order $e^2 g^2$ ensures that all diagrams contribute to the charge fluctuations with the correct relative signs and coefficients. It is now possible to calculate some numerical results.

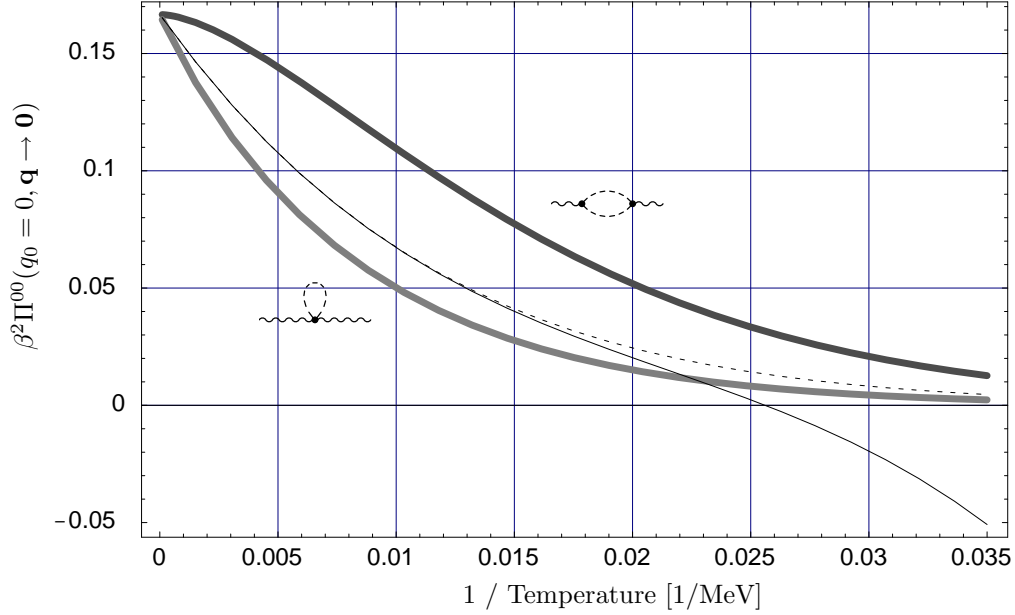


Figure 6.1: High temperature behavior of the bubble and the tadpole diagrams in sQED

6.2.1 The Tadpole Diagram and the Simple Bubble

Since all occurring diagrams can be expressed by the simple diagrams 4.9 and Fig 4.10, either directly or by a derivative in respect of β , it is sufficient to investigate the tadpole and the bubble diagram of sQED.

For details see B.1.

The High Temperature Limit

The dependency of both diagrams is shown in Fig 6.1. The thick black line represents the bubble C , the thick gray line the tadpole diagram D . The thin dashed line shows the high temperature fit (6.5), the thin solid line displays the simpler fit (6.6). The graphs are multiplied by the square of the inverse temperature β^2 which reveals their quadratic asymptotic behavior. Both diagrams seem to coincide for high temperatures. But note, that even differences linearly rising with T would disappear in this representation. And indeed, there is a linearly growing discrepancy $(C - D)$ as T is increased.

Both the integrals C and D are not analytically solvable. Therefore, we try to fit the integrals in the high- and low-temperature regime in order to investigate the asymptotic behavior. It is

$$D = \frac{1}{\pi^2} \int_{m_\pi}^{\infty} d\eta \frac{\sqrt{\eta^2 - m_\pi^2}}{e^{\beta\eta} - 1}.$$

If we set $\beta \ll 1$ and inspect high values of η , the denominator is still close to 0, increasing the influence of the squareroot in the numerator of D . There, the pion mass can be omitted for $\eta \gg 139$. This does not hold any longer for small values of η that always appear in the integration. But the resulting solution

of the simplified integral

$$D \simeq \frac{1}{\pi^2} \int_{m_\pi}^{\infty} d\eta \frac{\eta}{e^{\beta\eta} - 1} = \frac{1}{\pi^2} \frac{2\pi^2 + 3 m_\pi^2 \beta^2 - 6 m_\pi \beta \log [1 - e^{m_\pi \beta}] - 6 \text{Polylog} [2, e^{m_\pi \beta}]}{6 \beta^2} \quad (6.5)$$

fits surprisingly well regarding the fact that the omission of the pion mass in squareroot leads to a totally different shape of the integrand at $p \simeq m_\pi$.

In order to obtain a fit containing simpler functions, we perform a Taylor expansion of the numerator of (6.5) at $\beta = 0$. Note here that

$$\lim_{\beta \rightarrow 0} \left[3 m_\pi^2 \beta^2 - 6 m_\pi \beta \log [1 - e^{m_\pi \beta}] - 6 \text{Polylog} [2, e^{m_\pi \beta}] \right] = -\pi^2.$$

The expansion is cut after the third order and the result

$$\chi(\beta) = \frac{1}{\pi^2} \left(\frac{\pi^2}{6 \beta^2} - \frac{m_\pi}{\beta} + \frac{m_\pi^2}{4} - \frac{m_\pi^3 \beta}{36} [+O(\beta^2)] \right) \quad (6.6)$$

is shown in Fig. 6.1. There is no fit included for C . A fit for that function would have the same leading term, but due to the linearly with T increasing term ($C - D$) there occurs a correction to the next-to-leading-order term $-\frac{m_\pi}{\beta}$. Nevertheless, both fits reflect the correct high temperature limit of

$$\boxed{C \sim D \sim \frac{1}{6} T^2 + \mathcal{O}(T) \ (T \rightarrow \infty)} \quad (6.7)$$

There is no dependency on the mass, as one expects at high temperatures.

Low temperature Behavior

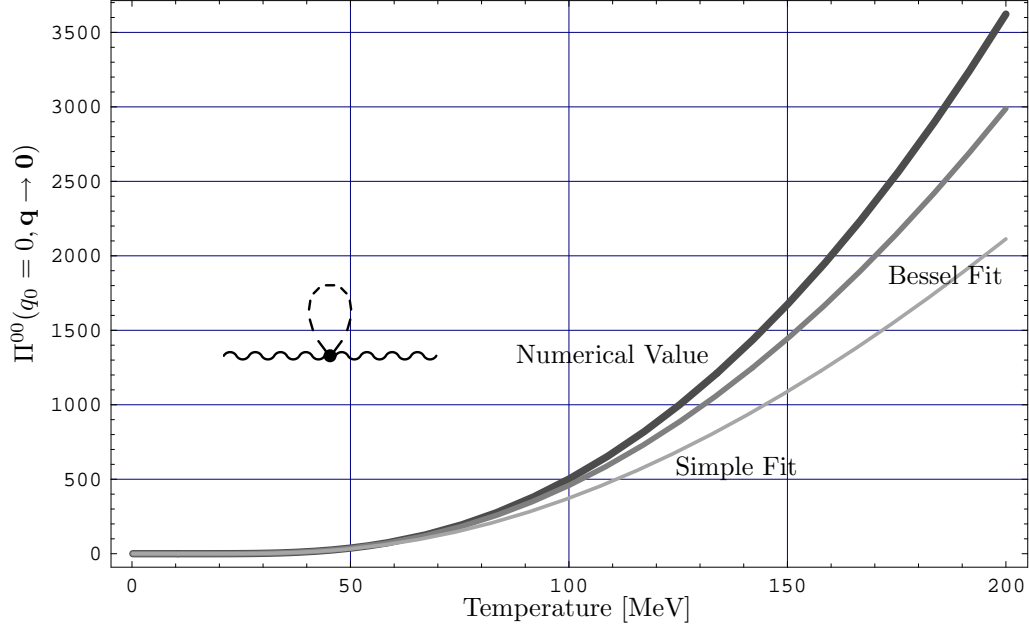
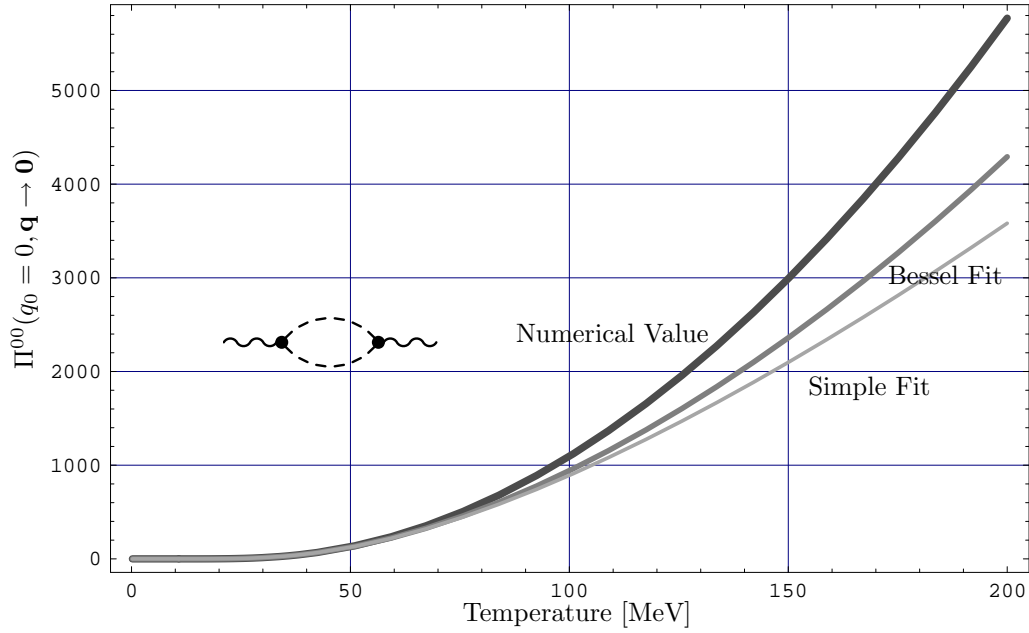
Since we calculated the pure matter part of all self energies (containing the maximum number of Bose factors of 2), we expect the contribution to vanish in the low temperature limit. Indeed, this is the case: The result for the tadpole diagram is shown in Fig 6.2, the bubble diagram values are shown in 6.3. Note in both cases the quadratic high temperature slope, but also the strong suppression at very small temperatures.

Both figures show the numerical result in the thick black line, the fit including the Bessel function in thick medium gray and the approximation of the Bessel function in thin light gray. Note that both fits in both cases give good values even above $T = 50 \text{ MeV}$.

The derivation of the fits are found in the appendix A.7. In the low temperature limit, the tadpole and the bubble diagrams obtain different fits. The results are:

Kind of Fit	Tadpole D	Bubble C
Limit $T \rightarrow \infty$	0	0
Mass Fit	$\frac{m_\pi}{\pi^2} T K_1 \left[\frac{m_\pi}{T} \right]$	$\frac{m_\pi}{\pi^2} T \left(K_1 \left[\frac{m_\pi}{T} \right] + \frac{m_\pi}{T} K_0 \left[\frac{m_\pi}{T} \right] \right)$
Mass Fit Approx.	$\sqrt{\frac{m_\pi}{2}} \left(\frac{T}{\pi} \right)^{\frac{3}{2}} e^{-\frac{m_\pi}{T}} [1 + \mathcal{O}(T/m_\pi)]$	$\sqrt{\frac{m_\pi T}{2\pi^3}} e^{-\frac{m_\pi}{T}} (m_\pi + T) [1 + \mathcal{O}(T/m_\pi)]$
$m_\pi = 139 \text{ MeV}$	$e^{-\frac{m_\pi}{T}} T^{\frac{3}{2}} (1.419 + 0.00592 T) + 0.085 e^{-0.0009(10.5+T)^2}$	$e^{-\frac{m_\pi}{T}} \sqrt{\frac{T}{m_\pi^3}} (m_\pi + T) [2047 + 567 e^{-0.000529(25+T)^2} + 9.7 T]$

The fits of the second line represent the solution of a simplified integral of D respectively C . In the third line, the limiting behavior of the Bessel functions K_0 and K_1 is employed. The last line displays

Figure 6.2: Low temperature behavior of the tadpole diagram D Figure 6.3: Low temperature behavior of the bubble diagram C

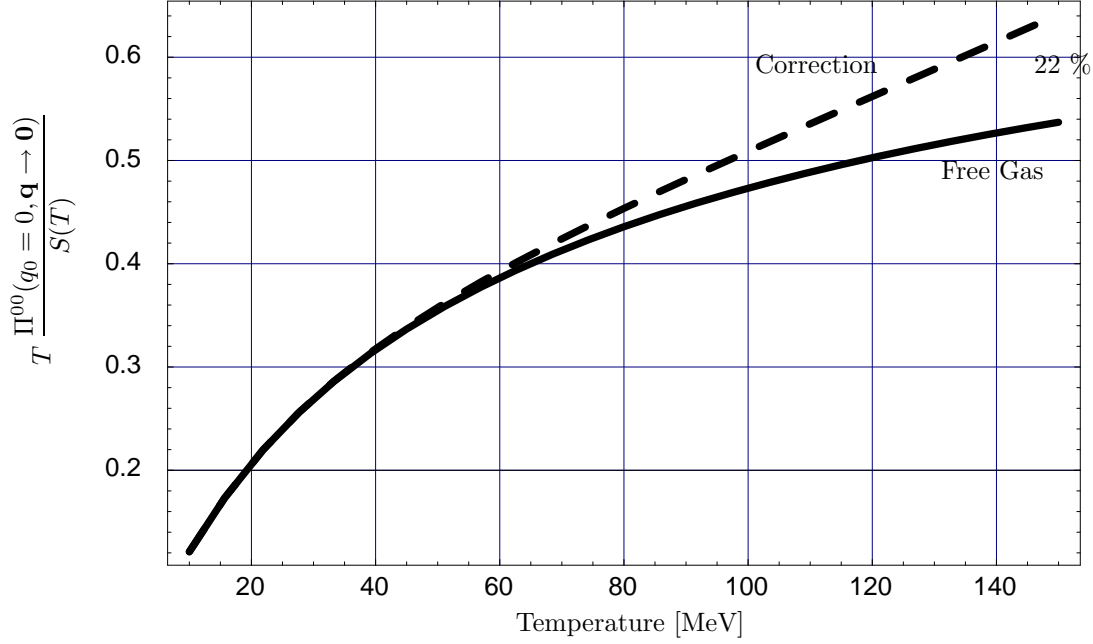


Figure 6.4: Correction to the Charge Fluctuations per Entropy in the Effective Model at the Two Loop Level (without π^0)

fits that were found at the *actual* mass of the pion. Those are the most precise ones ($< 1/1000$ relative error in the range $T \in [0, 140]$ MeV), but they do not contain the mass dependency any more.

The expected $T^{\frac{3}{2}}$ -dependency is clearly visible, however, there is an additional exponential suppression.

6.3 Charge Fluctuations per Entropy

We are ready to evaluate the sum (5.22) for the processes without π^0 . The integral resulting from the derivative with respect to β is solved separately. The result is shown in Fig. 6.4. Since the 0-order contributions $S_0 \sim T^3$ and $\Pi^{00}(q_0 = 0, \mathbf{q} \rightarrow \mathbf{0}) \sim T^2$, the charge fluctuations of the free Bose gas

$$\langle \delta \hat{Q}^2 \rangle = TV \left(\Pi_{0 \text{ mat}}^{00}(k_0 = 0, \mathbf{k} \rightarrow \mathbf{0}) \right), \quad (6.8)$$

divided by the (non-interaction) entropy, reach the constant value

$$\frac{\langle \delta \hat{Q}^2 \rangle_0}{S_0} \xrightarrow{T \rightarrow \infty} 0.76$$

in the high temperature limit. This value already includes the presence of two species of charged particles π^+ and π^- . If the result is divided by 3 (entropy!) and the multiplied by 16, we obtain $D_{\text{CF}} \simeq 4.053$ as $T \rightarrow \infty$ in full consistency with the previous result in section 2.2.2. At 150 MeV the correction is some 22%.

However, since $\Pi_{1 \text{ mat}}^{00}(k_0 = 0, \mathbf{k} \rightarrow \mathbf{0}) \sim T^4$, $S_0 \sim T^3$ and $S_1 \sim T^3$, the correction rises quadratically. Though, this behavior becomes visible at higher temperature only. The limiting behavior of the charge

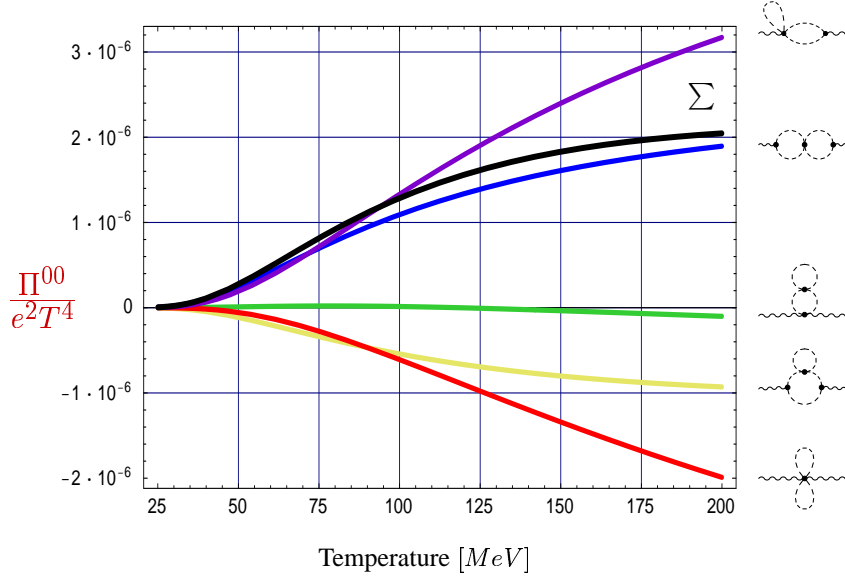


Figure 6.5: Contribution of the different diagrams

fluctuations per entropy, both in effective interaction, is

$$\frac{\langle \delta \hat{Q}^2 \rangle}{S} \xrightarrow{T \rightarrow \infty} 6.695 \cdot 10^{-6} T^2.$$

Both values have been evaluated by using the result (2.11) for the free entropy and (5.24)

In Fig. 6.5 the contribution of the different diagrams is shown. The black line is the sum of all contributions. In Fig. 6.6, the same is displayed but for high values of T . Both diagrams are normalized by T^4 .

Figure 6.7 shows a comparison of the self energy in the effective model with the results of Kapusta *et al.* [30]. There, the electrical mass is calculated and $m_{el}^2 = \Pi^{00}(q_0 = 0, \mathbf{q} \rightarrow \mathbf{0})$.

The curve for the free boson gas matches exactly our result. The chiral expansion shows a high rise in comparison with the two other models. The second model in [30] is a relativistic virial expansion. The fact is used, that the pressure of an interacting pion gas is nearly identical to the sum of the pressures of an ideal pion gas plus (Maxwellian) ρ -mesons up to rather large values of the temperature (indicated with " $\rho + \pi$ " in Fig. 6.7).

As the last result we want to show the Charge fluctuations per entropy, *including* the neutral pion π^0 . The result is shown in Fig. 6.8. The solid line again shows the free gas result, whereas the dashed line shows the correction by π^\pm interactions, identical with Fig. 6.4. The narrow dashing shows the correction if the processes of $\pi^0 - \pi^\pm$ -mixing are taken into account as well. The plot shows values up to 350 MeV for the entertainment of the reader since there is now significant contribution up to values of 150 MeV.

In order to see the influence of the correction we show the ratios (S_1/S_0) and (Π_1/Π_0) of the corrections with respect to free gas values in Fig. 6.9 (again, π^0 not included).

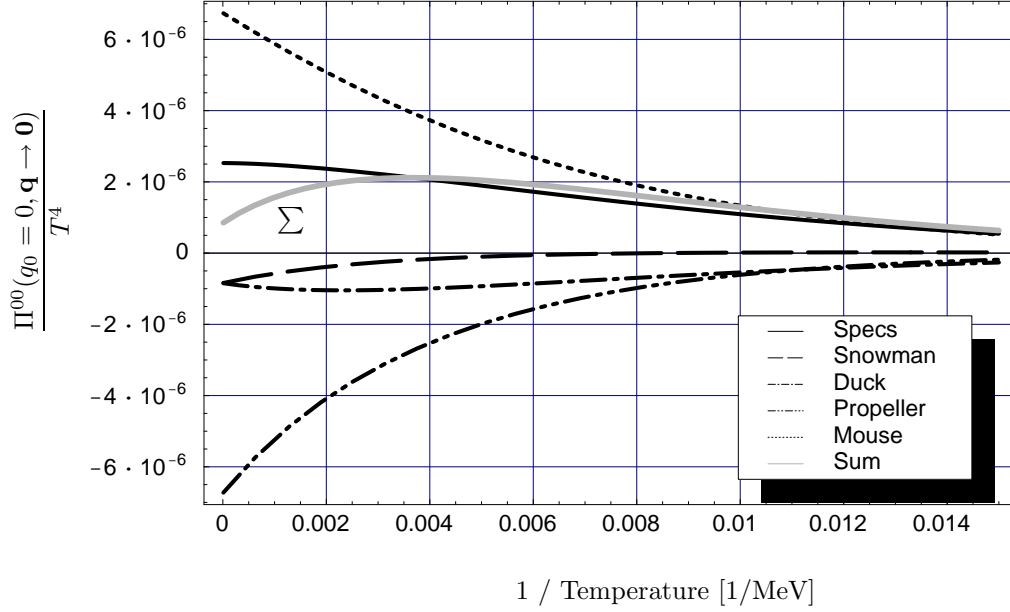


Figure 6.6: Contribution of the diagrams at high temperatures, normalized by T^4 . The sum of all diagrams is depicted in light gray.

6.4 The ρ -meson at Finite Mass

In the last chapter we derived a

$$\boxed{\text{correction of 22\%}}$$

(6.9)

to the charge fluctuation. This is a rather large value in the leading order $e^2 g^2$. Therefore, it is necessary to investigate further. This can be either approached by performing resummations of diagrams although current conservation becomes questionable. Furthermore, the ρ -mass can be set to its actual value of $m_\rho = 770$ MeV. In the order $e^2 g^2$, a new set of diagrams arises. A subset is shown in Fig. 6.10. Besides those shown there, the $2\pi 2\rho$ -vertex becomes relevant which we calculated at the beginning of this thesis but omitted, since it would lead to two-loop diagrams with only one Bose-factor, and those contributions are absorbed in the renormalization constants of the vacuum as discussed above.

Furthermore, the ρ -meson will obtain $\rho\gamma$ -interaction in the gauging process. In Fig. 6.10, only those diagrams are shown which contain the $\rho\pi\pi$ -vertex and its gauged equivalent. Diagram ⑧ and ⑩ can be calculated with not much more effort than the diagrams of the effective theory in (4.21) since the undetermined loop momenta factorize. Diagram ⑦ will not contribute at all since the ρ -meson carries no momentum. The diagrams that cause trouble are ⑤, ⑥ and ⑨. There, the two loop momenta *must* necessarily flow along the same line at one point, independent from the momentum assignment. They do not factorize. This leads to considerable difficulties which were the reason why to choose the effective model.

- Two Matsubara sums have to be performed. After performing the first one (let (ω, \mathbf{p}) be energy and momentum of the first summation / integration), the poles of the remaining loop amplitude (we assign (η, \mathbf{k})) depends on the energy ω of the first momentum. Since there is still the integration over \mathbf{p} , the poles start wandering in the k_0 -plane. That means, they can not only hit the integration

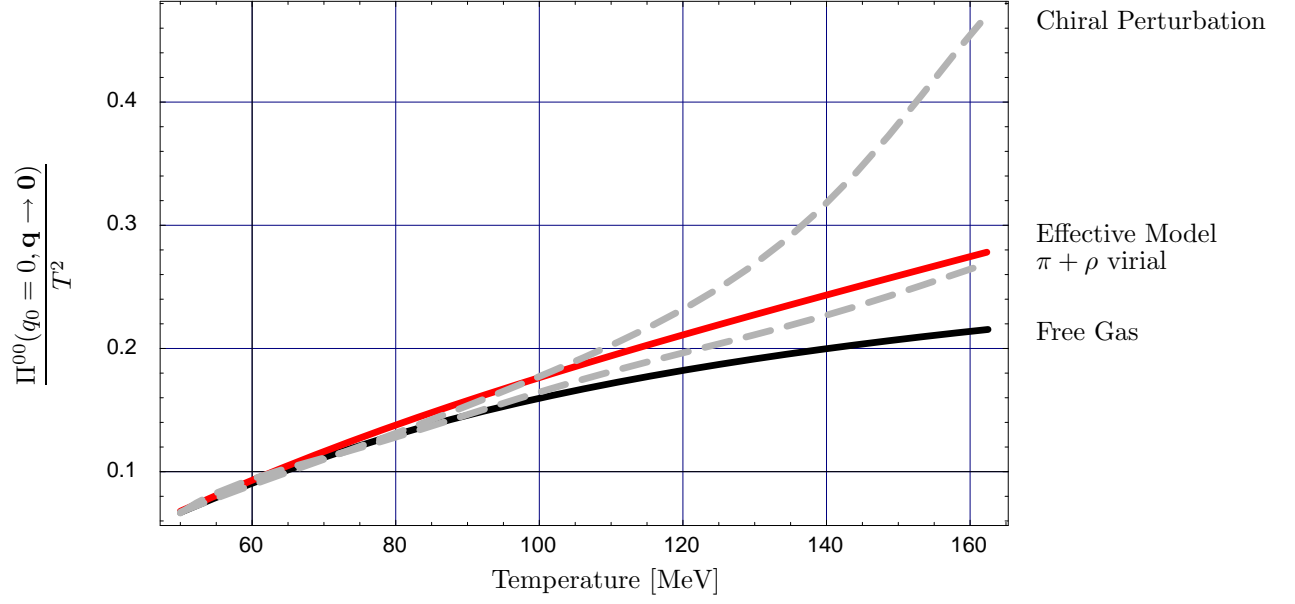
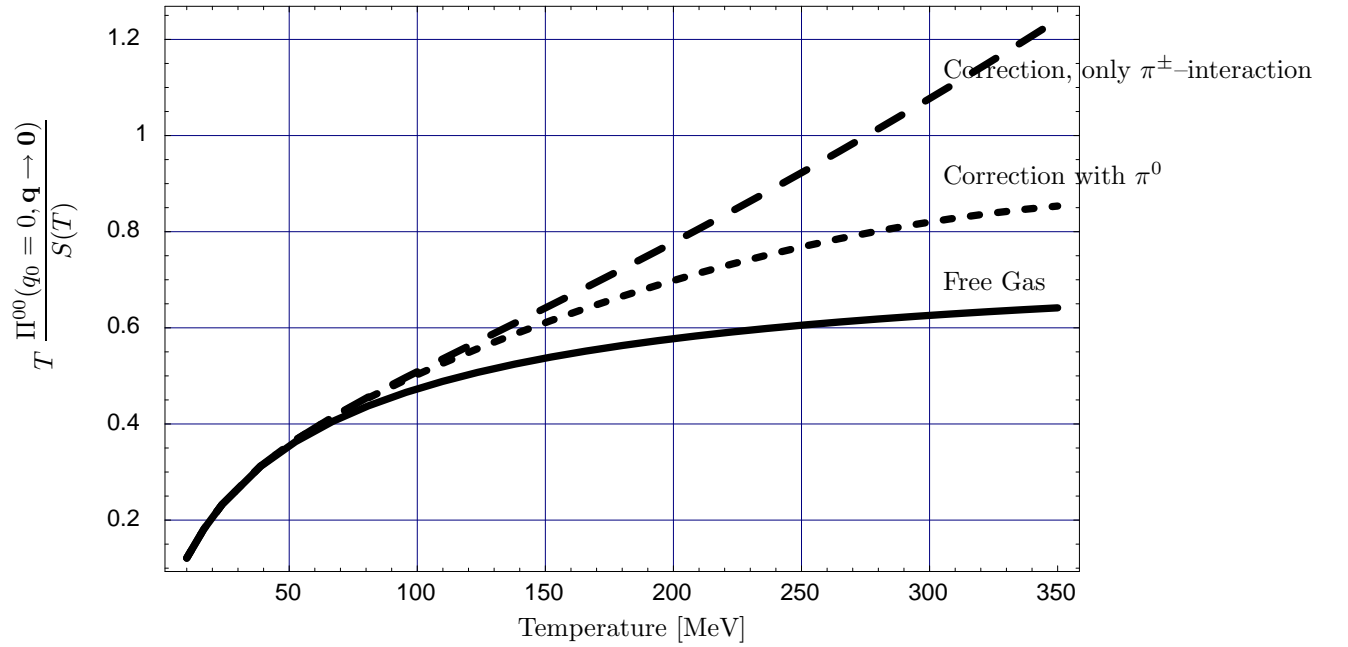


Figure 6.7: Comparison of our results with Kapusta et al. [30]

Figure 6.8: Correction to the Charge Fluctuations per Entropy in the Effective Model at the Two Loop Level (narrow Dashing: Process including π^0)

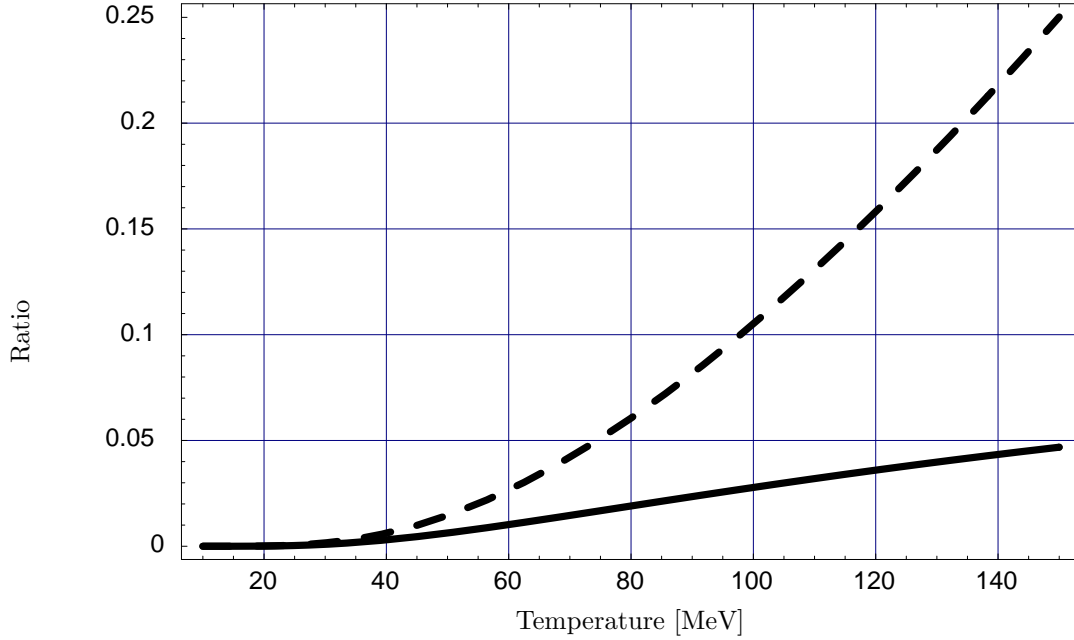


Figure 6.9: Ratios of corrections to free values; solid: entropy, dashed: self energy, processes with π^0 not included.

contour of the second Matsubara summation at one point, but also *leave* the right k_0 half plane. Then, the integration over \mathbf{k} must be performed by case distinction, since the integrand changes for certain values of the first integration over \mathbf{p} .

However, in the calculations it has been shown that those poles which leave the integration region of the right half plane at some point are fortunately all cancelled by other poles with same behavior.

- If in the static limit three poles coincide as it is the case in diagram ⑥, singularities of third order occur at finite values of the momentum \mathbf{k} . Those diverge when being evaluated by using the Cauchy principle value. Third order singularities are only finite within Cauchy principle value, if the second derivative of the denominator vanishes as it could be shown. Instead, one has to investigate carefully in the $+i\epsilon$ -prescription of the pion propagators. This has been omitted in this thesis completely because no singularities of this type occurred so far. Moreover, in our calculations we closed the integration contour far away from the poles so that this subtlety of *vacuum* field theory was irrelevant. In fact, one has to apply a finite value of ϵ . Then, the singularities are fitted better and better as $\epsilon \rightarrow 0$ as we could already find out, and the integral over this fitting function is indeed finite.

Diagram ⑤ and ⑥ have been reduced to a set of some 30 1-d-integrals each, some of them containing singularities as discussed above. After this reduction was achieved (which took about half the time of this thesis), it was not clear whether the current was conserved and a check of the result was hardly possible. Then the effective model was chosen, which could be solved in the order $e^2 g^2$. Since we have the effective behavior of the self energy, we can check the the results at finite ρ -mass by letting $m_\rho \rightarrow \infty$. This work is in progress.

In order to investigate diagrams with finite ρ -mass, the best strategy will be to have a simple comparison with the effective model. We can evaluate diagram ⑧ with not much more effort as the *Specs*

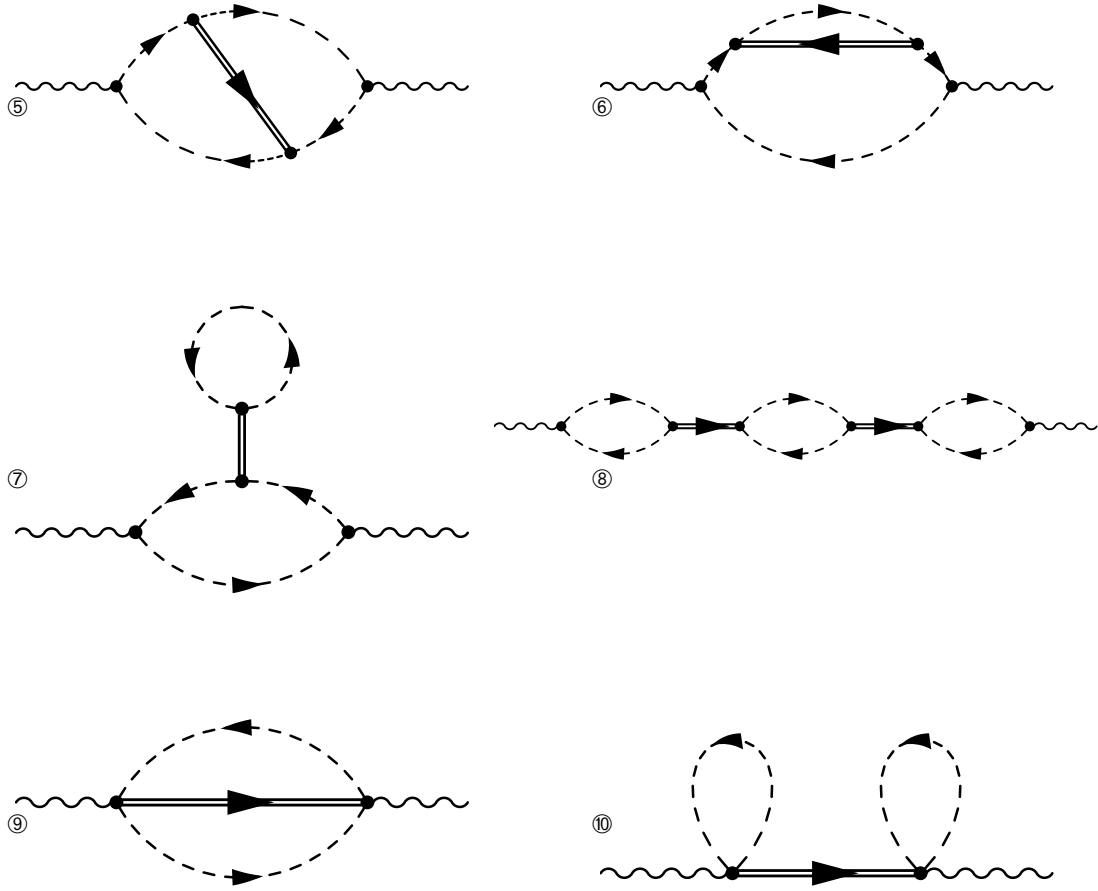


Figure 6.10: Overview of diagrams in $e^2 g^2$ at finite ρ -Mass (Chain diagram with one additional bubble), not including diagrams with $\gamma\rho$ -coupling or $2\rho 2\pi$ vertices.

diagram. Even the resummation of the *Specs* diagram can be performed at finite ρ -mass as well. All four results should be plotted and compared.

Chapter 7

Summary and Conclusions

Charge fluctuation was motivated as a possible signature for the existence of the Quark Gluon Plasma. An estimate for the fluctuation in a pion gas and the Quark Gluon Plasma showed the sensitivity of the quantity D on fractional charges and hence the QGP.

In order to investigate the enhancement or suppression of charge fluctuations in the hadronic phase, a pion gas including an interaction via the ρ -meson was considered. We constructed an effective Lagrangian with the constraint $m_\rho \rightarrow \infty$. For this, Ward–Takahashi identities for 2- and 4-point functions were found in sQED and in the effective theory. The simpler $\lambda(\phi\phi^*)^2$ -theory served as a link in different respects, since it shows direct interaction but without derivative couplings as in the effective theory.

The charge fluctuations were related to self energy diagrams in the static limit. This required the tool of finite temperature field theory. In the expansion of the effective Lagrangian we investigated two-loop diagrams in the leading order e^2g^2 . We constructed a set of five diagrams in a charge conserving way. The self energy has been calculated in the infrared limit and has been expressed in terms of simple self energy diagrams in e^2 . It has been shown that the infrared limit can be taken before the summation of Matsubara frequencies and before momentum integration.

The charge conservation of the set was shown by mapping the diagrams into scalar QED and exploiting the simpler properties of this theory. This is a completely new approach that corresponds to a considerable simplification in the proof of current conservation. It can also be used in order to construct sets of current conserving diagrams.

The result shows an enhancement of the charge fluctuations of about 20% at 150 MeV. This value is still within the range of other effects as the expected influence of resonances. The comparison with the literature in [30] shows that the result lies within the range of other predictions. However, this thesis is the first work in which the Ward–Takahashi–Identities are explicitly checked, which is a crucial point in the evaluation of charge fluctuations.

The relatively high correction of the charge fluctuations of about 20% gives rise to the question whether higher order corrections have to be taken into account. The attempts to perform resummations, which were touched upon in this thesis, will have to be extended. Solutions of the *Bethe–Salpeter equation* (which relates propagators to resummed interactions [27]) have to be sought. It would also be very promising to evaluate the charge fluctuations in the hadronic phase on the lattice.

In addition, the question at which temperatures the assumption of an effective interaction is tenable should be further investigated. There is an upper limit beyond which the Bose distribution no longer suppresses momenta transfers close to the mass of the ρ -meson. Therefore, the ρ -meson will have to be thermalized. This requires the calculation of non-factorizing two-loop diagrams. So far, the resulting terms have been reduced to a set of 1-d-integrals, which have to be solved numerically.

Appendix A

Details of Calculations

A.1 Motivation of the Path Integral

The Tr operation in the definition of the partition function needs to be performed over a complete set of states. We are therefore interested in the transition amplitude

$$\langle \phi_a | e^{-i\hat{H}t_f} | \phi_a \rangle \quad (\text{A.1})$$

from the state ϕ_a at time $t = 0$ back to ϕ_a after some time t_f .

Let $\hat{\phi}(\mathbf{x}, 0)$ be a Schrödinger-picture field operator at the time $t = 0$ and let $\hat{\pi}(\mathbf{x}, 0)$ its conjugate momentum operator. With the eigenstates of the field operators $|\phi\rangle$ and eigenvalues $\phi(\mathbf{x})$ ("wave functions") we have

$$\hat{\phi}(\mathbf{x}, 0)|\phi\rangle = \phi(\mathbf{x})|\phi\rangle.$$

The eigenstates $|\phi(\mathbf{x})\rangle$ obey the completeness and orthogonality relations

$$\int d\phi(\mathbf{x})|\phi\rangle\langle\phi| = \mathbf{1} \quad \text{and} \quad \langle\phi_a|\phi_b\rangle = \delta[\phi_a(\mathbf{x}) - \phi_b(\mathbf{x})], \quad (\text{A.2})$$

where the integral is over a complete set of fields.

Similarly, the eigenstates of the conjugate momentum field operator $|\pi\rangle$ (not to be mixed with the pion fields π^\pm, π^0) satisfy

$$\hat{\pi}(\mathbf{x}, 0)|\pi\rangle = \pi(\mathbf{x})|\pi\rangle.$$

The completeness relation (normalized by 2π) and the orthogonality are

$$\int d\pi(\mathbf{x})|\pi\rangle\langle\pi| = 2\pi \quad \text{and} \quad \langle\pi_a|\pi_b\rangle = \delta[\pi_a(\mathbf{x}) - \pi_b(\mathbf{x})]. \quad (\text{A.3})$$

The factor of 2π in the completeness relation for the π 's results from the Fourier transform.

The overlap between eigenstates of the position and the momentum operator in quantum mechanics is

$$\langle x|p\rangle = e^{ipx}. \quad (\text{A.4})$$

In field theory, the overlap is

$$\langle\phi|\pi\rangle = e^{i\int d^3\mathbf{x} \pi(\mathbf{x})\phi(\mathbf{x})}. \quad (\text{A.5})$$

This formula from [12] deserves an explanation: In quantum mechanics we obtain $\langle x|p\rangle = e^{ipx}$ from the integration of

$$i\frac{\partial}{\partial x} \langle x|p\rangle = \langle x|\hat{p}|p\rangle = p\langle x|p\rangle.$$

For the proof of (A.5) we have to show the field theoretical analog

$$i \frac{\delta \langle \phi(\mathbf{x}) | \pi(\mathbf{x}) \rangle}{\delta \phi(\mathbf{x})} = \pi(\mathbf{x}) \langle \phi(\mathbf{x}) | \pi(\mathbf{x}) \rangle.$$

With

$$I = I(f) = \int dx f(x) w(x) \quad (\text{A.6})$$

the functional derivative is defined as

$$\frac{\delta I(f)}{\delta f}(y) := w(y). \quad (\text{A.7})$$

Here, we have

$$I(f) := e^{\int dx f(x) w(x)}$$

and therefore

$$\frac{\delta I}{\delta f}(y) = w(y) e^{\int dx f(x) w(x)}.$$

Let now $w(x) = \pi(x)$ and $f(x) = \phi(x)$ and (A.5) follows.

As (A.4) is the relation for a single particle, we now have to integrate over the complete field which contains infinitely many degrees of freedom.

With the Hamilton density defined by

$$\hat{H} = \int d^3 \mathbf{x} \mathcal{H}(\hat{\pi}, \hat{\phi}) \quad (\text{A.8})$$

we have all necessary tools to evaluate (A.1). The time interval $(0, t_f)$ is divided in N equal steps of duration $\Delta t = t_f/N$ in order to linearize the exponential in (A.1). Alternating at each time interval, the completeness relations for $|\phi\rangle$ (A.2) and for $|\pi\rangle$ (A.3) are inserted:

$$\begin{aligned} \langle \phi_a | e^{-i\hat{H}t_f} | \phi_a \rangle &= \lim_{N \rightarrow \infty} \int \left(\prod_{i=1}^N \frac{d\pi_i d\phi_i}{2\pi} \right) \\ &\quad \langle \phi_a | \pi_N \rangle \langle \pi_N | e^{-i\hat{H}\Delta t} | \phi_N \rangle \langle \phi_N | \pi_{N-1} \rangle \\ &\quad \langle \pi_{N-1} | e^{-i\hat{H}\Delta t} | \phi_{N-1} \rangle \cdots \\ &\quad \langle \phi_2 | \pi_1 \rangle \langle \pi_1 | e^{-i\hat{H}\Delta t} | \phi_1 \rangle \langle \phi_1 | \phi_a \rangle \end{aligned} \quad (\text{A.9})$$

We have already found the values for the overlaps

$$\langle \phi_1 | \phi_a \rangle = \delta(\phi_1 - \phi_a) \quad (\text{A.10})$$

and

$$\langle \phi_{i+1} | \pi_i \rangle = e^{i \int d^3 \mathbf{x} \pi_i(\mathbf{x}) \phi_{i+1}(\mathbf{x})}. \quad (\text{A.11})$$

Since $\Delta t \rightarrow 0$, we can now expand

$$\begin{aligned} \langle \pi_i | e^{-i\hat{H}\Delta t} | \phi_i \rangle &\sim \langle \pi_i | 1 - i\hat{H}\Delta t | \phi_i \rangle \\ &= (1 - iH_i\Delta t) \langle \pi_i | \phi_i \rangle \\ &\stackrel{(\text{A.5})}{=} (1 - iH_i\Delta t) e^{-i \int d^3 \mathbf{x} \pi_i(\mathbf{x}) \phi_i(\mathbf{x})} \end{aligned} \quad (\text{A.12})$$

with eigenvalue H_i as the integral over the eigenvalue density

$$H_i = \int d^3\mathbf{x} \mathcal{H}(\pi_{\mathbf{i}}(\mathbf{x}), \phi_{\mathbf{i}}(\mathbf{x})) \quad (\text{A.13})$$

(note: π_i and ϕ_i are not operators any more as in (A.8)). Therefore

$$\langle \pi_i | e^{-i\hat{H}\Delta t} | \phi_i \rangle \sim e^{-i \int d^3\mathbf{x} [\Delta t \mathcal{H}(\pi_{\mathbf{i}}, \phi_{\mathbf{i}}) + \pi_{\mathbf{i}}(\mathbf{x}) \phi_{\mathbf{i}}(\mathbf{x})]} \quad (\text{A.14})$$

We can evaluate (A.9) now:

$$\begin{aligned} \langle \phi_a | e^{-i\hat{H}t_f} | \phi_a \rangle &= \lim_{N \rightarrow \infty} \int \left(\prod_{i=1}^N \frac{d\pi_i d\phi_i}{2\pi} \right) \underbrace{\delta(\phi_1 - \phi_a)}_{(\text{A.10})} \\ &\quad \exp \left[-i\Delta t \sum_{j=1}^N \int d^3\mathbf{x} \left(\underbrace{\mathcal{H}(\pi_j, \phi_j)}_{(\text{A.14})} - \pi_{\mathbf{j}} \left(\underbrace{\phi_{j+1}}_{(\text{A.11})} - \underbrace{\phi_j}_{(\text{A.14})} \right) \right) / \Delta t \right] \end{aligned} \quad (\text{A.15})$$

where $\phi_{N+1} = \phi_a = \phi_1$. We have denoted which equation was used in which part of the amplitude.

A.2 Gauging the Effective Lagrangian

We show the most intricate gauging procedure of the theories we are treating in this thesis. The gauging of the sQED Lagrangian with or without $\lambda(\phi\phi^*)^2$ -interaction follows directly from the gauging procedure of the effective interaction Lagrangian.

We will find that the Lagrangian (3.23) stays invariant under global $U(1)$ transformations (the equation of motion is form invariant). However, if the transformation is made local, we need to introduce a gauge field in order to preserve the invariance.

Let now Λ be a global (position independent) $U(1)$ transformation (or "transformation of the first kind")

$$\phi \rightarrow e^{-i\Lambda} \phi, \quad \phi^* \rightarrow e^{i\Lambda} \phi^*, \quad \phi_0 \rightarrow \phi_0$$

which leaves the separating third isospin component unchanged. The following calculation is done in analogy to the gauging of the charged scalar field in [20], part 3.3. The gauge transformation of the first kind reads

$$\delta\phi = -i\Lambda\phi, \quad \delta\phi^* = i\Lambda\phi^*, \quad \delta\phi_0 = 0$$

in its infinitesimal form. From this,

$$\delta(\partial_\mu\phi) = -i\Lambda\partial_\mu\phi, \quad \delta(\partial_\mu\phi^*) = i\Lambda\partial_\mu\phi^*, \quad \delta(\partial_\mu\phi_0) = 0.$$

The conserved current is determined by

$$J^\mu = \frac{\partial\mathcal{L}}{\partial(\partial_\mu\phi)} \Delta(\phi) + \frac{\partial\mathcal{L}}{\partial(\partial_\mu\phi^*)} \Delta(\phi^*) \underbrace{\frac{\partial\mathcal{L}}{\partial(\partial_\mu\phi_0)} \Delta(\phi_0)}_{=0} = i \left[\frac{\partial\mathcal{L}}{\partial(\partial_\mu\phi^*)} \phi^* - \frac{\partial\mathcal{L}}{\partial(\partial_\mu\phi)} \phi \right],$$

where $\Lambda\Delta(\phi^{(*)}) = \delta\phi^{(*)}$. The second term arises because there are two independent fields ϕ and ϕ^* . Inserting (3.23) leads to

$$J^\mu = j^\mu - \frac{g^2}{2m_\rho^2} i \left[\phi^* \frac{2j^\mu}{i} (-\phi) - \phi \frac{2j^\mu}{i} \phi^* \right] + J_{mix}^\mu = j^\mu (1 + b\phi\phi^*) + J_{mix}^\mu$$

where $b = \frac{2g^2}{m_\rho^2}$ and

$$J_{mix}^\mu = i \frac{g^2}{m_\rho^2} \phi_0 \left[\phi^\star \left(\phi_0 \overleftrightarrow{\partial}^\mu \phi \right) - \phi \left(\phi_0 \overleftrightarrow{\partial}^\mu \phi^\star \right) \right] \quad (\text{A.16})$$

contains the contribution of the mixing of ϕ_0 with ϕ and ϕ^\star . (A.16) can be simplified to

$$J_{mix}^\mu = \frac{g^2}{m_\rho^2} \phi_0^2 j^\mu$$

so that

$$J^\mu = j^\mu \left(1 + b \phi \phi^\star + \frac{b}{2} \phi_0^2 \right). \quad (\text{A.17})$$

The Lagrangian is not invariant under a variation of the the fields any more, if the transformation $\Lambda \rightarrow \Lambda(x_\mu)$ is made local (Transformation of the second kind). Still,

$$\delta\phi = -i\Lambda\phi, \quad \delta\phi^\star = i\Lambda\phi^\star, \quad \delta\phi_0 = 0$$

but

$$\delta(\partial_\mu\phi) = -i\Lambda(x_\mu)(\partial_\mu\phi) - i\phi(\partial_\mu\Lambda), \quad \delta(\partial_\mu\phi^\star) = i\Lambda(x_\mu)(\partial_\mu\phi^\star) + i\phi^\star(\partial_\mu\Lambda), \quad \delta(\partial_\mu\phi_0) = 0$$

has changed since the transformed quantity is a product of the spacetime dependent function $\Lambda(x_\mu)$ and the operator $\phi(x_\mu)^{(\star)}$. The non-covariant behavior of the Lagrangian is calculated now:

$$\begin{aligned} \delta\mathcal{L} &= \frac{\partial\mathcal{L}}{\partial\phi}\delta\phi + \frac{\partial\mathcal{L}}{\partial(\partial_\mu\phi)}\delta(\partial_\mu\phi) + \frac{\partial\mathcal{L}}{\partial\phi^\star}\delta\phi^\star + \frac{\partial\mathcal{L}}{\partial(\partial_\mu\phi^\star)}\delta(\partial_\mu\phi^\star) \quad \underbrace{(+0)}_{\phi_0\phi, \phi_0\phi^\star \text{ mixing}} \\ &= \partial_\mu \left[\frac{\partial\mathcal{L}}{\partial(\partial_\mu\phi)} \right] (-i\Lambda\phi) + \frac{\partial\mathcal{L}}{\partial(\partial_\mu\phi)} (-i\Lambda\partial_\mu\phi - i\phi\partial_\mu\Lambda) \\ &+ \partial_\mu \left[\frac{\partial\mathcal{L}}{\partial(\partial_\mu\phi^\star)} \right] (i\Lambda\phi^\star) + \frac{\partial\mathcal{L}}{\partial(\partial_\mu\phi^\star)} (i\Lambda\partial_\mu\phi^\star + i\phi^\star\partial_\mu\Lambda) \\ &= -i\Lambda\partial_\mu \left[\frac{\partial\mathcal{L}}{\partial(\partial_\mu\phi)} \phi \right] - i \frac{\partial\mathcal{L}}{\partial(\partial_\mu\phi)} (\partial_\mu\Lambda) \\ &+ i\Lambda\partial_\mu \left[\frac{\partial\mathcal{L}}{\partial(\partial_\mu\phi^\star)} \phi^\star \right] + i \frac{\partial\mathcal{L}}{\partial(\partial_\mu\phi^\star)} (\partial_\mu\Lambda) \\ &\rightarrow i(\partial_\mu\Lambda) \left[\frac{\partial\mathcal{L}}{\partial(\partial_\mu\phi^\star)} \phi^\star - \frac{\partial\mathcal{L}}{\partial(\partial_\mu\phi)} \phi \right] \\ &= J^\mu \partial_\mu\Lambda. \end{aligned} \quad (\text{A.18})$$

From the first to the second line, the first and the third term have been replaced by using the Euler-Lagrange equation of motion for the fields ϕ and ϕ^\star . Furthermore, the definitions of $\delta\phi^{(\star)}$ and $\delta(\partial_\mu\phi^{(\star)})$ have been used. The next equality is proven by applying the product rule backwards. Now the first and the third term vanish when integrating over them — surface terms (next line “ \rightarrow ”). By employing the Lagrangian explicitly one ends up with the result: The variation of the Lagrangian is proportional to the conserved current. This is a general result and does not depend on the particular form of the Lagrangian.

The next task is to find counterterms in the Lagrangian to cancel $\delta\mathcal{L}$.

Counter Terms

In order to cancel $\delta\mathcal{L}$ we introduce the gauge field A_μ and decree the transformation behavior under gauge transformations of the second kind

$$A_\mu \rightarrow A_\mu + \frac{1}{e}\partial_\mu\Lambda.$$

A first counterterm is defined by

$$\mathcal{L}_1 := -eJ^\mu A_\mu$$

and a second by

$$\mathcal{L}_2 := e^2 A_\mu A^\mu \phi^* \phi (1 + b\phi\phi^* + \frac{b}{2}\phi_0^2).$$

The variation of the sum cancels the variation of the Lagrangian under the local $U(1)$ -transformation. This has been explicitly evaluated, and the result of this lengthy procedure is (3.24). For the way how to find appropriate counter terms, see [20].

A.3 Vacuum Feynman Rules including Neutral Pions.

The results of section 3.4.1 are evaluated here. The Feynman rules including neutral pions are very similar to the pure π^\pm interaction.

Note however, that if in a diagram several vertices are combined we have a new restriction to care about: Take for example the "Specs" diagram in Fig. A.5. There, the two adjoint sQED 3-vertices forbid the involvement of any neutral pions in the process although this would be allowed by the central 4π -vertex. Usually this is taken into account by adding new isospin-subscripts to propagators and vertices. Those then have to be subsequently multiplied. Processes that are not allowed are automatically removed. We hesitate to explicitly introduce new confusion by more subscripts and investigate from case to case.

The term of the effective interaction that contain π_0 's in (3.24) can be expanded (same conventions as in the last section, subscripts partly suppressed). Again, we have for the coefficient $i\mathcal{L}_{\text{eff}}(\text{mixing}) = \frac{ig^2}{m_\rho^2}$ and multiply $i\mathcal{L}_{\text{eff}}(\text{mixing})$ with the inverse which is then undone at the end of each calculation.

$$\begin{aligned} \frac{m_\rho^2}{ig^2} i\mathcal{L}_{\text{int } \pi_0} &= (\phi_0 \partial_\mu \phi + ieA_\mu \phi_0 \phi - \phi \partial_\mu \phi_0) (\phi_0 \partial^\mu \phi^* - ieA^\mu \phi_0 \phi^* - \phi^* \partial^\mu \phi_0) \\ &= \phi_0^2 \partial\phi\partial\phi^* - \phi_0 \phi^* \partial\phi_0 \partial\phi - \phi_0 \phi \partial\phi_0 \partial\phi^* + \phi\phi^* (\partial\phi_0)^2 \quad (\text{term 1'-4'}) \\ &\quad - ieA_\mu \phi_0^2 (\phi^* \partial^\mu \phi - \phi \partial^\mu \phi^*) \quad (\text{term 5'}) \\ &\quad + e^2 A_\mu^2 \phi_0^2 \phi\phi^* \quad (\text{term 6'}). \end{aligned} \tag{A.19}$$

Furthermore, the field ϕ_0 can now be contracted to an incoming as well as to an outgoing propagator. That means for the replacement by free waves:

$$\phi_{0r} \rightarrow S_r e^{+ip_r x}, \quad \text{as well as} \quad \phi_{0r} \rightarrow S_r e^{-ip_r x}.$$

In the case of ϕ and ϕ^* , this possibility was not given.

(term 1'-4')

From (3.15) and (3.16) we found

$$D_F(x-y) = D_F(y-x) \quad \text{and} \quad \partial_x D_F(x-y) = -\partial_y D_F(x-y)$$

for the charged propagator. The same relations hold for the neutral case. In the charged case, the occurrence of a $\partial_z \phi(z)$ in a vertex at z means the following: The propagator from z to y is $D_F(z - y) = \phi(z)\phi^*(y)$ (outgoing line, see Fig. 3.1 for the definition of x , y and z). Therefore the derivative in $\partial_z \phi$ acts on the first argument of the propagator which results in a factor of $(-ip)^\mu$ according to (3.16). Comparison with (3.26) shows that we are indeed working in a consistent picture. The case $\partial_z \phi^*(z)$ is analogous.

If there is a derivative acting on a ϕ^0 that is contracted into an incoming propagator, it results in a $(+ip^\mu)$ in momentum space according to (3.15). A derivative acting on a π^0 that is contracted into an outgoing propagator produces a factor of $(-ip)^\mu$ according to (3.16).

Do we have to distinguish three cases for the effective 4-vertex: "Both π^0 's are incoming lines, both are outgoing, one is incoming and one is outgoing"? No, because from the above it is clear that the two charged field operators ϕ^* (ϕ) always "occupy" one incoming (outgoing) state so that only the last possibility survives. p_1 and p_2 are incoming momenta and p_3 and p_4 are outgoing momenta by definition according to (term 1-3). We assign p_1 and p_3 to the neutral pions and p_2 and p_4 to the charged ones without loss of generality.

After these considerations, (term 1'-4') results in

$$\begin{aligned} & 2(-ip_4)(ip_2) - [(-ip_4)(ip_1) + (-ip_4)(-ip_3)] - [(ip_2)(ip_1) + (ip_2)(-ip_3)] + 2(ip_1)(-ip_3) \\ \rightarrow & \frac{ig^2}{m_\rho^2} (2p_2p_4 - p_1p_4 + p_3p_4 + p_1p_2 - p_2p_3 + 2p_1p_3) \end{aligned} \quad (\text{A.20})$$

The $[\dots]$ -brackets in the first line sum the two possibilities for the ϕ_0 . E.g. in the first $[\dots]$ -bracket, the term $\partial\phi_0$ can be connected into an incoming propagator (ip_1) or to an outgoing line ($-ip_3$). The factors of 2 in the first and the last term of the first line indicate the 2 possibilities for the ϕ_0 resulting in identical terms.

In the self energy diagrams we want to calculate, the neutral pion only occurs in a closed loop. That means $p_1 = p_3 =: k$ and $p_2 = p_4 =: p$ and the Feynman rule for the 4-vertex simplifies to

$$\frac{ig^2}{m_\rho^2} (p^2 + k^2). \quad (\text{A.21})$$

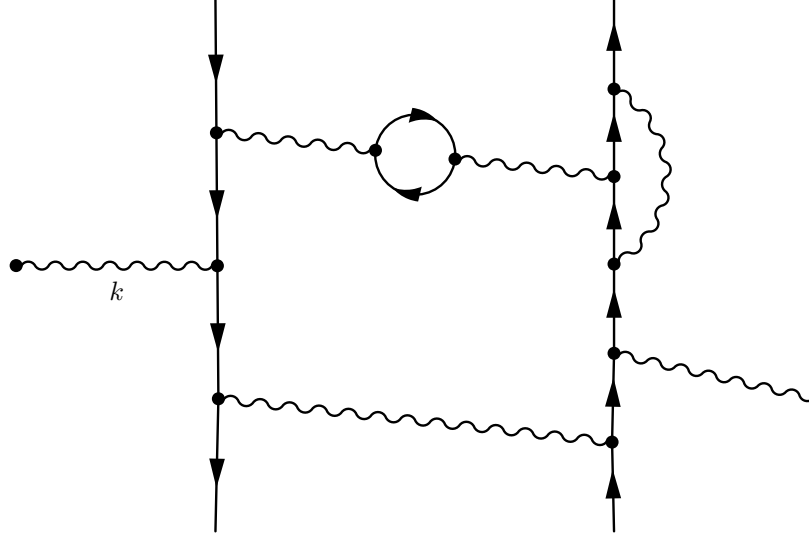
Here, a division by 2 has been applied since there is now only one possibility for the ϕ^0 to couple (not two distinguishable external fields any more).

(term 5')

There are two possibilities for ϕ_0 to contract with external fields but only one combination for ϕ and ϕ^* now in contrast to (term 4). Replacing the operators with free waves gives

$$\begin{aligned} & -ie\epsilon_\mu^*(k)e^{i(p_3+p_4+k-p_1-p_2)}2S_{\phi_0}^2(S_\phi S_{\phi^*}(-ip_\phi - ip_{\phi^*})) \\ \rightarrow & -\frac{2ieg^2}{m_\rho^2}(p_\phi + p_{\phi^*})\delta(k + p_3 + p_4 - p_1 - p_2). \end{aligned} \quad (\text{A.22})$$

The last line, which displays the vertex rule, deserves an explanation. We do not know whether the π^0 is an incoming or outgoing state (whether it has a positive or negative sign in the momentum conserving δ -function). Therefore we first have to draw the vertex, assign momenta and then decide how to identify p_1 to p_4 with the two p_{ϕ_0} 's, p_ϕ and p_{ϕ^*} . This subtlety is rather of formal nature. Our calculations of self energy diagrams in the order e^2g^2 will always (if π^0 allowed at all) contain a closed π^0 -loop. Then we get a symmetry factor of 1/2 for the vertex rule since there is only one way left how to connect the two ϕ_0 's.

Figure A.1: A typical feynman diagram with an external photon of momentum k **(term 6')**

In contrast to (term 5), the factor of 4 from the expansion of the square is missing as well as the $2 \cdot 2$ possibilities to contract to incoming / outgoing states. Still, the squared photon field gives a factor of two and we obtain a new factor of two from the ϕ_0 . After all, the rule for the $2\gamma 4\pi$ -vertex reads

$$\frac{4ie^2 g^2}{m_\rho^2} g^{\mu\nu} \delta(k_1 + k_2 + p_3 + p_4 - p_1 - p_2).$$

If the two ϕ_0 's are contracted to a loop, this vertex gets a symmetry factor of $1/2$ (as it will be the case in the diagram resulting from (term 5)).

We conclude from the Feynman rules for the $\pi^0 \pi^\pm$ -mixing that they are very similar to the pure π^\pm case up to multiplicity. In the case of the 4-vertex we did not show this explicitly. In fact, the effective $0\gamma 4\pi$ -vertex in the mixing case does not reveal the interesting factorization behavior of (3.30). However, in the special case that the π^0 is only occurring in the form of loops, the result will be equal to the π^\pm -case up to a (positive) constant as we will see soon.

A.4 Calculations in the Frame of the Ward–Takahashi Identity (WTI)

A.4.1 Proof of the WTI for sQED (see 4.3)

WTI for Fermions

For fermions the Ward–Takahashi identity reads (see [13], chapter 7.4):

Suppose a Feynman diagram in QED with external fermion and photon lines (see the diagram in Fig. A.1). Those do not necessarily need to be on-shell. It may contain fermion loops. Let the associated Fourier transformed correlation function, which it contributes to, be $\mathcal{M}^\mu(k)$, where k indicates the momentum of an external photon. Of course, there are in general many

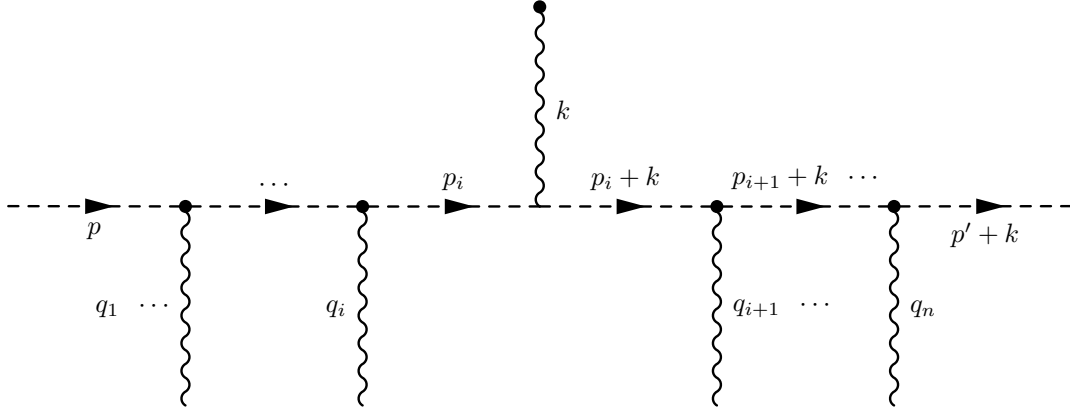


Figure A.2: Proof of the WTI — throughgoing boson line

other diagrams in the same order of perturbation theory that contribute to $\mathcal{M}^\mu(k)$. The WTI reads:

$$k_\mu \mathcal{M}^\mu(k) = x, \quad (\text{A.23})$$

where x represent terms that do not contribute to the scattering matrix S . If all external lines are on-shell, this implies

$$k_\mu \mathcal{M}^\mu(k) = 0.$$

By removing the external photon, a simpler diagram is defined which contributes to the simpler amplitude \mathcal{M}_0 . Reinserting the photon at any place of the reduced diagram leads to another contribution to $\mathcal{M}^\mu(k)$. Summing over all diagrams that contribute to \mathcal{M}_0 and within each diagram summing over all possible insertion point diagram rebuilds the full correlation $\mathcal{M}^\mu(k)$.

Then, an equivalent statement to (A.23) is:

The Ward–Takahashi–identity is separately true for each diagram contributing to \mathcal{M}_0 , once we sum over all insertion points.

Furthermore, there exists a special case of the WTI, which is often referred to as Ward identity which can also be formulated in the differential form with vanishing external photon momentum k .

We will show, that the WTI does indeed fully hold for sQED, although only by including a wider set of insertion points.

Proof of the WTI for Scalar QED — Throughgoing Lines Insertions

An algebraic proof of the WTI for n -point functions is given in [29], p. 407 ff, for 2-point function and in more clarity in [35], p.447 ¹. In both, the fermionic case is treated and this cannot directly be applied to our case. We choose a diagrammatic proof similar to [13], p. 238 ff which has the advantage of vividness.

¹A hint how to change the proof for bosons (in the notation of Weinberg): About one page of operator algebra shows, that (10.4.21) also holds for bosons. (10.4.22) and (10.4.23) are not true in sQED any more. In contrast, another 4 pages of algebra including creation and annihilation operators as well as the canonical commutation relations give

$$\left[J^0(\mathbf{x}, t), \phi(\mathbf{y}, t) \stackrel{x_0=y_0}{=} -iq\delta^3(\mathbf{x} - \mathbf{y}) \right]$$

There are two different possibilities for a boson line in a diagram (see (A.1)): either it is a throughgoing line or a closed loop. In order to examine the first possibility we consider the subdiagram in Fig. A.2. It consists of n incoming photon lines with momenta q_i and the external photon inserted between the i^{th} and the $(i+1)^{th}$ insertion point.

The inserted photon in Fig. A.2 leads to an additional vertex $(-ie(2p_i + k))$ and an additional propagator with momentum $p_i + k$. Since we conventionally choose the additional photon momentum to flow along the boson line, all propagators on the right side are shifted by the momentum k . The product of k_μ with the new vertex multiplied with the adjacent propagators is

$$ie \left(\frac{2p_i k + k^2}{((p_i + k)^2 - m_\pi^2)(p_i^2 - m_\pi^2)} \right) = e \left(\frac{i}{p_i^2 - m_\pi^2} - \frac{i}{(p_i + k)^2 - m_\pi^2} \right). \quad (\text{A.24})$$

The square has been completed in the numerator, the fraction is separated and appropriate terms cancel. Therefore the diagram with the photon inserted at position i has the structure

$$= e \cdots \frac{i}{(p_{i+1} + k)^2 - m_\pi^2} V^{i+1}(k) \left(\frac{i}{p_i^2 - m_\pi^2} - \frac{i}{(p_i + k)^2 - m_\pi^2} \right) V^i \frac{i}{p_{i-1}^2 - m_\pi^2} V^{i-1} \cdots,$$

where $V(k)$ indicates the dependency of the vertex of k . Analogously, the diagram with the photon inserted at position $i-1$ has the structure

$$= e \cdots \frac{i}{(p_{i+1} + k)^2 - m_\pi^2} V^{i+1}(k) \frac{i}{(p_i + k)^2 - m_\pi^2} V^i(k) \left(\frac{i}{p_{i-1}^2 - m_\pi^2} - \frac{i}{(p_{i-1} + k)^2 - m_\pi^2} \right) V^{i-1} \cdots.$$

Note that in the case of fermions, the calculation is totally equivalent up to this point (except the different propagator) and the first term in brackets in the second diagram cancels the second term in brackets of the first diagram. This happens in the fermionic case successively with all insertion points and one is left with two diagrams with insertion points after the last vertex and before the first vertex, which both are e times the original diagram. (see equation (7.66) in [13]).

Unfortunately no cancellation takes place in sQED: In the lower diagram the vertex V^i also depends on the momentum. The difference of both diagrams and the previous one with insertion point before

and

$$\left[J^0(\mathbf{x}, t), \phi^*(\mathbf{y}, t) \stackrel{x_0=y_0}{=} i q \delta^3(\mathbf{x} - \mathbf{y}) \right]$$

so that (10.4.21) reads

$$\frac{\partial}{\partial x^\mu} = T \left[J^\mu(x) \phi(y) \phi^*(z) \right] = -q \delta^4(x - y) \phi^*(z) + q \delta^4(x - z) \phi(z)$$

where T is the time ordered product. With these new expressions, the bosonic analogs of (10.4.19) and (10.4.20) have to be attacked.

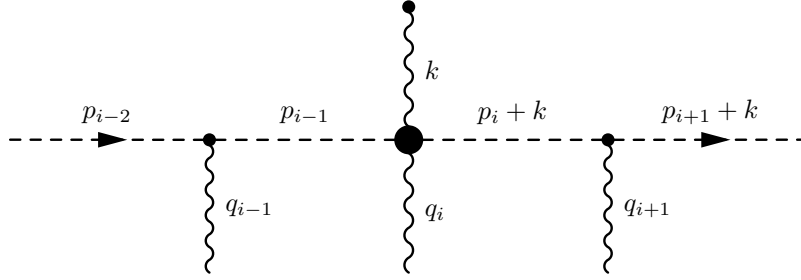


Figure A.3: Proof of the WTI — throughgoing boson line: Building a 4-vertex out of a 3-vertex by inserting the photon $\gamma(k)$ at V_{old}^i .

V^{i-1} is

$$\begin{aligned}
 & \dots + \left[V^i(k) - V^i \right] \left(\dots \frac{i}{(p_{i+1} + k)^2 - m_\pi^2} V^{i+1}(k) \frac{i}{(p_i + k)^2 - m_\pi^2} \frac{i}{p_{i-1}^2 - m_\pi^2} V^{i-1} \dots \right) \\
 & + \left[V^{i-1}(k) - V^{i-1} \right] \left(\dots \frac{i}{(p_i + k)^2 - m_\pi^2} V^i(k) \frac{i}{(p_{i-1} + k)^2 - m_\pi^2} \frac{i}{p_{i-2}^2 - m_\pi^2} V^{i-2} \dots \right) \\
 & + \dots \\
 & \simeq x_i + x_{i-1} + \dots
 \end{aligned} \tag{A.25}$$

Fortunately, the difference of the vertices is independent of the p_i :

$$V^i(k) - V^i = (-ie(p_{i-1} + p_i + 2k)^\mu) - (-ie(p_{i-1} + p_i)^\mu) = -2iek^\mu.$$

The sum over all terms x_i of the n different insertion points can be obtained by the following procedure: You get the term x_i from the original diagram without insertion x_0 in the following way:

- Erase vertex V^i in x_0 .
- Multiply x_0 with $-2iek^\mu$.
- The sum over the x_i implies that the insertion before the first point and the one after the last point is only half each contained in the x_i (You see this in (A.25) by noting, that every diagram has been split into two parts and the x_i contain one half from diagram i and another half from diagram $i - 1$).

Although there is no cancellation so far, we have not exhausted all possible insertion points in our throughgoing boson line: It is also possible to insert the photon at an existing 3-vertex, transforming it into a 4-vertex.

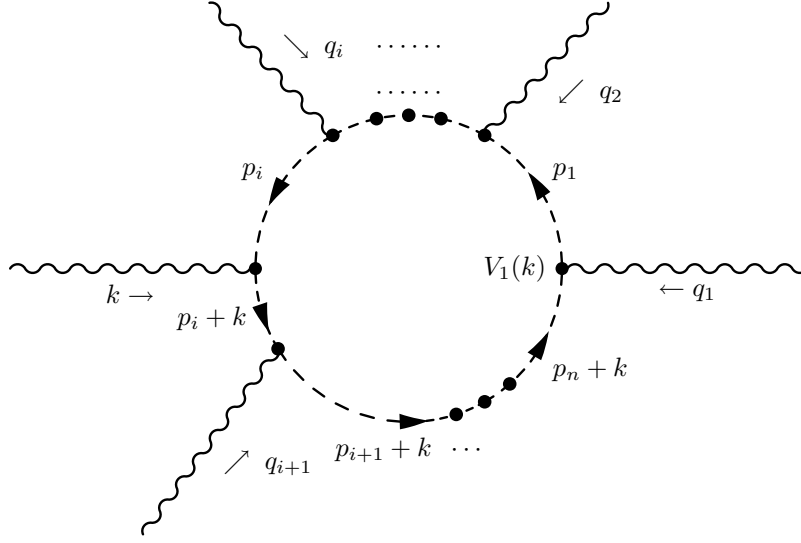
Consider the diagram in Fig. A.3 The corresponding amplitude of the new diagram is

$$\dots V^{i-1} \frac{i}{p_{i-1}^2 - m_\pi^2} (2ie^2 k^\mu) \frac{i}{(p_i + k)^2 - m_\pi^2} V^{i+1} \frac{i}{(p_{i+1} + k)^2 - m_\pi^2} \dots$$

or

$$(-ie(p_{i-2} + p_{i-1})) \frac{i}{p_{i-1}^2 - m_\pi^2} (2ie^2 k^\mu) \frac{i}{(p_i + k)^2 - m_\pi^2} (-ie(p_i + p_{i+1} + 2k)) \frac{i}{(p_{i+1} + k)^2 - m_\pi^2} \tag{A.26}$$

Note, that the inserted momentum is again chosen to flow along the boson line. If we call the new diagram y_i , the rule to obtain it from x_0 is:

Figure A.4: Loop insertion of the photon $\gamma(k)$

- Erase V^i in x_0 .
- Multiply x_0 with $+2ie^2 k^\mu$.

As it is obvious, the 3-vertex insertion term, that consists of half of the insertion before V^i and of half of the insertion after V^i , cancels the $3 \rightarrow 4$ -vertex insertion at V^i in diagram A.3. That means that only the first half of the term at the insertion before the first photon and the second half of the term at the insertion behind the last photon survive. If we call the diagram without photon insertion $d(p, p')$, then the sum of these unpaired terms is

$$e[d(p, p') - d(p + k, p' + k)] = e[d(p, q - k) - d(p + k, q)] \quad (\text{A.27})$$

with the replacement $p' := q - k$ for the sake of symmetry.

Note further that no integration shift has been applied in the whole calculation. We could have shifted the internal integration by e.g. $p_i \rightarrow p_i + k$ as it is necessary at loop insertions (see below). Shifts may, if the integral is ultraviolet divergent, destroy the conservation of current. This needs to be cured by a new Pauli-Villard regularization or dimensional regularization. (see §7.5 in [13])

Introducing 4-vertices

If the original diagram without photon insertion contains 4-vertices, the situation changes. Imagine for clarity that the photon that attaches the boson line with momentum q_i in diagram A.2 proceeds its way upwards and is therefore coupled by a 4-vertex. This simply means that the derivative coupling at the 4-vertex is replaced by a non-derivative one – which has the same structure as the fermionic case. Then the two 3-point insertions of the attached external photon at momentum k right and left from the 4-vertex cancel directly as in the proof of the fermionic case and nothing has to be done further.

A.4.2 Loop Insertion

Consider a boson loop with n external photon lines as in Fig. A.4. By convention, let the inserted momentum k flow along the loop in counter clockwise direction and exit via the photon line at $V_1(k)$. The following is a shortcut of the proof in [13], p. 241.

If we cut the boson line directly before and directly after $V_1(k)$ we get a throughgoing line with momentum p_1 entering and p_n exiting the line. If this throughgoing line is multiplied with $V_1(k)$ we have restored the amplitude of the complete loop. Note that in all insertions there is an additional momentum of k at $V_1(k)$ according to our convention of momentum flow. Except the insertion at V_1 itself. But this insertion is not a regular insertion of the newly defined throughgoing line. The summation over all regular insertion points results in (see above)

$$e\left(d(p_1, p_n) \underbrace{(-ie(p_1 + p_n + k)^\mu)}_{V_1(k)} - d(p_1 + k, p_n + k) \underbrace{(-ie(p_1 + p_n + k)^\mu)}_{V_1(k)}\right). \quad (\text{A.28})$$

$d(x, y)$ is the amplitude of the throughgoing line with momentum x entering and y exiting the line.

We perform the shift $p_i + k \rightarrow p_i$ for $i = 1, \dots, n$ in the second term. Note that this shift is only allowed if the diagram is properly regularized. (A.28) simplifies to

$$e\left(d(p_1, p_n)(-ie(2k^\mu))\right). \quad (\text{A.29})$$

So far, we have not used the insertion possibility at V_1 . Since the direct vertex is $2ie^2 g^{\mu\nu}$ we see that the remaining insertion exactly cancels (A.29).

There are different diagrams contributing to the amplitude \mathcal{M}_0 without the photon, each of them consisting of throughgoing lines, loops and photons. We have shown that each summation over insertion points in a diagram contributing to \mathcal{M}_0 is of the form (A.27). If we sum first over the insertion possibilities of a diagram and then sum over all diagrams we finally obtain $\mathcal{M}^\mu(k)$. Therefore the product of this with the external photon momentum k_μ reads

$$k_\mu \mathcal{M}^\mu(k; p_1, \dots, p_n; q_1, \dots, q_n) = e \sum_i \left[\mathcal{M}_0(p_1, \dots, p_n; q_1, \dots, (q_i - k), \dots, q_n) - \mathcal{M}_0(p_1, \dots, (p_i + k), \dots, p_n; q_1, \dots, q_n) \right]. \quad (\text{A.30})$$

This is the WTI for sQED for the amplitude $\mathcal{M}^\mu(k)$ with n incoming and n outgoing boson lines (and arbitrarily many outgoing/incoming photon lines of \mathcal{M}_0). In Fig. 4.8 this is visualized.

Furthermore, it is clear now that the full statement of the WTI can be applied in the bosonic case.

A.4.3 Proof of the WI for Four-Point Functions in the Effective Theory

In the following we want to give the exact proof of the WI (4.20) (for four-point functions) for the effective interaction (see 4.6).

Mapping the Problem

If we are able to find a set of sQED diagrams that correspond to the sum over all insertion point diagrams of the 4-point function in the effective theory, we are practically done due to the WTI for scalar QED. The heuristic considerations from above about the diagrams 3.1 and 4.7 give a hint how these sQED diagrams should look like. Indeed, by writing down the amplitudes, we find two identities. The first one

is for 4-point functions:

$$= \frac{\left(\frac{ig^2}{m_\rho^2}\right)}{(-ie)^2} \frac{q^2}{i} \left(\text{t-channel diagram} + \text{u-channel diagram} \right). \quad (\text{A.31})$$

The coefficient of the righthand side simply consists of the ratio of the vertex constants and the inverse photon propagator. We can even state another version of (A.31): Add an external photon with momentum k to any of the four legs of the diagram on the lefthand side (by a 3-vertex) as well as to the two diagrams on the righthand side. We call these four new identities I_1 to I_4 . They will be needed for the proof of the WTI.

The second identity, defined as I_5 , is for 5-point functions and reads

$$= \frac{\left(\frac{-4ie g^2}{m_\rho^2}\right)}{2(-ie)(2ie^2)} \frac{q^2}{i} \left(\text{t-channel diagrams} + \text{u-channel diagrams} \right). \quad (\text{A.32})$$

The righthand side has been split up in two equal parts representing the t - respectively u -channel of the scattering process. We are very lucky: both identities I_1 to I_4 and I_5 show the same proportionality $-\frac{g^2 q^2}{e^2 m_\rho^2} \frac{q^2}{i}$.

Comparing I_1 to I_5 shows: We can map insertion diagrams of the 4-point function of the effective theory in sQED. This is possible because of the same proportionality of I_1 to I_4 and I_5 . The two diagrams on the righthand side of (A.31) are the "core diagrams" of all insertion diagrams. Every diagram on the righthand side of I_1 to I_5 can be obtained by inserting a photon at all possible insertion points of

these two "core diagrams". Then, the sum over all insertion diagrams of the effective 4-point coupling (including external leg insertions as well as central insertion) is proportional to the sum of all insertion point diagrams of the sum of the two diagrams on the right side of (A.31).

We are practically done now. We can identify two throughgoing lines for each diagram on the righthand side of I_1 to I_5 . The Ward identity (4.9) for sQED can be applied now for the righthand side of I_1 to I_5 . If we introduce the 4-point function $G^{(2)}(p_1, p_2, p_3, p_4)$ as in the case of the $\lambda(\phi^\star\phi)^2$ -theory with the assignment of momenta as in Fig 4.5, the WI for the sum of the core diagrams on the right side of (A.31), now defined as S , reads

$$\begin{aligned} k_\mu \sum_{\text{insertion points}} S &= e \left(G^{(2)}(p_1, p_2, p_3, p_4) - G^{(2)}(p_1 + k, p_2, p_3 + k, p_4) \right. \\ &\quad + G^{(2)}(p_1, p_2, p_3, p_4) - G^{(2)}(p_1, p_2 + k, p_3, p_4 + k) \\ &\quad + G^{(2)}(p_1, p_2, p_3, p_4) - G^{(2)}(p_1 + k, p_2, p_3, p_4 + k) \\ &\quad \left. + G^{(2)}(p_1, p_2, p_3, p_4) - G^{(2)}(p_1, p_2 + k, p_3 + k, p_4) \right). \end{aligned} \quad (\text{A.33})$$

In order to obtain differential ratios, we have to expand every line as it is shown here for the first line:

$$\begin{aligned} G^{(2)}(p_1, p_2, p_3, p_4) - G^{(2)}(p_1 + k, p_2, p_3 + k, p_4) &= [G^{(2)}(p_1, p_2, p_3, p_4) - G^{(2)}(p_1 + k, p_2, p_3, p_4)] \\ &\quad + [G^{(2)}(p_1 + k, p_2, p_3, p_4) - G^{(2)}(p_1 + k, p_2, p_3 + k, p_4)]. \end{aligned} \quad (\text{A.34})$$

Therefore the righthand side of (A.33) divided by the external momentum k_μ reads in the limit $k_\mu \rightarrow 0$

$$-2e \sum_{i=1, \dots, 4} \frac{\partial G^{(2)}(p_1, \dots, p_4)}{\partial p_{i\mu}} \rightarrow -2e \frac{\partial G^{(2)}(p)}{\partial p_\mu} \quad \text{for } p_1, \dots, p_4 \rightarrow p.$$

The identity (4.18) has been used again. We are ready to write down the Ward identity for 4-point functions in the effective theory:

$$\Gamma_{\text{full}}^\mu(p) = -2e \frac{\partial}{\partial p_\mu} G^{(2)}(p). \quad (\text{A.35})$$

Imagine we have an arbitrary higher order 4-point function in the effective theory. We can always apply identities similar to I_1 to I_5 in order to translate the problem into the language of sQED diagrams. Therefore (4.20) is true in all orders and the desired non-perturbative statement for the two particle propagator is found.

A.4.4 Vacuum Part in e^2 : Dimensional Regularization

If we call $S(p)$ the sum of the arguments of (4.23) and (4.22) (for the simple vacuum diagrams in e^2 in Fig. 4.9 and Fig. 4.10), we can write

$$S(p) = e^2 \left[\frac{(2p^\mu + q^\mu)(2p^\nu + q^\nu) - 2g^{\mu\nu}((p+q)^2 - m_\pi^2)}{(p^2 - m_\pi^2)((p+q)^2 - m_\pi^2)} \right]. \quad (\text{A.36})$$

Here, the factor T of both expressions is omitted².

The self energy is supposed to have the structure

$$\Pi^{\mu\nu}(q) = (q^2 g^{\mu\nu} - q^\mu q^\nu) \Pi(q^2). \quad (\text{A.37})$$

²We switched back to the vacuum case and therefore have to apply the vacuum Feynman rules in the determination of the amplitudes of Fig. 4.9 and Fig. 4.10. However, all changes cancel by switching to the vacuum case.

By looking at (A.36) we notice a "bad" term proportional to $g^{\mu\nu}m_\pi^2$ in the numerator in contrast to the form of the expression we have to obtain. The term cannot be cancelled by anything. From this we conclude that it is not enough just to manipulate the integrand without evaluating the integral. The integral has to be somehow evaluated and a method has to be found to transform another term of the numerator into the $g^{\mu\nu}$ tensor structure in order to attack the m_π^2 -term. A good candidate is the $q^\mu q^\nu$ -structure, because we might be able to apply the identity

$$q^\mu q^\nu \rightarrow \frac{1}{d} q^2 g^{\mu\nu}, \quad (\text{A.38})$$

which is valid when the replacement is performed in an integral whose integrand is symmetric (see [13], p. 251, (7.87), p. 191, (6.46)). Here, the denominator is not symmetric due to the external momentum q . The first step is therefore to combine the denominators to a symmetric integrand by introducing Feynman parameters:

$$\frac{1}{(p^2 - m_\pi^2)((p+q)^2 - m_\pi^2)} = \int_0^1 dx \frac{1}{(l^2 + x(1-x)q^2 - m_\pi^2)^2},$$

where $l = p + xq$. This transforms the numerator of (A.36) into

$$\begin{aligned} \text{numerator (A.36)} &= e^2 ((2l^\mu + q^\mu(1-2x))(2l^\nu + q^\nu(1-2x)) - 2g^{\mu\nu}((l + q(1-x))^2 - m_\pi^2)) \\ &= e^2 (4l^\mu l^\nu - 2g^{\mu\nu}l^2 + (1-2x)^2 q^\mu q^\nu + 2g^{\mu\nu}(m_\pi^2 - (1-x)^2 q^2)) \\ &+ e^2 \underbrace{(2(1-2x)(l^\mu q^\nu + l^\nu q^\mu) - 4g^{\mu\nu}l \cdot q(1-x))}_{\text{proportional to } l}. \end{aligned} \quad (\text{A.39})$$

The terms linear in l have been separated. The denominator of the new integral is now $(l^2 - \Delta)^2$ with $\Delta = m^2 - x(1-x)q^2$. In order to understand why the integration over terms with a numerator proportional to l vanishes, a Wick rotation is performed by switching the time like integration variable $l^0 = il_e^0$. (The correct rotation sense due to the location of poles is obeyed.) The result is

$$\int \frac{d^4 p}{(2\pi)^4} S(p) = ie^2 \int_0^1 dx \int_{\text{euklidian}} \frac{d^4 l_e}{(2\pi)^4} \frac{-g^{\mu\nu}l_e^2 + 2g^{\mu\nu}l_e^2 + (1-2x)^2 q^\mu q^\nu + 2g^{\mu\nu}(m^2 - (1-x)^2 q^2)}{(l_e^2 + \Delta)^2}. \quad (\text{A.40})$$

Two more things have been changed here: First, the identity (A.38) has been applied since the integrand is now symmetric in l_e . Second, the linear terms in l_e have been omitted, since these terms are antisymmetric and give no contribution to the integral. The Wick rotated euklidian 4-integral is now expressed in d dimensions in order to apply the method of dimensional regularization. For reasons that will become obvious soon, the first two terms of the numerator of (A.40) are not combined. In d dimensions the first two terms of (A.40) read

$$\begin{aligned} 2ie^2 \int \frac{d^d l_e}{(2\pi)^2} \frac{(-\frac{2}{d} + 1)g^{\mu\nu}l_e^2}{(l_e^2 + \Delta)^2} &= 2ie^2 \frac{-1}{(4\pi)^{\frac{d}{2}}} \left(1 - \frac{d}{2}\right) \Gamma\left[1 - \frac{d}{2}\right] \left(\frac{1}{\Delta}\right)^{1-\frac{d}{2}} g^{\mu\nu} \\ &= 2ie^2 \frac{1}{(4\pi)^{\frac{d}{2}}} \Gamma\left[2 - \frac{d}{2}\right] \left(\frac{1}{\Delta}\right)^{2-\frac{d}{2}} (-\Delta g^{\mu\nu}). \end{aligned} \quad (\text{A.41})$$

Here, the identity

$$\int \frac{d^d l_e}{(2\pi)^d} \frac{l_e^2}{(l_e^2 + \Delta)^n} = \frac{1}{(4\pi)^{\frac{d}{2}}} \frac{d}{2} \frac{\Gamma\left[n - \frac{d}{2} - 1\right]}{\Gamma[n]} \left(\frac{1}{\Delta}\right)^{n-\frac{d}{2}-1} \quad (\text{A.42})$$

has been used as well as $x\Gamma[x] = \Gamma[x+1]$.

The $\Gamma(z)$ -function has isolated poles at $z = 0, -1, -2, \dots$. Therefore the integral (A.41) has isolated poles at $z = 4, 6, 8, \dots$. However, the pole at $d = 4$ is cancelled by $(1 - d/2)$ in the numerator of (A.41). It has paid off that we did not combine the first two terms of (A.40) before we generalized the integral to d dimensions.

The first two terms of (A.40) consist of contributions from both Fig. 4.9 and Fig. 4.10. Only if both diagrams are taken into account with the correct coefficients and relative sign, the cancellation of poles becomes possible. From the identity

$$\int \frac{d^d l_e}{(2\pi)^d} \frac{1}{(l_e^2 + \Delta)^n} = \frac{1}{(4\pi)^{\frac{d}{2}}} \frac{\Gamma[n - \frac{d}{2}]}{\Gamma[n]} \left(\frac{1}{\Delta}\right)^{n - \frac{d}{2}} \quad (\text{A.43})$$

the evaluation of the terms of (A.40) containing no l_e^2 follows.

In the second line of (A.41) appears the term Δ in the numerator that depends on the pion mass and will cancel the unwanted mass term of (A.36).

Now, (A.40) can be readily evaluated

$$\begin{aligned} \Pi^{\mu\nu}(q) &= ie^2 \int_0^1 dx \frac{1}{(4\pi)^{\frac{d}{2}}} \frac{\Gamma[2 - \frac{d}{2}]}{\Delta^{2 - \frac{d}{2}}} \left(2g^{\mu\nu} \underbrace{(-\Delta)}_{-m_\pi^2 + x(1-x)q^2} + (1-2x)^2 q^\mu q^\nu + 2g^{\mu\nu} (m_\pi^2 - (1-x)^2 q^2) \right) \\ &= ie^2 \frac{1}{(4\pi)^{\frac{d}{2}}} \int_0^1 dx \frac{\Gamma[2 - \frac{d}{2}]}{\Delta^{2 - \frac{d}{2}}} \left(2g^{\mu\nu} q^2 \underbrace{\left(x(1-x) - (1-x)^2 \right)}_{=-2x^2 + 3x - 1} + (1-2x)^2 q^\mu q^\nu \right). \end{aligned} \quad (\text{A.44})$$

The Ward identity is proven if it can be shown that the integrals which represent the coefficients of $g^{\mu\nu} q^2$ and $q^\mu q^\nu$ are equal with opposite sign:

$$\begin{aligned} \int_0^1 dx \frac{1}{\Delta^{2 - \frac{d}{2}}} (2(-2x^2 + 3x - 1) + (1-2x)^2) &= 2 \int_0^1 dx \frac{x - \frac{1}{2}}{(m_\pi^2 - x(1-x)q^2)^{2 - \frac{d}{2}}} \\ &= 2 \int_{-\frac{1}{2}}^{\frac{1}{2}} dy \frac{y}{(m_\pi^2 - y^2 q^2)^{2 - \frac{d}{2}}} = 0. \end{aligned} \quad (\text{A.45})$$

This shows that the Ward identity in the vacuum is preserved in second order in sQED. The self energy can now be expressed as

$$\Pi^{\mu\nu}(q) = \frac{8ie^2}{(4\pi)^{\frac{d}{2}}} (q^\mu q^\nu - g^{\mu\nu} q^2) \underbrace{\int_{-\frac{1}{2}}^{\frac{1}{2}} dy \frac{\Gamma[2 - d/2] y^2}{\Delta^{2 - \frac{d}{2}}}}_{=\Pi(q^2)}. \quad (\text{A.46})$$

Since

$$\frac{\Gamma(2 - d/2)}{\Delta^{2 - d/2}} \rightarrow \frac{2}{\epsilon} - \log \Delta - \gamma + \log(4\pi) \quad \text{for } d \rightarrow 4$$

with $\epsilon = 4 - d$ and $\gamma \approx .5772$ the Euler-Mascheroni constant, the integral is analytically solvable, but the solution is rather lengthy.

Shortcut of the Proof of the Ward Identity in the Vacuum

Multiplying (A.36) directly with q_μ gives (by completing the square in the first term):

$$\begin{aligned} q_\mu \cdot (A.36)^{\mu\nu} &= 2e^2 \left[\frac{(((p+q)^2 - m_\pi^2) + m_\pi^2 - p^2)(2p^\nu + q^\nu)}{((p+q)^2 - m_\pi^2)(p^2 - m_\pi^2)} - \frac{2q^\nu}{p^2 - m_\pi^2} \right] \\ &= 2e^2 \left[\frac{2p^\nu + q^\nu - 2q^\nu}{p^2 - m_\pi^2} - \frac{2p^\nu + q^\nu}{(p+q)^2 - m_\pi^2} \right]. \end{aligned} \quad (A.47)$$

$$(A.48)$$

Shifting the integration in the second term from $(p^\nu + q^\nu) \rightarrow l^\nu$ and renaming $l^\nu = q^\nu$ shows that both terms are equal with different signs, so the sum is 0. There is one remark to make about shifts in integration variables. Since the integrals are ultraviolet divergent, the high momentum cutoff would be shifted as well resulting in a destruction of the transversality of self energy. So either one has to introduce a new Pauli-Villard regulator or one works consistently in dimensional regularization. Both (where the second is simpler) give a justification of the shift. In thermal field theory, shifts are not a problem because of the Bose suppression. The advantage of the shortcut taken here is of course its brevity. The unwanted mass term in the numerator of (A.36) disappeared at once.

A.5 Evaluation of the Self Energy in $e^2 g^2$

A.5.1 Further Analysis of the *Duck* Diagram in Fig. 5.1

Vacuum Part of the Pion Loop Insertion

The first integral of (2.46) describes the vacuum part. If we switch the imaginary integration into a real one by $k_4 = ik_0$ over k_4 we obtain the euklidian integral

$$-\frac{g^2}{m_\rho^2} \int \frac{d^4 k}{(2\pi)^4} \frac{(\mathbf{k} + \mathbf{p})^2 + k_4^2 - p_0^2}{k_4^2 + \mathbf{k}^2 + m_\pi^2}$$

from the amplitude (5.8) for the pion loop. According to [12], a high moment cutoff is applied at $\Lambda_c = \sqrt{k_4^2 + \mathbf{k}^2}$. The four dimensional volume differential is

$$d^4 x = r^3 \sin^2 \omega \sin \theta d\phi d\theta d\omega dr.$$

Let \mathbf{p} point towards the direction $\omega = 0$:

$$-\frac{g^2}{m_\rho^2} \frac{1}{(2\pi)^4} \int_0^{\Lambda_c} dr \int_0^\pi d\omega \int_0^\pi d\theta \int_0^{2\pi} d\phi r^3 \sin^2 \omega \sin \theta \frac{r^2 + 2|\mathbf{p}|r \cos \omega + \mathbf{p}^2 - p_0^2}{r^2 + m_\pi^2}$$

The integration over θ and ϕ results in a factor 4π . Then, the integration over ω is performed with the result

$$-\frac{g^2}{2m_\rho^2} \frac{1}{(2\pi)^2} \frac{r^3(\mathbf{p}^2 - p_0^2 + r^2)}{r^2 + m_\pi^2}.$$

The following integration over r gives

$$-\frac{g^2}{8m_\rho^2} \frac{1}{(2\pi)^4} \left(\Lambda_c^4 + 2(p_0^2 - \mathbf{p}^2 + m_\pi^2) \left(m_\pi^2 \log \left[\frac{m_\pi^2 + \Lambda_c^2}{m_\pi^2} \right] - \Lambda_c^2 \right) \right).$$

Note the somewhat more complicated form of this result compared to (3.42) in [12]. For a large cutoff parameter this simplifies to

$$\rightarrow -\frac{g^2}{8m_\rho^2} \frac{1}{(2\pi)^4} \left(\Lambda_c^4 + 2(p_0^2 - \mathbf{p}^2 + m_\pi^2) \left(m^2 \log \left[\frac{\Lambda_c^2}{m_\pi^2} \right] - \Lambda_c^2 \right) \right).$$

Matter Part of the Pion Loop of the *Duck* diagram in Fig. 5.1

The matter part of the pion loop is

$$-\frac{g^2}{m_\rho^2} \int \frac{d^3\mathbf{k}}{(2\pi)^2} \frac{1}{2\pi i} \int_{-i\infty+\epsilon}^{i\infty+\epsilon} dp_0 \frac{2p_0^2 + 2k_0^2 - 2(\mathbf{p} + \mathbf{k})^2}{k_0^2 - \omega^2} n(k_0).$$

The integration contour is closed in the right k_0 half plane and contains a single pole at $k_0 = \omega$. The summation results in

$$\frac{g^2}{m_\rho^2} \int \frac{d^3\mathbf{k}}{(2\pi)^3} \frac{n(\omega)}{\omega} \underbrace{(p^2 + m_\pi^2)}_{\text{integral I}} \underbrace{-2\mathbf{k}\mathbf{p}}_{\text{integral II}}, \quad p^2 = p_\mu p^\mu = p_0^2 - \mathbf{p}^2.$$

There is an additional factor of (-1) due to the clockwise integration contour. The sum is split in two parts referring to the different dependency on \mathbf{k} .

Integral I

$$\frac{g^2}{m_\rho^2} (p^2 + m_\pi^2) \int \frac{d^3\mathbf{k}}{(2\pi)^3} \frac{n(\omega)}{\omega} = 2 \frac{g^2}{m_\rho^2} (p^2 + m_\pi^2) \int_0^\infty \frac{dk}{(2\pi)^2} k^2 \frac{n(\omega)}{\omega}$$

Integral II

$$-\frac{2g^2}{m_\rho^2} \int \frac{d^3\mathbf{k}}{(2\pi)^3} \mathbf{k}\mathbf{p} \frac{n(\omega)}{\omega} = -\frac{g^2}{m_\rho^2} \frac{2}{(2\pi)^2} \int_0^\pi d\theta \int_0^\infty dk (k^2 \sin \theta) (|\mathbf{p}| k \cos \theta) \frac{n(\omega)}{\omega} = 0, \quad (\text{A.49})$$

as it is obvious after the angle integration.

Example of a Full Contraction for the *Duck* Diagram in Fig 5.1

We show how to fully contract the field operators of a diagram in order to transform τ -ordered products in normal ordered products, using the modified Wicks theorem at finite temperature in the imaginary time formalism [27]. We have

$$\begin{aligned} & \overbrace{\phi_l^* \leftrightarrow \partial \phi_l}^{\quad} \overbrace{(\phi_v^* \leftrightarrow \partial \phi_v)(\phi_v^* \leftrightarrow \partial \phi_v)}^{\quad} \overbrace{\phi_r^* \leftrightarrow \partial \phi_r}^{\quad}, \\ & \overbrace{\phi_l^* \leftrightarrow \partial \phi_l}^{\quad} \overbrace{(\phi_v^* \leftrightarrow \partial \phi_v)(\phi_v^* \leftrightarrow \partial \phi_v)}^{\quad} \overbrace{\phi_r^* \leftrightarrow \partial \phi_r}^{\quad}, \\ & \overbrace{\phi_l^* \leftrightarrow \partial \phi_l}^{\quad} \overbrace{(\phi_v^* \leftrightarrow \partial \phi_v)(\phi_v^* \leftrightarrow \partial \phi_v)}^{\quad} \overbrace{\phi_r^* \leftrightarrow \partial \phi_r}^{\quad}, \\ & \overbrace{\phi_l^* \leftrightarrow \partial \phi_l}^{\quad} \overbrace{(\phi_v^* \leftrightarrow \partial \phi_v)(\phi_v^* \leftrightarrow \partial \phi_v)}^{\quad} \overbrace{\phi_r^* \leftrightarrow \partial \phi_r}^{\quad} \end{aligned}$$

and the same combinations again except that the uttermost contraction is not from the first to the last operator but from the second to the penultimate:

$$\phi_l^* \overleftrightarrow{\partial} \phi_l \overbrace{(\phi_v^* \overleftrightarrow{\partial} \phi_v)(\phi_v^* \overleftrightarrow{\partial} \phi_v)} \phi_r^* \overleftrightarrow{\partial} \phi_r.$$

Therefore, we do not have four contractions as the Feynman rules decree but 8. Diagrammatically, this corresponds to the possibility, that the *Duck* in Fig. 5.1 can also swim upside down, meaning the pion loop insertion g is attached to the lower boson line.

Remark on the *Duck* Diagram in the High Mass Limit

It was already stated that the *Duck* diagram originates from ⑥ of Fig. 6.10 in the high mass limit. This can be understood by shrinking the ρ -line in the diagram ⑥ of Fig. 6.10 into a point. The result is then Fig. 5.1.

Is there is another contribution to the diagram in Fig. 5.1 resulting from the diagram ⑦ in Fig 6.10 in the high mass limit? This would simply lead to another assignment of momenta in (3.17): There, $p - q \rightarrow p$, $k + q \rightarrow k$ or equivalently $q = 0$. Therefore,

$$f(p, k, q)_{\text{offFig. 6.10}} = 4g^2 pk.$$

This quantity would then add to the $[(p + k)^2 + 4pk]$ in (5.8). The amplitude of the resulting pion loop is

$$-\frac{2g^2}{m_\rho^2} \int \frac{d^3\mathbf{k}}{(2\pi)^3} \frac{1}{2\pi i} \int_{-i\infty+\epsilon}^{+i\infty+\epsilon} \frac{4p_0 k_0 - 4\mathbf{p}\mathbf{k} - 4p_0 k_0 - 4\mathbf{p}\mathbf{k}}{k_0^2 - \omega^2} = 0$$

since integrals over mixed products vanish as it is shown in the calculation of *integral II* (A.49). The result of the summation of Matsubara frequencies (5.9) stays the same. Contributions of diagrams where the ρ carries no momentum vanish at finite temperature. In the vacuum, these "vacuum polarizations" or tadpole diagrams contribute to the field renormalization.

A.5.2 The *Specs* Diagram

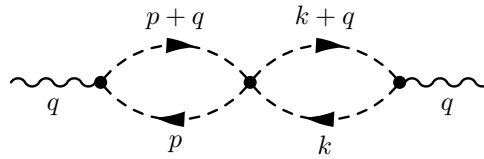


Figure A.5: Simplification of the diagram ⑤ of Fig. 6.10: The *Specs* diagram

The two-loop diagram in Fig. A.5 results from the high mass limits of the diagrams ⑤ and the two-loop version of ⑧ Fig. 6.10 both.

Chosing the vertices from the cubic term in the perturbation series expansion $\mathcal{L}_{\text{int}}^3$ and performing the contractions, it turns out that there is no overall factor for the *Specs* diagram.

The amplitude for the self energy is

$$\begin{aligned}
\Pi_{\text{Fig. A.5}}^{\mu\nu}(q_0, \mathbf{q}) &= T^2 \sum_{\substack{k_0=-\infty, \dots, +\infty \\ p_0=-\infty, \dots, +\infty}} \int \frac{d^3\mathbf{k}}{(2\pi)^3} \frac{d^3\mathbf{p}}{(2\pi)^3} \\
&\quad (-e(2p+q)^\mu) \frac{-g^2}{m_\rho^2} ((2p+q)(2k+q) + (2q+k+p)(k+p)) (-e(2k+q)^\nu) \\
&\quad (-1)^4 \frac{1}{p^2 - m_\pi^2} \frac{1}{(p+q)^2 - m_\pi^2} \frac{1}{k^2 - m_\pi^2} \frac{1}{(k+q)^2 - m_\pi^2} \\
&= \frac{2e^2 g^2 T^2}{m_\rho^2} \sum_{\substack{k_0=-\infty, \dots, +\infty \\ p_0=-\infty, \dots, +\infty}} \int \frac{d^3\mathbf{k}}{(2\pi)^3} \frac{d^3\mathbf{p}}{(2\pi)^3} \\
&\quad \frac{(2p+q)^\mu (2k+q)^\nu [(2p+q)(2k+q) + (2q+k+p)(k+p)]}{(p^2 - m_\pi^2)((p+q)^2 - m_\pi^2)(k^2 - m_\pi^2)((k+q)^2 - m_\pi^2)}. \tag{A.50}
\end{aligned}$$

In the limit, the 00-component of the self energy is therefore

$$\begin{aligned}
\Pi^{00}(q_0 = 0, \mathbf{q} \rightarrow 0) &= \frac{4e^2 g^2 T^2}{m_\rho^2} \sum_{\substack{k_0=-\infty, \dots, +\infty \\ p_0=-\infty, \dots, +\infty}} \int \frac{d^3\mathbf{k}}{(2\pi)^3} \frac{d^3\mathbf{p}}{(2\pi)^3} \\
&\quad \frac{k_0 p_0 [4(k_0 p_0 - \mathbf{k}\mathbf{p}) + (k_0 + p_0)^2 - (\mathbf{k} + \mathbf{p})^2]}{(p_0^2 - \eta^2)^2 (k_0^2 - \omega^2)^2}, \tag{A.51}
\end{aligned}$$

which looks considerably more difficult than the amplitude of the *Duck* diagram in Fig. 5.1. Here, $\eta^2 = \mathbf{p}^2 + m_\pi^2$, $\omega^2 = \mathbf{k}^2 + m_\pi^2$.

Quadratic Terms of the Amplitude

Dismiss all terms in the numerator of (A.51) that do not contain the term $k_0^2 p_0^2$. The resulting amplitude is

$$\frac{24e^2 g^2 T^2}{m_\rho^2} \frac{k_0^2 p_0^2}{(p_0^2 - \eta^2)^2 (k_0^2 - \omega^2)^2}$$

and the resulting integration respectively summation factorizes at once:

$$\Pi_{k_0^2 p_0^2 - \text{term}}^{00}(q_0 = 0, \mathbf{q} \rightarrow 0) = \frac{24e^2 g^2}{m_\rho^2} \left(T \sum_{s_0=-\infty, \dots, +\infty} \int \frac{d^3\mathbf{s}}{(2\pi)^3} \frac{s_0^2}{(s_0^2 - \lambda^2)^2} \right)^2$$

where $\lambda^2 = \mathbf{s}^2 + m_\pi^2$.

The result (see B.1) is

$$\begin{aligned}
\Pi_{k_0^2 p_0^2 - \text{term}}^{00}(q_0 = 0, \mathbf{q} \rightarrow 0) &= \frac{24e^2 g^2}{m_\rho^2} \left(-\frac{1}{2} \int \frac{d^3\mathbf{s}}{(2\pi)^3} \left(\frac{n[\lambda]}{\lambda} + n'[\lambda] \right) \right)^2 \\
&= \frac{3e^2 g^2}{2m_\rho^2} \left(\frac{1}{\pi^2} \int_0^\infty ds s^2 \left[\frac{n[\lambda]}{\lambda} + n'[\lambda] \right] \right)^2 \\
&= \frac{3e^2 g^2}{2m_\rho^2} \left(-\frac{1}{\pi^2} \int_{m_\pi}^\infty d\lambda n[\lambda] \left(s - s + \lambda \frac{\lambda}{s} \right) \right)^2
\end{aligned}$$

$$= \frac{3e^2 g^2}{2m_\rho^2} \left(\frac{1}{\pi^2} \int_{m_\pi}^{\infty} d\lambda \frac{\lambda^2}{s} n[\lambda] \right)^2 \quad (\text{A.52})$$

The minus sign in the first line inside the brackets originates from the clockwise integration contour
The *Specs* diagram in Fig. A.5 is therefore

$$\Pi_{\text{Fig. A.5}}^{00}(q_0 = 0, \mathbf{q} \rightarrow 0) = \frac{3e^2 g^2}{2m_\rho^2} C^2 \quad (\text{A.53})$$

Terms linear in $k_0 p_0$ in (A.51)

Terms linear in $k_0 p_0$ in (A.51) cancel because of the summation technique in (2.46). This is still true for all terms of the form $k_0 p_0^2$ and $k_0^2 p_0$.

A.5.3 Chain Diagrams — Resummation

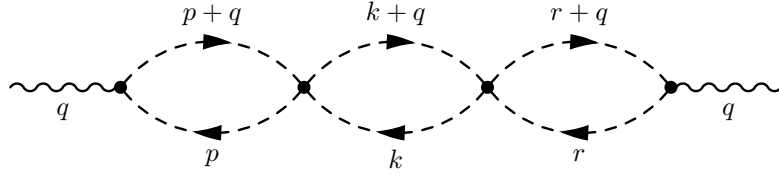


Figure A.6: Generalization of Fig. A.5

The diagram in Fig. A.5 can easily be enlarged to arbitrarily many bubbles that are all coupled by the effective interaction. The diagram to be computed can be seen in Fig. A.6. To get further insight, we investigate in the difference between Fig. A.5 and Fig. A.6: What expression corresponds to the insertion of an additional bubble into the diagram of Fig. A.5?

The numerator of (A.51) with an additional bubble of the momentum r at the righthand side of the kp – double bubble can be rewritten as

$$4p_0 \underbrace{[4kp + (k+p)^2]}_{4\pi\text{-vertex}} k_0 \rightarrow 4p_0 \underbrace{[4pk + (k+p)^2]}_{4\pi\text{-vertex}} \underbrace{[4kr + (k+r)^2]}_{4\pi\text{-vertex}} r_0.$$

The denominator of the new expression depends on r_0^2 , not on r_0 . By using the calculation technique (2.46) we know that terms linear in the 0-components cancel. Therefore the summations are performed from the left bubble to the right one in order to simplify the numerator.

- Summation over p_0 :

$$4p_0 [4pk + (k+p)^2] [4kr + (k+r)^2] r_0 \rightarrow 4p_0 [2p_0 2k_0 + 2p_0 k_0] [4kr + (k+r)^2] r_0 = 4 \cdot 6 p_0^2 r_0 k_0 [4kr + (k+r)^2].$$

The first bracket is simplified by omitting all terms linear in p_0 .

- Summation over k_0 :

$$4 \cdot 6 p_0^2 r_0 k_0 [4kr + (k+r)^2] \rightarrow 4 \cdot 6 p_0^2 r_0 k_0 [2k_0 2r_0 + 2k_0 r_0] = 4 \cdot 6 \cdot 6 p_0^2 r_0^2 k_0^2.$$

- The summation over r_0 leads to no new cancellations by symmetric integration since the term depends only on r_0^2 .

Therefore the r -bubble insertion is

$$\begin{aligned}
& T \sum_{r_0=-\infty}^{\infty} \int \frac{d^3 \mathbf{r}}{(2\pi)^3} 6r_0^2 \frac{g^2}{m_\rho^2} \left(-\frac{1}{r_0^2 - \omega^2} \right)^2 \\
&= -\frac{6g^2 T}{m_\rho^2} \left(\frac{1}{2} \right) \int \frac{d^3 \mathbf{s}}{(2\pi)^3} \left[\frac{n[\lambda]}{\lambda} + n'[\lambda] \right] = \frac{6g^2 T}{m_\rho^2} \frac{1}{4} \frac{1}{\pi^2} \int_{m_\pi}^{\infty} d\lambda \frac{\lambda^2}{s} n[\lambda] \\
&= \frac{3g^2}{2m_\rho^2} C.
\end{aligned} \tag{A.54}$$

Here, C is the static limit of self energy of the single bubble diagram in Fig. 4.9 in e^2 . The quantity C has been evaluated in (5.3). The necessary partial integration has been performed to get rid of the n' -term (gives the factor (-1)) and the clockwise integration contour has been taken into account (second factor of (-1)). Note that the clockwise integration contour plays a role if the number of bubbles in a chain is odd.

The resummation can be performed:

$$\begin{aligned}
& \text{Diagram 1} + \text{Diagram 2} + \text{Diagram 3} + \dots \\
&= e^2 C + \frac{3e^2 g^2}{2m_\rho^2} C^2 + \frac{9e^2 g^4}{m_\rho^4} C^3 + \dots \\
&= e^2 C \left(1 + \frac{3g^2}{2m_\rho^2} C + \left(\frac{3g^2}{m_\rho^2} C \right)^2 + \dots \right) \\
&= e^2 C \frac{1}{1 - \frac{3g^2}{2m_\rho^2} C} = \frac{e^2 2m_\rho^2 C}{2m_\rho^2 - 3g^2 C}.
\end{aligned} \tag{A.55}$$

A.5.4 The *Snowman* Diagram

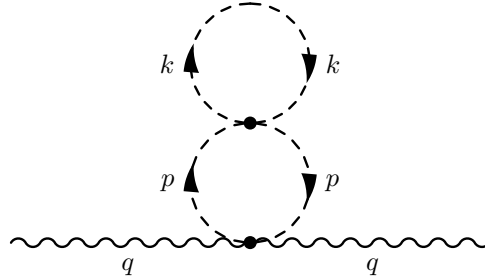


Figure A.7: The *Snowman* Diagram

The contraction of the field operators of this diagram shows that there is no symmetry factor. The diagram originates from second order in perturbation theory $\mathcal{L}_{\text{int}}^2$, so there are two ways to choose one four-vertex in e^2 and one in g^2 which cancels the $1/2!$ from the perturbation series expansion.

The amplitude of the *Snowman* diagram is

$$\begin{aligned}\Pi_{\text{Fig. A.7}}^{00}(q_0, \mathbf{q}) &= T \sum_{p_0=-\infty, +\infty} \int \frac{d^3 \mathbf{p}}{(2\pi)^3} (2e^2) (a(p_0^2 - \mathbf{p}^2 + m_\pi^2)) \left(-\frac{1}{p_0^2 - \eta^2} \right)^2 \\ &= 2e^2 a T \sum_{p_0=-\infty, +\infty} \int \frac{d^3 \mathbf{p}}{(2\pi)^3} \frac{p_0^2 - \mathbf{p}^2 + m_\pi^2}{(p_0^2 - \eta^2)^2}.\end{aligned}\quad (\text{A.56})$$

Here, "a" denotes the closed k-loop as calculated before. The result of the summation is

$$\Pi^{00}(q_0 = 0, \mathbf{q} \rightarrow 0) = \Pi^{00}(q_0, \mathbf{q}) = -\frac{e^2 a}{\pi^2} \int_0^\infty dp p^2 \left(\frac{n(\eta)}{\eta} + \frac{m_\pi^2}{\eta^3} (n'(\eta) \eta - n(\eta)) \right). \quad (\text{A.57})$$

See also B.1. Note that in the case of the sQED 4-vertex as in the *Snowman* diagram, the limit ($q_0 = 0, \mathbf{q} \rightarrow 0$) is irrelevant. The result (A.57) can be further simplified: Consider the integral over the second term, first part (coefficients suppressed) in (A.57)

$$\begin{aligned}m_\pi^2 \int_0^\infty dp p^2 \frac{n'(\eta)}{\eta^2} &= m_\pi^2 \int_{m_\pi}^\infty d\eta \frac{p}{\eta} n'(\eta) \\ &= \underbrace{m_\pi^2 \left[\frac{p}{\eta} n(\eta) \right]_{m_\pi}^\infty}_{=0} - m_\pi^2 \int_{m_\pi}^\infty d\eta n(\eta) \frac{\frac{p}{\eta} - p}{\eta^2} = -m_\pi^2 \int_{m_\pi}^\infty d\eta n(\eta) \left(\frac{1}{p} - \frac{p}{\eta^2} \right).\end{aligned}\quad (\text{A.58})$$

The other part of the second term in the integral (A.57) is

$$-m_\pi^2 \int_0^\infty dp p^2 \frac{n(\eta)}{\eta^3} = -m_\pi^2 \int_{m_\pi}^\infty \frac{p}{\eta^2} n(\eta).$$

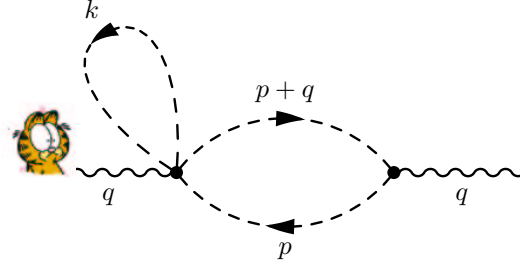
Adding both terms up results in

$$-m_\pi^2 \int_{m_\pi}^\infty d\eta \frac{n(\eta)}{p} = -m_\pi^2 \int_0^\infty dp \frac{n(\eta)}{\eta}.$$

With this simplification of (A.57), the result of the *Snowman* diagram can be rewritten as

$$\Pi_{\text{Fig. A.7}}^{00}(q_0 = 0, \mathbf{q} \rightarrow 0) = -e^2 a \left(D - \underbrace{\frac{m_\pi^2}{\pi^2} \int_0^\infty dp \frac{n(\eta)}{\eta}}_{C-D} \right) = -\frac{e^2 g^2}{2m_\rho^2} D(2D - C). \quad (\text{A.59})$$

The D outside the brackets results from the insertion of the pion loop ("a"), the other from the 4-vertex of sQED (So the result is somewhat more complicated than $\sim D^2$ as one would naively expect.)

Figure A.8: The *Mouse* Diagram

A.5.5 The *Mouse* Diagram

The 5-fold coupling has already the order eg^2 , so that the only vertex it can be combined with is the 3-fold coupling of sQED. The resulting diagram is depicted in Fig. A.8.

The structure of field operators that have to be contracted is from (3.29)

$$4ieA_\mu\phi_v^\star\phi_v(\phi_v^\star\overleftrightarrow{\partial}\phi_v)(\phi_r^\star\overleftrightarrow{\partial}\phi_r).$$

The constraining rule to build the correct topology is that both operators of the 3-vertex have to be connected to the 5-fold vertex.

Performing the contractions shows that there do not occur symmetry factors.

Fig. A.8 originates from the *squared* interaction Lagrangian $\mathcal{L}_{\text{int}}^2$. There exist two possibilities to extract one 3-vertex and one 5-fold vertex from this term. This cancels the $1/2!$ from the perturbation series expansion. Since it is possible for the external photons to exchange their connection point to the diagram, there is an overall factor of 2 for this diagram.

Therefore, the *Mouse* is

$$\begin{aligned}\Pi^{\mu\nu}(q_0, \mathbf{q}) &= 2T^2 \sum_{\substack{k_0=-\infty, \dots, +\infty \\ p_0=-\infty, \dots, +\infty}} \int \frac{d^3\mathbf{k}}{(2\pi)^3} \frac{d^3\mathbf{p}}{(2\pi)^3} \left(\frac{-4e^2g}{m_\rho^2} (p + (p+q) + k + k)^\mu \right) \\ &\quad (-1)^3 \frac{1}{k^2 - m_\pi^2} \frac{1}{p^2 - m_\pi^2} \frac{1}{(p+q)^2 - m_\pi^2} (-e(p+p+q)^\nu) \\ &= -\frac{8e^2g^2}{m_\rho^2} T^2 \sum_{\substack{k_0=-\infty, \dots, +\infty \\ p_0=-\infty, \dots, +\infty}} \int \frac{d^3\mathbf{k}}{(2\pi)^3} \frac{d^3\mathbf{p}}{(2\pi)^3} \frac{(2k+2p+q)^\mu (2p+q)^\nu}{(p^2 - m_\pi^2)(k^2 - m_\pi^2)((p+q)^2 - m_\pi^2)}.\end{aligned}\tag{A.60}$$

This can be simplified:

$$\begin{aligned}\Pi^{00}(q_0 = 0, \mathbf{q} \rightarrow 0) &= -\frac{32e^2g^2}{m_\rho^2} T^2 \sum_{\substack{k_0=-\infty, \dots, +\infty \\ p_0=-\infty, \dots, +\infty}} \int \frac{d^3\mathbf{k}}{(2\pi)^3} \frac{d^3\mathbf{p}}{(2\pi)^3} \frac{(k_0 + p_0)p_0}{(p_0^2 - \eta^2)^2(k_0^2 - \omega^2)} \\ &= -\frac{16e^2g^2}{m_\rho^2} \int \frac{d^3\mathbf{k}}{(2\pi)^3} \frac{d^3\mathbf{p}}{(2\pi)^3} \frac{n[\omega]}{\omega} \left(\frac{n[\eta]}{\eta} + n'[\eta] \right) \\ &= -\frac{16e^2g^2}{m_\rho^2} \frac{(4\pi)^2}{(2\pi)^6} \int_0^\infty dk dp k^2 p^2 \frac{n[\omega]}{\omega} \left(\frac{n[\eta]}{\eta} + n'[\eta] \right)\end{aligned}$$

$$\begin{aligned}
&= -\frac{4e^2g^2}{m_\rho^2} \frac{1}{\pi^4} \int_{m_\pi}^{\infty} d\omega \, d\eta \, k p \, n[\omega] \, (n[\eta] + \eta \, n'[\eta]) \\
&= -\frac{4e^2g^2}{m_\rho^2} \left(\frac{1}{\pi^2} \int_{m_\pi}^{\infty} d\omega \, k \, n[\omega] \right) \left(\frac{1}{\pi^2} \int_{m_\pi}^{\infty} d\eta \, p(n[\eta] + \eta \, n'[\eta]) \right) \\
&= -\frac{4e^2g^2}{m_\rho^2} \left(\frac{1}{\pi^2} \int_{m_\pi}^{\infty} d\omega \, k \, n[\omega] \right) \frac{1}{\pi^2} \left(\underbrace{\left[p\eta \, n[\eta] \right]_{m_\pi}^{\infty}}_{=0} - \int_{m_\pi}^{\infty} d\eta \, (p\eta)' \, n[\eta] + \int_{m_\pi}^{\infty} d\eta \, p \, n[\eta] \right) \\
&= -\frac{4e^2g^2}{m_\rho^2} \left(\frac{1}{\pi^2} \int_{m_\pi}^{\infty} d\omega \, k \, n[\omega] \right) \frac{1}{\pi^2} \left(\int_{m_\pi}^{\infty} d\eta \, n[\eta] \left(p - p - \frac{\eta^2}{p} \right) \right) \\
&= \frac{4e^2g^2}{m_\rho^2} \left(\frac{1}{\pi^2} \int_{m_\pi}^{\infty} d\omega \, k \, n[\omega] \right) \left(\frac{1}{\pi^2} \int_0^{\infty} dp \, \eta \, n[\eta] \right) \tag{A.61}
\end{aligned}$$

with $\omega = \sqrt{\mathbf{k}^2 + m_\pi^2}$.

Therefore, the static limit of the self energy can be denoted as

$$\Pi^{00}(q_0 = 0, \mathbf{q} \rightarrow 0) = \frac{4e^2g^2}{m_\rho^2} \left(\frac{1}{\pi^2} \int_{m_\pi}^{\infty} d\omega \, k \, n[\omega] \right) \left(\frac{1}{\pi^2} \int_0^{\infty} dp \, \eta \, n[\eta] \right). \tag{A.62}$$

The result of the *Mouse* diagram in Fig. A.8 can now be expressed as

$$\Pi_{\text{Fig. A.8}}^{00}(q_0 = 0, \mathbf{q} \rightarrow 0) = \frac{4e^2g^2}{m_\rho^2} CD \tag{A.63}$$

according to (A.62).

A.5.6 The Propeller Diagram

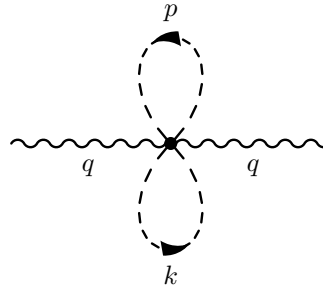


Figure A.9: Photon Self Energy in the order e^2g^2 — The 6-Vertex Case

The 6-fold vertex (3.32) already has the order e^2g^2 in the coupling constant, so it is the only vertex in this self energy diagram. The resulting diagram is displayed in Fig. A.9.

Symmetry Factors

The inspection of the vertex

$$-4e^2 A_\mu A_\nu g^{\mu\nu} \phi^* \phi^* \phi \phi,$$

led us to the vertex factor of $-4 \cdot 2 \cdot 4 = -32$ in the evaluation of the Feynman rules. The coefficient consists of the factor 4 from the expansion of the Lagrangian (3.29), two possibilities to connect external photons to the A -operators and a factor of 4 for the ways the 4 external operators $\phi\phi\phi^*\phi^*$ can connect to the four operators of the Lagrangian.

The last factor must be reduced to 2 now, because both lines close to themselves. The overall factor we have to apply to the calculation is $\frac{1}{2}$.

Calculation of the Self Energy

The resulting matter amplitude is

$$\Pi^{\mu\nu}(q_0, \mathbf{q}) = \frac{1}{2} \frac{16e^2 g^2}{m_\rho^2} g^{\mu\nu} T^2 (-1)^2 \sum_{\substack{k_0=-\infty, \dots, +\infty \\ p_0=-\infty, \dots, +\infty}} \int \frac{d^3 \mathbf{k}}{(2\pi)^3} \frac{d^3 \mathbf{p}}{(2\pi)^3} \frac{1}{k^2 - m_\pi^2} \frac{1}{p^2 - m_\pi^2}, \quad (\text{A.64})$$

and the associated limit is

$$\begin{aligned} \Pi^{00}(q_0 = 0, \mathbf{q} \rightarrow 0) &= \frac{8e^2 g^2}{m_\rho^2} \left(T \sum_{p_0=-\infty, \dots, +\infty} \int \frac{d^3 \mathbf{p}}{(2\pi)^3} \frac{1}{p_0^2 - \eta^2} \right)^2, \quad \eta = \sqrt{\mathbf{p}^2 + m_\pi^2} \\ &= \frac{8e^2 g^2}{m_\rho^2} \left(-\frac{1}{2} \left[\frac{1}{\pi^2} \int_0^\infty dp p^2 \frac{n[\eta]}{\eta} \right] \right)^2 \\ &= -\frac{2e^2 g^2}{m_\rho^2} \left(\frac{1}{\pi^2} \int_0^\infty dp p^2 \frac{n(\eta)}{\eta} \right)^2. \end{aligned} \quad (\text{A.65})$$

See B.1 for details.

The result of the limit of the *Propeller* diagram (A.65) is now prepared to be expressed in terms of D :

$$\Pi_{\text{Fig. A.9}}^{00}(q_0 = 0, \mathbf{q} \rightarrow 0) = -\frac{4e^2 g^2}{m_\rho^2} D^2. \quad (\text{A.66})$$

A.5.7 Numerical Test of the Computation of Contour Integrals

A numerical simulation is performed with the value of $\eta = 1$, $n(p_0) = \frac{1}{e^{p_0} - 1}$ (see B.1). The integration limits are from $-i\infty + \epsilon$ to $+i\infty + \epsilon$, slightly shifted from the imaginary p_0 -axis (see Fig. 5.2).

$$\frac{2}{2\pi i} \int_{\Gamma} dp_0 \left(\frac{1}{p_0^2 - \eta^2} \right)^2 \frac{1}{p_0^2 - \eta'^2} n(p_0) \rightarrow f_{\text{num}}(\eta', \epsilon) = \frac{1}{\pi} \int_{-\infty}^{\infty} dt \left(\frac{1}{(it + \epsilon)^2 - 1} \right)^2 \frac{1}{(it + \epsilon)^2 - \eta'^2} \frac{1}{e^{it+\epsilon} - 1},$$

where the i from the derivative of the path cancels the i from the coefficient. The limit $\eta' \rightarrow 1$ is the interesting part.

The result is consistent with the complex calculus methods: f_{num} is a smooth function in the interval $\epsilon \in [0.8, 1.2]$ (no significant dependence on ϵ) and $f_{\text{num}}(1) = 0.81253$ (with $\epsilon = 0.1$). If one applies the residue theorem on the function (5.18), meaning that the limit is taken before summation (pole of the order of 3), it returns the value of 0.81253 as well.

A.6 Proof of J_D as Conserved Current — no π^0

In order to proof that J_D is the conserved current, the new equations of motion must be derived. This is first done for the sQED case. Then the results are applied for the effective theory. We will omit the term in J_D containing π^0 -mixing since this term has the same structure as the pure π^\pm effective interaction and results in no new complications in the proof apart from length.

With the Lagrangian

$$\mathcal{L} = -\frac{1}{4}F_{\mu\nu}^2 + (D_\mu\phi)(D^\mu\phi)^* - m^2\phi^*\phi \quad (\text{A.67})$$

the three equations of motion

$$\partial_\mu \left(\frac{\partial \mathcal{L}}{\partial (\partial_\mu \phi)} \right) - \frac{\partial \mathcal{L}}{\partial \phi}$$

lead to

$$\begin{aligned} (D_\mu^*)^2 \phi^* + m_\pi^2 \phi^* &= 0 \quad [= \partial^2 \phi^* - ie\phi^* \partial_\mu A^\mu - 2ieA^\mu \partial_\mu \phi^* - e^2 A_\mu A^\mu \phi^* + m_\pi^2 \phi^*] \\ D_\mu^2 \phi + m_\pi^2 \phi &= 0 \quad [= \partial^2 \phi + ie\phi \partial_\mu A^\mu + 2ieA^\mu \partial_\mu \phi - e^2 A_\mu A^\mu \phi + m_\pi^2 \phi] \\ \partial_\mu F^{\mu\nu} &= eJ_D^\nu. \end{aligned} \quad (\text{A.68})$$

Then,

$$\begin{aligned} \partial_\mu j_D^\mu &= i \left[\phi^* \partial^2 \phi - \phi \partial^2 \phi^* + 2ie\phi\phi^* (\partial_\mu A^\mu) + 2ieA^\mu (\phi^* \partial_\mu \phi + \phi \partial_\mu \phi^*) \right] \\ &= i \left[-ie\phi^* \phi (\partial_\mu A^\mu) - 2ieA^\mu \phi^* (\partial_\mu \phi) - ie\phi\phi^* (\partial_\mu A^\mu) - 2ieA^\mu \phi (\partial_\mu \phi^*) \right. \\ &\quad \left. + 2ie\phi\phi^* (\partial_\mu A^\mu) + 2ieA^\mu (\phi^* \partial_\mu \phi + \phi \partial_\mu \phi^*) \right] \\ &= 0, \end{aligned} \quad (\text{A.69})$$

where the first two equations of motion for ϕ and ϕ^* have been used from the first to the second line.

From the Lagrangian of the effective theory (without π^0 -mixing)

$$\mathcal{L} = -\frac{1}{4}F_{\mu\nu}^2 + (D_\mu\phi)(D^\mu\phi)^* - m_\pi^2\phi\phi^* + \frac{b}{4}(\phi^* D_\mu\phi - \phi D_\mu\phi^*)^2$$

follow the three equations of motion

$$\begin{aligned} (D_\mu^*)^2 \phi^* + m_\pi^2 \phi^* + \frac{b}{2i} \phi^* (\partial_\mu j_D^\mu) + b \frac{j_D^\mu}{i} (D_\mu\phi)^* &= 0 \\ D_\mu^2 \phi + m_\pi^2 \phi - \frac{b}{2i} \phi (\partial_\mu j_D^\mu) - b \frac{j_D^\mu}{i} D_\mu\phi &= 0 \\ \partial_\mu F^{\mu\nu} &= eJ_D^\nu. \end{aligned} \quad (\text{A.70})$$

Note that there is a linear term in the derivative in the equation of motion for ϕ and ϕ^* . This might be understood as positive / negative damping for ϕ^*/ϕ . It depends on the density of the particles (j_D) and also goes proportional with the effective ρ -coupling constant. The damping for one particle is the negative of the damping for the other particle: They exchange energy as expected. Note that the damping term is imaginary because b is real.

Furthermore there are two new terms in the equations of motion for ϕ respectively ϕ^* , proportional to $\phi^{(*)} j_D^\mu$. This might be seen as a mass shift which is proportional to the derivative of the conserved current of the process without effective ρ -coupling.

As expected, the derivate of the Maxwell tensor couples to the conserved current with the strength e (see also the case of sQED above).

We return to our original goal, the proof of $\partial_\mu J_D^\mu = 0$. The situation has changed in two respects: if we calculate $\partial_\mu j_D^\mu$ it is not longer 0 due to the new equations of motion. Secondly, we have new terms in the conserved current. But we know from the last calculation how to proceed: Evaluate every occurring $\partial_\mu j_D^\mu$, replace terms of the form $\partial^2 \phi^{(*)}$ by the equations of motion and watch out for cancellations.

Inserting the expressions

$$\underline{\partial^2 \phi^*} = 2ieA^\mu(\partial_\mu \phi^*) + ie\phi^*(\partial_\mu A^\mu) + e^2 A_\mu A^\mu \phi^* - m_\pi^2 \phi^* - \frac{b}{2} \phi^*(\partial_\mu j_D^\mu) - bj_D^\mu(D_\mu \phi)^*$$

and

$$\underline{\partial^2 \phi} = -2ieA^\mu(\partial_\mu \phi) - ie\phi(\partial_\mu A^\mu) + e^2 A_\mu A^\mu \phi - m_\pi^2 \phi + \frac{b}{2} \phi(\partial_\mu j_D^\mu) + bj_D^\mu(D_\mu \phi)$$

from the equations of motion in the expansion of $\partial_\mu j_D^\mu$ in line 1 of (A.69) one ends up with

$$\frac{1}{i} \partial_\mu j_D^\mu = b\phi\phi^*(\partial_\mu j_D^\mu) + bj_D^\mu(\phi^* D_\mu \phi + \phi(D_\mu \phi)^*), \quad (\text{A.71})$$

and therefore

$$(\partial_\mu j_D^\mu)(1 + b\phi\phi^*) = -bj_D^\mu(\phi^* \partial_\mu \phi + \phi \partial_\mu \phi^*) \quad (\text{A.72})$$

Then,

$$\begin{aligned} \partial_\mu J_D^\mu &= \partial_\mu (j_D^\mu(1 + b\phi\phi^*)) \\ &= (\partial_\mu j_D^\mu)(1 + b\phi\phi^*) + bj_D^\mu \partial_\mu (\phi\phi^*) \\ &\stackrel{(\text{A.72})}{=} 0 \end{aligned} \quad (\text{A.73})$$

by using (A.72).

A.7 Fitting the Bubble and the Tadpole Diagram

See section B.1 for a list of the notebooks concerning the fitting procedure.

The Bose factor is replaced by a simple exponential in the low temperature limit in order to solve the integral analytically. The replacement by the Maxwell distribution is usually performed for high temperature approximations, but it turns out to fit very well in this case, too. The result of the simplified integration of D is

$$\frac{1}{\pi^2} \int_{m_\pi}^{\infty} d\eta \sqrt{\eta^2 - m_\pi^2} e^{-\beta\eta} = \frac{m_\pi K_1[m_\pi\beta]}{\pi^2 \beta},$$

where $K_n[x]$ is the first Bessel function of the second kind (or "MacDonald function") which is one solution of the differential equation $x^2 y''(x) + xy' - (x^2 + n^2)y(x) = 0$. Remember that the Bessel functions are solutions to differential equations whose first derivative has a singularity. The functions obey a certain asymptotic behavior (see [22], p. 505, section 9.1.2.6.2.3) and can be fitted with

$$\frac{m_\pi K_1[m_\pi\beta]}{\pi^2 \beta} \rightarrow \frac{m_\pi^{\frac{1}{2}}}{\sqrt{2}\pi^{\frac{3}{2}}\beta^{\frac{3}{2}}} e^{-m_\pi\beta} \left[1 + O\left(\frac{1}{\beta}\right) \right] \quad \text{for } \beta \rightarrow \infty.$$

This fit is still good for reasonably high values of the temperature as the light gray line in Fig 6.2 and Fig. 6.3 shows. The low temperature behavior for D is therefore of the form $\sim T^{\frac{3}{2}} e^{1/T}$. As a last step we try to apply an empirical fit to the numerical result. From the approximation we know which form to expect. If we multiply all three graphs of Fig 6.2 and Fig. 6.3 with the inverse of $T^{\frac{3}{2}} e^{1/T}$, the fit is a

constant and the numerical result (and the Bessel function as well) appear as almost straight lines with different slopes. We add a linear term to the constant fit so that the new fit intersects the numerical result at $T = 100 \text{ MeV}$. This new linear term (only linear in this representation of course) intersects the precise result again at around $T = 300 \text{ MeV}$ and can therefore count as really good. Putting the added linearity inside the coefficients that linearized the curves leads to the better fit

$$D \sim \frac{m_\pi^{1/2}}{\sqrt{2}\pi^{3/2}} e^{-\frac{m_\pi}{T}} T^{\frac{3}{2}} (1 + 0.00343985T).$$

Note here that the correction term implicitly contains the mass of the pion. Therefore this formula is only valid for the *actual* mass of the pion $m_\pi = 139 \text{ MeV}$.

The relative error of the new fit never exceeds 2% in the interval of T between 0 MeV and 300 MeV with maximal relative error at $T = 40 \text{ MeV}$ (fit is higher than numerical result) and $T = 180$ (fit is below numerical result).

We can an even better fit if we try to remove the very low temperature ditch as in the case of C below by introducing an additional gaussian (see below). The the result of the best empirical fit is

$$D \sim e^{-\frac{m_\pi}{T}} t^{(3/2)} (1.419 + 0.00592t) + 0.085e^{-0.0009(10.5+T)^2}.$$

The relative error within the T -interval $(0, 140) \text{ MeV}$ is only 2/1000!

The diagram C cannot be integrated directly by replacing the Bose factor with a negative exponential. Therefore, the difference integral $(C - D)$ (5.7) is solved and then added to the fit of D . The result consists again of modified Bessel functions and is

$$C \sim \frac{m_\pi}{\pi^2 \beta} \left[K_1[m_\pi \beta] + m_\pi \beta K_0[m_\pi \beta] \right].$$

The two Bessel functions can be fitted now as in case of diagram D by

$$\frac{1}{\sqrt{2}\pi^{(3/2)}} e^{-\frac{m_\pi}{T}} m_\pi \sqrt{\frac{T}{m}} (m_\pi + T).$$

Normalizing and linearizing the numerical curve by this approximation shows that it is linear above $T \sim 60 \text{ MeV}$, but displaced from its intersection point at $T = 0$ by a deviation at low temperatures (the fit of D shows the same behavior). The difference to a linear function resembles the right side of a gaussian which is then indeed used to fit very low temperature behavior. The resulting empirical fit is only valid for the *actual* value of m_π and reads

$$C \sim e^{-\frac{m_\pi}{T}} \frac{\sqrt{T}}{m^{(3/2)}} (m_\pi + T) \left[2047 + 567e^{-0.000529(25+T)^2} + 9.7T \right]$$

and has a relative error $< 2/1000$ with respect to the numerical result up to a temperature of 160 MeV.

A.8 A Questionable Calculation

In sQED we have the Ward Identity (4.12). It can be rewritten as

$$k_\mu V^\mu(k, p) = e(\mathcal{G}(p) - \mathcal{G}(p + k)).$$

V^μ is the sum of all vertex diagrams, including 3- and 4-vertices and still has the external legs of the throughgoing boson line. (This is the "raw" version of the WI which transform in the usual WI by multiplying on both sides with inverse propagators). We multiply with $(2p + k)_0$ on both sides. Now

we integrate over p on both sides respectively denote the Matsubara summation. Finally we perform the limit $\mathbf{k} \rightarrow \mathbf{0}$. By doing this, the product on the left side, summed over μ , reduces to the product of the 0-components. The result is (without phase space factors)

$$\int d^3\mathbf{p} \sum_{p_0} (2p+k)_0 k_0 V^0(k_0, \mathbf{k} \rightarrow \mathbf{0}, \mathbf{p}) = \int d^3\mathbf{p} \sum_{p_0} (-e)(2p+k)_0 [\mathcal{G}(p_0+k_0, \mathbf{p}) - \mathcal{G}(p_0, \mathbf{p})].$$

We can now divide by k_0 . Additionally we perform the shift in the energy variable $p^0 \rightarrow p^0 - k^0$ for the term containing $\mathcal{G}(p_0+k_0, \mathbf{p})$.³

The right side results in

$$(2p+k)_0^0 \frac{\mathcal{G}((p+k)^0, \mathbf{p}) - \mathcal{G}(p^0, \mathbf{p})}{k^0} \rightarrow \frac{(2p-k)^0 - (2p+k)^0}{k^0} \mathcal{G}(p_0, \mathbf{p}) = -2\mathcal{G}(p_0, \mathbf{p})$$

so that the equation is (with $k_0 = 0$ and multiplying with $(-e)$ on both sides)

$$\int d^3\mathbf{p} \sum_{p_0} (-e)(2p+k)_0 V^0(k_0=0, \mathbf{k} \rightarrow \mathbf{0}, \mathbf{p}) = \int d^3\mathbf{p} \sum_{p_0} (-e)(-e) (-2\mathcal{G}(p_0, \mathbf{p}))$$

now. This means

$$\Pi_D^{00}(k_0=0, \mathbf{k} \rightarrow \mathbf{0}) = \Pi_B^{00}(k_0=0, \mathbf{k} \rightarrow \mathbf{0}).$$

The subscript D denotes the fully dressed direct coupling self energy in Fig. 4.4 and B the fully dressed self energy bubble in Fig. 4.3.

This result is questionable. For sure, it is not true order-by-order since $C \neq D$ (although $C \sim D \sim (1/6)T^2$).

³How can we shift the 0-component by a constant without changing the result? This question arises because instead of an integration over the energy component we have a sum now. Whereas in an finite valued integral shifts are allowed this is not longer true in case of series: Imagine

$$\sum_{n=-\infty}^{\infty} \delta(n) = 1$$

from the $n=0$ -term but any non-integer shift gives 0 for this series. However, the Matsubara summation has the amazing feature that it can be expressed as an integral along the complex axis (see (2.46)).

So a shift, supposed k is purely imaginary, is allowed. We just shift the integration contour along its own direction.

If the reader is not convinced, we repeat the whole calculation in the vacuum. There we have no summation and the integral shift in the energy component is allowed for sure.

Appendix B

References

B.1 *Mathematica*® Notebooks

Most of the calculations have been carried out using *Mathematica*®. This is a (preliminary) list of the relevant notebooks and their reference to this thesis. They can be found shortly on the web under <http://theory.gsi.de/>, personal homepage of the author.

Name	Reference	Comments
<i>numerical_Values_2.nb</i>	chapter 6	Evaluation of simple Bubbles C and D Evaluation of $\partial/\partial\beta(C - D)$ Evaluation of charge fluctuations Fits for all curves
<i>specs.nb</i>	(A.52)	Calculation of the <i>Specs</i> diagram
<i>duck.nb</i>	(5.13)	Calculation of the <i>Duck</i> diagram Different limits
<i>mouse.nb</i>	(A.62)	Calculation of the <i>Mouse</i> diagram
<i>external.nb</i>	(5.21)	e^2 -Bubble with finite external momentum

B.1.1 Reference of Software

- Numerical integrations and algebraic computations have been done with *Mathematica*®, Version 4.0 on the UNIX cluster of the Gesellschaft für Schwerionenforschung (GSI) in Darmstadt. More informations can be found under www.wolfram.com
- For text editing, L^AT_EX has been used. A good introduction into L^AT_EX can be found in [31]. Furthermore, the package *feynmp*, developed by Thorsten Ohl, TH Darmstadt and the *wick.sty*, developed by T. Kugo have been used. The first is a programming environment which makes it possible to draw Feynman diagrams with L^AT_EX using METAPOST. The second is a *.sty* file that defines a L^AT_EX-command to draw Wick contraction brackets.
- The drawings have been done using *xfig*.

Bibliography

- [1] From the STAR-Collaboration Homepage under
http://www.star.bnl.gov/STAR/imagelib/collisions2001/ev53_front.jpg
- [2] T.Matsui, H.Satz, Phys. Rev. Lett. (**B 178**), 416–422, (1986)
- [3] *Proceedings of the Quark Matter Conference 2001*, Nucl. Phys. (**A 698**), (2002)
- [4] M. Gylassy, Nucl. Phys. (**A 418**), 59C, (1985)
- [5] J. Cleymans, R.V. Gavai, E. Suhonen, Phys. Rep. (**130**), 218, (1986)
- [6] *Proceedings of the Strange Quark Matter Conference*, to be published
- [7] S. Jeon, V. Koch, Phys.Rev.Lett. (**85**), 2076–2079, (2000)
- [8] M. Asakawa, U. Heinz, B. Müller, Phys.Rev.Lett (**85**), 2072–2075, (2000)
- [9] S. Jeon, V. Koch, Phys. Rev. Lett (**83**), 5435–5438, (1999)
- [10] G. Bertsch: Phys. Rev. Lett. (**72**), 2349–2350 (1994)
- [11] T. Fliessbach: *Statistische Physik*,
Spektrum Akademische Verlag, 3rd edition, Heidelberg 1999
- [12] J. I. Kapusta: *Finite-Temperature Field Theory*,
Cambridge 1989
- [13] Michael E. Peskin, Daniel V. Schroeder: *An introduction to Quantum Field Theory*,
Cambridge 1995
- [14] L.D. Landau, E.M. Lifschitz: *Statistische Physik*,
Berlin 1971
- [15] G. Baym: *Lectures On Quantum Mechanics*,
9th edition, W.A. Benjamin Advanced Book Program, Reading, MA, 1981
- [16] H. Arthur Weldon: Phys. Rev. **D 47**, 594–600, (1993)
- [17] W. Weise *Trends in Nuclear Physics, 100 Years Later (Les Houches, Session LXVI 1996)*,
Elsevier 1998, p. 427–515

- [18] S.L. Adler, R. Dashen: *Current Algebras and Applications to Particle Physics*, Benjamin, New York, 1968
- [19] V.Koch: *Aspects of Chiral Symmetry*, International Journal of Modern Physics **E 6**, No. 2, 203–249. (1997)
- [20] Lewis H. Ryder: *Quantum Field Theory*, Cambridge 1985
- [21] Chris Quigg: *Gauge Theories of the Strong, Weak, and Electromagnetic Interactions*, Reading, Massachusetts 1983
- [22] Bronstein et al.: *Taschenbuch der Mathematik*, 4th edition, Frankfurt am Main 1999
- [23] C. Gale, J.I. Kapusta, Nucl. Phys. (**B 357**), 65-89, (1991)
- [24] C. Song, Phys. Rev. (**D48**), 1375–1389, (1993)
- [25] H.A. Weldon: hep-ph/0203057v1 (5 Mar 2002)
- [26] G. Baym, N.D. Mermin, J. Math. Phys., (**2**), 232, (1961)
- [27] Alexander L. Fetter, John D. Walecka: *Quantum Theory of Many Particle Systems*, McGraw – Hill, 1971
- [28] S. Gottlieb *et al.*, Phys Rev. (**D 27**), 140, (1983)
- [29] C. Itzykson, J.-B. Zuber: *Quantum Field Theory*, McGraw–Hill 1980
- [30] V.L. Eletsky, J. Kapusta, R. Venugopalan, Phys. Rev.D (**48**), 4398–4407, (1993)
- [31] H. Kopka: *L^AT_EX, Eine Einführung*, 4th edition, Addison–Wesley, 1992
- [32] E.M. Lifschitz, L.P. Pitaevski: *Statistical Physics, Part1*, 3rd edition, Pergamon Press, (1980)
- [33] F. Reif: *Fundamentals of statistical and thermal physics*, McGraw–Hill, 1965
- [34] M.Prakash, R. Rapp, J. Wambach, I. Zahed, hep-ph/0110070 v1 (4 Oct 2001)
- [35] S. Weinberg: *The Quantum Theory Of Fields*, Cambridge 1995

Appendix C

Acknowledgement

Ich versichere gemäss der Prüfungsordnung, diese Diplomarbeit selbst angefertigt zu haben. Alle übernommenen Resultate sind klar zitiert und im Literaturverzeichnis angeführt. Insbesondere ist in der Einleitung stets markiert, auf welches Autors Gedankengang Bezug genommen wurde. Die verwendeten Hilfsmittel sind in den Referenzen bezeichnet.

Zu allererst möchte ich meinen Eltern danken, die mir immer moralisch und finanziell beigestanden haben.

Volker Koch möchte ich für seine Betreuung danken. Ich kann mir keine bessere vorstellen. Nicht nur, dass er unkompliziert und schnell die Zusage gab und mir das Einleben in Berkeley erleichterte, er erreichte auch eine finanzielle Unterstützung durch das Lawrence Berkeley Lab. Während der gesamten Zeit der Diplomarbeit konnte ich ständig zu ihm mit meinen Fragen kommen, die er immer geduldig und ausführlich beantwortet hat, stundenlang und auch Freitags nachmittags. Ausserdem: Truthahn an Thanksgiving and Weihnachten (!) für den Diplomanden fern von zu Hause. Und wenn's nötig war, auch gelinder Druck.

Spass an der Physik zu haben, mit Mitphysikern locker und herzlich umzugehen und Fragen der Physik gleichzeitig anschaulich aber auch exakt anzugehen — ich fand es klasse. Danke.

Herrn Professor Münster möchte ich danken, dass er so unkompliziert einen Diplomanden akzeptiert hat, der sich dann sofort für ein Jahr ins Ausland verdrückte.

Dem Lawrence Berkeley Laboratory möchte ich für finanzielle Unterstützung danken.

Furthermore, I want to thank my colleagues from GSI and LBNL. In particular, Luis Alvarez-Ruso and Hendrik van Hees for fruitful discussions and the help with physics and computers. In both laboratories I enjoyed the open and relaxed atmosphere. In addition to Dr. Volker Koch and Prof. Dr. Gernot Münster I would like to thank Kate Jones, Andreas Krüger, and Alexis Pong for proofreading.

Schliesslich sage ich auch danke allen Freunden, mit denen ich viel Spass hatte, in Berkeley, auf ausgedehnten Reisen im letzten Sommer im Südwesten der USA (thanks to Pasi for his convertible) und hier an der GSI.